CHEMICO-MECHANICAL IMPROVEMENT OF BENTONITE BARRIERS FOR POLLUTANT CONTAINMENT

A THEORETICAL AND EXPERIMENTAL STUDY

SARA PUMA

PH.D. IN WATER AND TERRITORY MANAGEMENT ENGINEERING

ADVISOR: PROF. MARIO MANASSERO

CO-ADVISOR: DR. ANDREA DOMINIJANNI

POLITECNICO DI TORINO

DEPARTMENT OF STRUCTURAL, GEOTECHNICAL AND BUILDING ENGINEERING

May 2013

CONTENTS

INTRODUCTION VII

References XII

CHAPTER 1 – BENTONITE BARRIERS 1

1.1. Bentonite crystalline structure and microstructure 1

1.2. Swelling and mechanical properties of bentonite influenced by the microscopic scale structure 6

1.2.1 Sodium and calcium bentonite 7

1.2.2 Index properties measurement: Swell Index and Atterberg Limits 7

1.2.3 Swelling tests and loading/unloading/reloading tests under isotropic conditions 11

1.2.3.1 Swelling tests under isotropic conditions 11

1.2.3.2 Loading/unloading/reloading tests under isotropic conditions 13

1.3. Geosynthetic clay liners (GCLs) 17

1.4. Clay membrane barriers 21

1.5. Bentonite based barriers 23

References 24

CHAPTER 2 – CONTAINMENT PERFORMANCE OF NATURAL AND POLYMER-MODIFIED BENTONITE BARRIERS SUBJECTED TO PHYSICAL PRE-TREATMENTS 29

Puma et al., 2013. **The role of physical pretreatments on the hydraulic conductivity of natural and polymer modified sodium bentonites.** (Submitted in November 2012 to the journal *Geotextiles and Geomembranes*). In revision.

2.1. Abstract 31
2.2. Keywords 32
2.3. Introduction 33
2.4. Material and specimen preparation 35
2.4.1 Materials 36
2.4.2 Permeant liquids 37
2.4.3 Soluble salt removal 37
2.4.4 Polymer modification 38
2.4.5 Pre-hydration and pre-consolidation. 39
2.5. Experimental method and testing procedures 40
2.6. Results 42
2.6.1 Natural bentonite specimens 42
2.6.2 Polymer modified specimens 47
2.6.3 Termination criteria 51
2.7. Discussions and conclusions 53
Acknowledgements 55
References 56

CHAPTER 3 – OSMOTIC AND SWELLING PROPERTIES OF BENTONITE BARRIERS 59

Dominijanni et al.,2013. **Coupled chemical-hydraulic-mechanical behaviour of bentonites.** *Géotechnique* 63, No. 3, 191-205.

3.1. Abstract 61
3.2. Keywords 61
3.3. Introduction 62
3.4. Theory 63
3.4.1 Equilibrium conditions 64
3.4.2 Transport equations 72
3.5. Material and methods 80
3.5.1 Materials 80
3.5.1.1 Bentonite preparation 80
3.5.2. Testing apparatus and procedures 82
3.5.2.1 Chemico-osmotic test 82
3.5.2.2 Swelling pressure test 85

Dominijanni, A., Manassero, M., Puma, S. (2013). **Coupled chemical...** *Geotechnique* 63, No. 3.

3.6. Results 87
3.6.1 Chemico-osmotic test results 87
3.6.2 Swelling pressure test results 93
3.7. Interpretation of the test results 96
3.8. Conclusions 102
References 103
3.9. Further results of chemico-osmotic tests and confront with data from literature 106
3.9.1 Chemico-osmotic properties of calcium bentonite 106
3.9.2 Second chemico-osmotic test on sodium bentonite 110
3.9.3 Confront with data from literature 112
3.10 A new apparatus to measure together the swelling and osmotic behaviour of bentonites 113

CHAPTER 4 – CONTAINMENT PERFORMANCES OF POLYMER MODIFIED BENTONITE TOWARDS HYDROCARBONS 117
4.1. Capillarity in porous media 118
4.1.1 Characteristic curve 118
4.1.2 Characteristic curve models 120
4.2. Characteristic curve of sodium bentonite 121
4.2.1 Specimen preparation 121
4.2.2 The vapour equilibrium technique 122
4.2.3 Testing procedure and results 125
4.3. Hydrocarbon behaviour in charged porous media 131

Puma et al., 2011. **Performance of GCLs with Diesel Oil and Polymer Treatment Proposal.** Geosynthetics Middle East.

4.4. Abstract 135
4.5. Introduction 135
4.6. Materials and methods 137
4.6.1 Bentonites 137
4.6.1.1 Geosynthetic Clay Liner and natural sodium bentonite 137
4.6.1.2 Modified bentonites 138
4.6.2 Permeant liquids 138

Puma et al., 2011. **Performance of GCLs with Diesel Oil and Polymer Treatment Proposal.** Geosynthetics Middle East.

4.6.3 Testing methods and equipments 139
4.6.3.1 Free swell test 139
4.6.3.2 Hydraulic conductivity test 139
4.7. Results 140
4.7.1 Free swell tests 140
4.7.2 Hydraulic conductivity tests 141
4.8. Conclusions 144
Acknowledgements 145
References 146

CHAPTER 5 – CONTAINMENT PERFORMANCE OF A BENTONITE-BASED BARRIER CONSTITUTED OF MUNICIPAL SOLID WASTE BOTTOM ASHES 149

Puma et al., 2013. **Reuse of MSWI bottom ash mixed with natural sodium bentonite as landfill cover material.** Waste Management and Research.

5.1. Abstract 151
5.2. Keywords 151
5.3. Introduction 152
5.4. Materials and methods 154
5.5. Results and discussions 160
5.5.1 Swelling performance of the sodium bentonite in MSWI BA-bentonite mixtures 160
5.5.2 Hydraulic conductivity of the BA-bentonite mixture 163
5.5.3 Leachate characterization 165
5.6. Conclusions 166
References 168

CHAPTER 6 – FINITE DIFFERENCE MODELLING OF DIFFUSIVE FLUX OF CALCIUM THROUGH A BENTONITE BARRIER IN IN-SITU CONDITIONS 175
6.1. Engineering problem 175
6.1.1 Use of GCLs in landfill 175
6.1.2 Simplification of the problem: GCL inside a landfill barrier 176
6.1.2.1 Advective flux approach (Shackelford, 2005) 177
6.1.2.2 Diffusive flux approach 180
6.2. From the engineering problem to the mathematical problem 181
6.2.1 Porous medium characteristics 181

6.2.2 Momentum Balance Equations 182
6.2.3 Solute transport equation for a semi-permeable porous medium 186
6.2.4 Equations describing the mathematical model 189
6.3. Solution method 193
6.3.1 Dimensionless equations 194
6.3.2 Finite-difference method solution 195
6.3.3 Initial and boundary conditions – Study of the partition mechanism in the pore solution 199
6.3.3.1 Initial conditions 200
6.3.3.2 Boundary conditions 202
6.4. Matlab® implementation 204
6.5. Simulation results 213
6.5.1 Case A results: 10 mm bentonite layer alone 213
6.5.2 Case B results: composite barrier 217
6.5.3 Confront with literature experimental data 220
6.5.4 Result discussion 224
References 226

FINAL CONCLUSIONS 227

FINAL ACKNOWLEDGEMENTS 233

INTRODUCTION

Pollution control represents one of the main problems of public interest in all industrialised countries. Nowadays, the widespread issue of urban waste disposal has highlighted the necessity of developing advanced technological solutions aimed at improving waste containment facilities, since the major component of the solid waste disposal system to this day is still the landfill, in almost every country.

Since the 1970s, when the engineering of waste containment began, the overall objective of Environmental Geotechnics was to limit contaminant discharge to groundwater and subsoil (Benson, 2000). Initially, clay liners and clay caps were introduced to provide isolation of waste leachate from the subsoil (or the groundwater beneath), in the case of liners, or to guarantee long-term control of percolation into the waste, and thus control the generation of leachate, in the case of covers.

Since the 1990s design engineers and environmental agencies have shown a growing interest in the use of geosynthetic clay liners (GCLs) as an alternative to compacted clays in cover systems or in bottom lining of waste containment facilities because they have very low hydraulic conductivity to water and relatively low cost (Bouazza, 2002).

GCLs contain a thin layer of sodium bentonite with a dry thickness between 5 and 10 mm, sandwiched between two geotextiles or glued to a geomembrane, GM. The

excellent hydraulic performances of GCLs have to be attributed to bentonite characteristics (Shackelford et al., 2000) and, since these last are greatly influenced by the chemical composition of the environment surrounding the barrier and by the state parameters, the performances of GCLs can be altered, and then worsened, by a simple variation of the chemical or physical boundary conditions.

Aimed at solving this last issue, clay liners and GCLs have undergone great change during the last two decades, with new material being introduced (i.e. polymers) and new design methods being adopted (i.e. membrane behaviour investigation, contaminant diffusion estimation). These new technologies have been used in several applications for pollution control to offer higher levels of safety, to guarantee maintenance of excellent performances, even in the long term, and to reduce the overall cost of liner construction (i.e. cheaper raw material and more practical installation).

The research project developed during the Ph.D. has been focused on bentonite barriers. The term "bentonite barriers" includes bentonite or bentonite-based barriers which find application both in urban waste landfill, hazardous or radioactive wastes final disposal and in hydrocarbon containment.

The developed theoretical and experimental study has had the aim of evaluating the possible improvement of containment performance of the bentonite barriers, towards standard (i.e. de-ionized water, DW) and non standard liquids (i.e. sodium and calcium chloride solutions or diesel oil), acting on their state parameters, chemical composition, and boundary conditions at installation.

The whole laboratory activity has been developed at Politecnico di Torino, in the laboratory of soil mechanics of the Department of Environment, Land and Infrastructure Engineering and in the Disaster Planning Laboratory of the Department of Structural, Geotechnical and Building Engineering, with an exception for the swell pressure tests, which have been performed at ISMGEO (Seriate, Milan, Italy).

The contents of this thesis cover the main topic analysed during the development of the 3-years Ph.D. research programme. A short summary is reported below:

Chapter 1 – Bentonite barriers

This chapter is an introduction to the topic of the research activity: the improvement of contaminant containment performances of the bentonite barrier. Chapter 1 gives a phenomenological and physical description of the mineralogical, chemical and physical properties of sodium and calcium bentonite. Moreover, the main features and issues concerning Geosynthetic Clay Liners, and bentonite barriers in general, are introduced.

Chapter 2 – Containment performances of natural and polymer-modified bentonite barriers subjected to physical pre-treatments

The role of physical pre-treatments, such as pre-hydration, pre-consolidation and salt removal, applied to sodium and polymer modified bentonites, has been analyzed in the Paper reported in chapter 2, titled: "THE ROLE OF PHYSICAL PRETREATMENTS ON THE HYDRAULIC CONDUCTIVITY OF NATURAL AND POLYMER MODIFIED SODIUM BENTONITES". Moreover, the effect of the presence or absence of needling across the bentonite layer has been studied.

All these variables have been shown to influence the hydraulic performances of bentonite through hydraulic conductivity change in both short and long term conditions. Physical pre-treatments and polymer addiction, in fact, influence the swelling behaviour of bentonite and its response to the cation exchange phenomenon.

Chapter 3 – Osmotic and swelling properties of bentonite barriers

In the Paper included in this chapter, titled "COUPLED CHEMICAL-HYDRAULIC-MECHANICAL BEHAVIOUR OF BENTONITES", a theoretical approach has been proposed in order to derive constitutive equations which describe the coupled chemical-hydraulic-mechanical behaviour of bentonite barriers, with the aim to assess their long term performance. The phenomenological parameters that govern the transport of electrolyte solutions through bentonites, i.e. the hydraulic

conductivity, the reflection coefficient, which is also called the chemico-osmotic efficiency coefficient, and the osmotic effective diffusion coefficient, have been measured through laboratory tests on a natural sodium bentonite The obtained results have been interpreted by assuming that the microscopic deviations of the pore solution state variables from their average values are negligible. In this way, it is possible to interpret the macroscopic behaviour on the basis of the physical and chemical properties of the bentonite mineralogical components.

At the end of the chapter two further chemico-osmotic tests are described aimed at analysing (1) the osmotic behaviour of calcium bentonite and (2) the effects induced on osmotic behaviour by stress-strain properties. Moreover, the osmotic results are confronted with data from literature.

Finally, the design of a new osmotic apparatus to measure both the swelling pressure and the reflection coefficient is proposed. This apparatus will be produced in the laboratories of ISMGEO (Seriate, Milan, Italy).

Chapter 4 – Hydrocarbon containment performances of natural and polymer-modified bentonite barriers

Background information on hydrocarbon behaviour in soils is reported in the first part of this chapter. In particular, the effects of capillary forces on the distribution of immiscible fluids in porous media and the theoretical aspects, regarding the formation of tactoids induced by the low dielectric constant that characterizes the most of hydrocarbon species, are studied.

An experimental study is presented in the Paper titled "HYDRAULIC PERFORMANCE OF GCLS WITH DIESEL OIL AND POLYMER TREATMENT PROPOSAL", which is aimed at evaluating the hydraulic performance of a needle-punched GCL using both standard liquids (i.e. de-ionized water) and diesel oil in order to estimate the change in hydraulic conductivity and swelling ability upon contact or permeation with hydrocarbons. Moreover, the hydraulic conductivity to diesel oil of GCL samples saturated at different initial gravimetric water contents was investigated with the aim to analyse the effect of initial water saturation on hydrocarbon containment performances. Finally, the swelling and hydraulic

performances to diesel oil of an innovative material, obtained by mixing sodium bentonite with a polymer, were measured.

Chapter 5 – Containment performances of a bentonite-based barrier constituted of municipal solid waste bottom ashes

The research described in the Paper included in this chapter, titled "REUSE OF MSWI BOTTOM ASH MIXED WITH NATURAL SODIUM BENTONITE AS LANDFILL COVER MATERIAL" has the aim of evaluating the reuse of incinerator slag, mixed with sodium bentonite, for landfill capping system components. A chemical, hydraulic and mechanical characterization was performed on pure bottom ash (BA) samples from an incinerator in the North of Italy and on the BA-bentonite mixture. This study qualifies the BA-bentonite mixture as a suitable material for landfill cover in Italy. Moreover, owing to the low release of toxic compounds from BA, the proposed cover system does not affect the leachate quality in the landfill.

Chapter 6 – Finite difference modelling of diffusive flux of Calcium through a bentonite barrier in in-situ conditions

The evidence of the strong degradation induced in the hydraulic performances of sodium bentonite barriers by the cation exchange phenomenon has been highlighted in the previous chapters. This experimental result underlines the need to study the transitional development of the cation exchange phenomenon with the aim to compare that to the period in which landfill barrier performances have to be guaranteed in in-situ conditions.

The mathematical study developed in this chapter is focused on the evaluation of the role of the diffusive component of Calcium flux in the cation exchange phenomenon which can develop in a sodium bentonite barrier, placed in an environment inexorably rich in chemical compounds containing soluble Calcium (i.e. the natural soil, the aquifer, the drainage layer saturated with waste leachate or raining water).

References

Benson, C. H. (2000). Liners and covers for waste containment. *In* Proceeding 4th Kansai Intl. Geotechnical Forum, Creation of a New Geo-Environmental, Japanese Geotechnical Society, Kyoto, Japan, May 24-26, 2000, 1-40.

Bouazza, A. (2002). Geosynthetic clay liners. Review article. Geotextiles and Geomembranes, **20**, 3-17.

Shackelford, C. D., Benson, C. H., Katsumi, T., Edil, T. B., and Lin, L. (2000). Evaluating the hydraulic conductivity of GCLs permeated with nonstandard liquids. Geotextiles and Geomembranes, **18**(2-4) 133–162.

Chapter 1

BENTONITE BARRIERS

This chapter is an introduction to the topic of the research activity: the improvement of contaminant containment performances of the bentonite barriers. Chapter 1 gives a phenomenological and physical description of the mineralogical, chemical and physical properties of bentonite. Moreover, the results of a laboratory study regarding the difference in the swelling and mechanical behaviour of sodium and calcium bentonite are reported. Finally, the main features and the main issues concerning Geosynthetic Clay Liners and bentonite barriers in general are introduced.

1.1 BENTONITE CRYSTALLINE STRUCTURE AND MICRO-STRUCTURE

Clay minerals consist of hydrous silicates or alumino silicates and their structure is composed by layers of silica and alumina sheets joined together. The crystalline structure and the microstructure are the main factors which influence the physical and chemical properties of clay minerals.

Clay minerals can be divided into: kaolinites, illites, attapulgites, chlorites and smectites. Each one of these categories presents some differences in the crystalline structure and, for this reason, each one is characterized by different properties.

In general, as described by Luckham (1999), every clay mineral is constituted by two structural units:

- the first one is the octahedral sheet, consisting of an octahedral structure in which aluminium, iron or magnesium atoms are equidistant from the oxygen atoms or the hydroxyls.
- the second one is called tetrahedral sheet, consisting of a tetrahedral structure in which a silicon atom is equidistant from the oxygen atoms or the hydroxyls.

Both networks are repeated indefinitely to form a sheet.

Bentonite is a clay soil composed by at least 70% of montmorillonite, which belongs to smectite clay minerals, also called 'three-layer minerals' or 2:1 phyllosilicates. The main feature of this class is to be formed by a certain number of unit layers, consisting of the combination of an octahedral (alumina or magnesia) sheet and two tetrahedral (silica) sheets, one on each side, as shown in Fig. 1.1 and Fig. 1.2. The sheets are joined because they share oxygen atoms (covalent bonds).

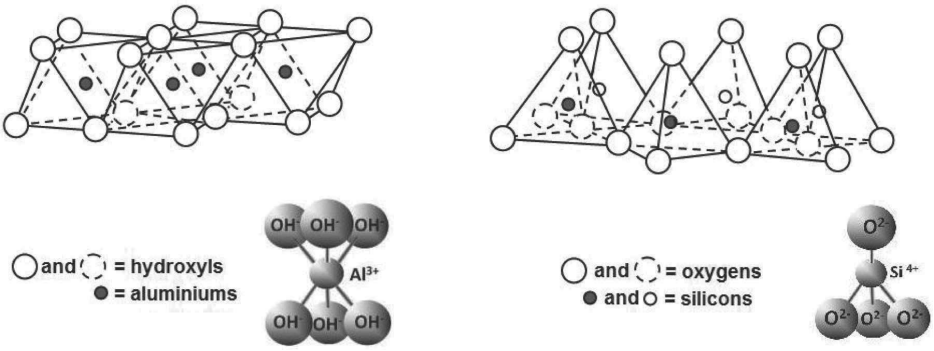

Figure 1.1 - Unit layer forming the montmorillonite crystalline structure.

The unit layers are pooled together face-to-face to form the crystal lattice. In this case they are held together by Van Der Waals forces (see Fig. 1.2).

Clay minerals present a charge due to the isomorphous substitutions of lower charge species as Mg^{2+}, Fe^{2+} or Mn^{2+} for Al^{3+} in the octahedral sheet, and to the substitution of Al^{3+} or Fe^{3+} for Si^{4+} in the tetrahedral sheet. In this way a charge deficiency is established and this deficiency determines a negative electric potential at the

surfaces of the particles, which is compensated by the cations contained in the pore solution. The ideal unit cell formula of montmorillonite is $\{(OH)_4Si_8Al_{3.44}Mg_{0.66}O_{20}\cdot nH_2O^{0.66-}\}$ with a typical surface charge of 0.66 equivalent per unit cell.

The cation exchange capacity, CEC, is defined as the total amount of cations necessary to compensate the negative clay charge and it's expressed in milliequivalents per hundred grams of dry clay. A typical CEC value for montmorillonite is 80-100 meq/ 100g.

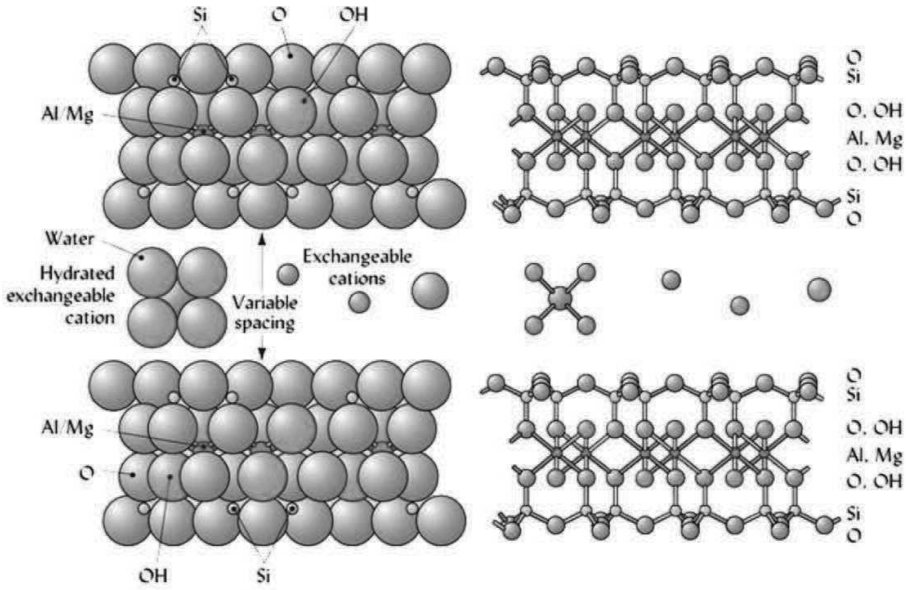

Figure 1.2 - Montmorillonite crystal lattice.

Montmorillonite crystals consist of parallel-aligned elementary alumino-silicate lamellae, which are approximately 10 Å thick and 1000-2000 Å in the lateral extent. The unit cell parameters are a = 5.17 Å and b = 8.95 Å, which correspond to a unit cell area of 92.5 $Å^2$, or one unit charge per 140 $Å^2$. The corresponding surface charge, σ, is equal to 0.114 $C\cdot m^{-2}$. The total specific surface, S, available for water adsorption is approximately equal to 760 $m^2\cdot g^{-1}$, assuming a solid density, ρ_{sk} = 2.65 $g\cdot cm^{-3}$.

Montmorillonite particles can be represented as infinitely extended platy particles. The half distance, b (m), between the montmorillonite particles can be estimated from the total porosity, n (-), or the void ratio, e = n/(1-n) (-). Norrish (1954) showed that bentonite can have a dispersed structure in which clay particles are present, as well separated units, or an aggregated structure that consists of packets of particles, or tactoids, within which several clay platelets or lamellae are in a parallel array, with a characteristic interparticle distance of 9 Å.

The formation of tactoids has the net result of reducing the surface area of the montmorillonite, which then behaves like a much larger particle with the diffuse double layer only fully manifesting itself on the outside surfaces of the tactoids (see Fig. 1.3).

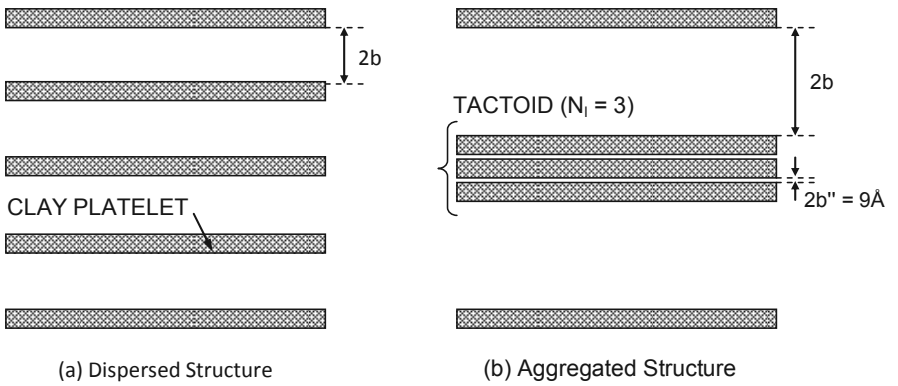

Figure 1.3 - Microscopic structure of clay soils containing montmorillonite as the main mineralogical component. The structure can be dispersed (a), if the lamellae of montmorillonite (or clay platelets) are present as individual units, or aggregated (b), if the lamellae are condensed to form the so-called tactoids. Symbols: N_l = number of clay platelets per tactoid; b = half-spacing of the conducting pores; b'' = half spacing of the intra-tactoid pores containing immobile water.

The formation of tactoids is due to internal flocculation of the clay platelets, and depends on the concentration and the valence of the ions in the soil solution. The number, N_l, of clay platelets or lamellae forming tactoids increases with an increase of the ion concentration and valence of cations in the soil solution. Unfortunately, the number of platelets in a tactoid cannot be predicted and has to be estimated from

macroscopic measurements of the transport parameters (e.g. hydraulic conductivity). A complicating factor is the non-uniform distribution of ions in mixed systems. For instance, in Na^{+}-Ca^{2+} systems, the distribution of the ions is not random, but the charges within the tactoids are mainly neutralized by Ca^{2+} whereas those on the outer surfaces are substantially enriched in Na^{+} over Ca^{2+}.

The average half spacing, b, in dispersed clays may be estimated assuming a uniform distribution of the clay platelets in a parallel orientation, from the relation:

$$b = \frac{e}{\rho_{sk} S} \tag{1.1}$$

If the clay has an aggregated structure, only the external surface of the tactoids is in contact with the mobile fluid, therefore the void space within the platelets in the tactoids should be subtracted from the total void space to obtain the void space with reference to the conducting pores (see Fig. 1.3). If N_l is the number of platelets per tactoid, the external specific surface, S', and the internal specific surface, S'', are given by:

$$S' = \frac{S}{N_l} \tag{1.2a}$$

$$S'' = S - S' = \frac{(N_l - 1)}{N_l} S \tag{1.2b}$$

The average half spacing between the platelets in the tactoids, as determined by means of X-ray measurements, is b'' = 4.5 Å (Shainberg et al., 1971). The total void index, e_T, of the bentonite is given by the sum of the void index inside the tactoid, e'', and the void index, e, of the conducting pores. The water in the tactoids can be considered part of the solid particles and is excluded from the transport mechanisms. The void index associated with the internal surfaces of the tactoid, e'', can be estimated as follows:

$$e'' = b'' \rho_{sk} S'' \tag{1.3}$$

where ρ_{sk} = density of the solid particles (kg/m^3).

The corrected half spacing, b, between the tactoids, in the case of an aggregate microstructure of bentonite, can be estimated from a similar equation to Eq.1.1:

$$b = \frac{e}{\rho_{sk} S'} \tag{1.4}$$

where $e = e_T - e_0$ = void ratio referring to the void space between the tactoids and S' = effective specific surface of the tactoids.

When the number, N_l, of clay platelets in the tactoids increases, the external specific surface decreases and the half spacing, b, between the tactoids increases, even though the total void ratio remains constant and the void ratio referring to the pore volume available for the transport decreases.

Guyonnet et al. (2005), through a comparison of the results of hydraulic conductivity tests and microscopic analyses of bentonite structure based on small angle X-ray scattering and transmission electron microscopy, showed that high values of the hydraulic conductivity are related to an aggregated structure (also called the hydrated-solid phase), while low values of the hydraulic conductivity are related to a dispersed structure (also called the gel phase). These experimental results can be explained by the increase in the average pore size, due to tactoid formation (see Fig. 1.3).

1.2 SWELLING AND MECHANICAL PROPERTIES OF BENTONITE INFLUENCED BY THE MICROSCOPIC SCALE STRUCTURE

This paragraph summarizes the main results of a laboratory study, developed during the Ph.D. activity, aimed at analysing the influence of the microscopic scale structure of montmorillonite lamellae on the swelling and mechanical properties of bentonite. At the microscopic scale, two main and distinct montmorillonite structures can be distinguished: a dispersed structure of separated lamellae, typical of sodium bentonite, and an aggregated structure formed by packets of lamellae united in a parallel face-to-face array, called tactoids, which are typical of calcium bentonite.

In this paragraph the results of swell index tests, liquid limit determinations, swelling tests under isotropic conditions and loading/unloading tests under isotropic conditions performed on sodium and calcium bentonite are reported, with the aim to highlight the influence of microscopic scale structure (dispersed/aggregated) on macroscopic scale properties of bentonite, such are the swelling behaviour and the mechanical properties.

1.2.1 Sodium and calcium bentonite

The powdered sodium bentonite used in the Ph.D. laboratory activity is an Indian sodium bentonite that is used for the production of a needle-punched GCL. The bentonite is characterized by a cation exchange capacity (CEC, measured using the methylene blue adsorption method) of 105 meq/100g. The mineralogical composition, evaluated through x-ray diffraction analysis, indicates a bentonite that is primarily composed of smectite (> 98%) with traces of calcite, quartz, mica and gypsum. More information on sodium bentonite is reported in the paragraph 2.4.1.

Calcium bentonite has been obtained through an accelerated degradation of sodium bentonite that was promoted by the cation exchange of calcium for sodium. Sodium bentonite was kept in contact with a highly concentrated (1M) calcium chloride solution for a week. In this way, sodium bentonite exchanged sodium cations with calcium cations present in the equilibrium solution. Excess soluble calcium salts, contained in the exchanged calcium bentonite (due to the usage of a 1M $CaCl_2$ solution as equilibrium solution), were successively removed by a series of hydration with de-ionized water and settlement cycles. Calcium bentonite was left to settle in de-ionized water and, when complete settlement was reached, excess water was removed and the material was hydrated once again. This procedure was stopped when the electrical conductivity of the equilibrium solution was less than 700 μS/cm.

1.2.2 Index properties measurement: Swell Index and Atterberg Limits

Swell index tests can estimate the volume change of bentonite after hydration (Katsumi et al., 2008). These tests can be used to obtain a qualitative measurement of the swelling behaviour of bentonite subjected to several electrolyte

concentrations. High swell index, SI, means high swelling performance of bentonite in equilibrium with a specific electrolyte solution at a specific molarity.

Swell index tests (ASTM D5890) were performed on sodium and calcium bentonite regarding the equilibrium conditions with sodium chloride (2 mM, 5 mM, 10 mM, 20 mM, 50 mM, 100 mM, 500 mM and 1 M solutions) and calcium chloride (2 mM, 5 mM, 10 mM and 50 mM solutions), respectively. Moreover, swell index was measured with de-ionized water, DW, for both sample.

More information on the testing solutions is reported in the paragraph 2.4.2.

The swell index trend obtained for sodium and calcium bentonite is reported in Figure 1.4 as a function of the NaCl and $CaCl_2$ concentration, respectively.

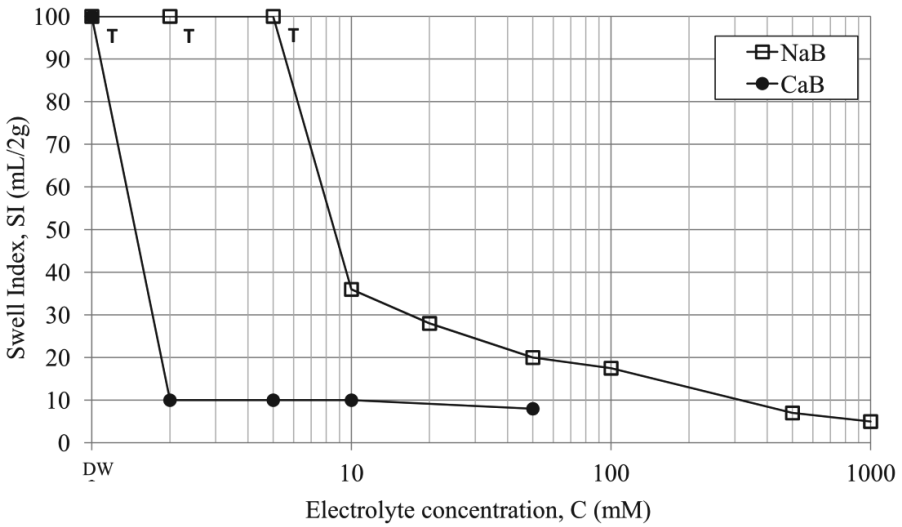

Figure 1.4 - Swell index as a function of the NaCl and $CaCl_2$ concentration, for sodium (NaB) and calcium (CaB) bentonite, respectively (ASTM D5890).

The swelling behaviour of the sodium bentonite (NaB) and calcium bentonite (CaB) shows turbid samples ('T' in the graph), which do not present a precise interface between the settled bentonite and the upper clear solution. In these cases, bentonite forms a stable suspension and it is not possible to evaluate a value of SI. As a consequence, a conventional value of SI of 100 mL/2g has been assigned to the turbid solutions (actually, without recognising how much the suspension is turbid).

Regarding sodium bentonite, the results presented in Fig. 1.4 highlight that the stability of bentonite suspensions decreases when the electrolyte concentration increases: the material behaves as a stable suspension for very low molarity values and for deionised water, while swelling behaviour is inhibited for a higher NaCl concentration than 0.5 M. Whereas if calcium bentonite is concerned, the swelling is substantially inhibited for every calcium chloride molarities, while the test performed with DW presents significant swelling behaviour.

Atterberg Limits are water contents of soil that represent qualitatively the passage between two different states of aggregation. The liquid limit (LL), in particular, is the water content, in percent, of a soil at the boundary between the semi-liquid and plastic state. LL represents how much moisture a soil material can hold until reaching a liquid state.

Under a qualitative point of view, LL value can be related to the external specific surface of montmorillonite particles, S′, as described by Farrar and Coleman (1967).

The term S′ represents the surface of the clay soil external to the tactoid, referred to the volume of the solid particles. The external surface is able to absorb a significant amount of water, and, as a consequence, is responsible for the extent of the swelling behaviour during imbibition. Moreover, as reported in Equation 1.2(a), S′, is a function of the microscopic structure of the montmorillonite particles, and, in particular, of the number of platelets per tactoid (N_l). When bentonite structure is dispersed (low N_l), as for sodium bentonite, the external specific surface will be high, while, when the bentonite lamellae are aggregated in large tactoids, as for calcium bentonite, S′ will assume a low value.

LL determination was performed by means of Casagrande's device accordingly to ASTM 4318 (multipoint liquid limit method) on sodium and calcium bentonite hydrated with sodium chloride (10 mM and 500 mM solutions) and calcium chloride (50 mM solution), respectively. Moreover, the test was performed on both bentonites hydrated with DW.

Table 1.1 shows the LL of sodium (NaB) and calcium (CaB) bentonite hydrated with the above electrolyte concentrations.

Table 1.1 – Liquid limit of powdered sodium and calcium bentonite with sodium and calcium chloride solution respectively (ASTM 4318).

	Liquid limit, LL [%]			
	DW	10 mM	50 mM	500 mM
sodium bentonite + NaCl solutions	525	524	-	111
calcium bentonite + $CaCl_2$ solutions	152	-	144	-

The results show that LL decreases when bentonite is exposed to high molarities electrolyte solutions as a consequence of S′ reduction, induced by the tactoid formation, which decreases the water adsorption capacity of montmorillonite at the microscopic scale. Moreover, the LL value of sodium bentonite with respect to the 500 mM NaCl solution (LL = 111%) is considerably lower than the value measured for calcium bentonite with DW (LL = 152%). This result proves the higher value of swell index obtained for CaB with DW and low molarity $CaCl_2$ solutions than that obtained for NaB with high molarity NaCl solution.

In any case, LL values obtained for sodium bentonite are notably higher than those obtained for calcium bentonite at similar molarity values.

Farrar and Coleman (1967) gave the following regression equation (with the 95% confidence limit in the brackets) between the surface area, S, and the liquid limit, LL, of several British clay soils:

$$S = -14 + 1.48 \cdot LL \quad (\pm 33), \quad \text{where } [S] = m^2/g \text{ ; } [LL] = \% \qquad [1.5]$$

The values of specific surface, S, found for calcium and sodium bentonite on the basis of the results of LL test using equation 1.5 are reported in Table 1.2.

Table 1.2 – Specific surface values, S, obtained on the basis of the results of LL test (see table 1.1) using the equation 1.5 (after Farrar and Coleman, 1967).

	Specific surface, S (± 33) [m^2/g]			
	DW	10 mM	50 mM	500 mM
sodium bentonite + NaCl solutions	763	762	-	150
calcium bentonite + $CaCl_2$ solutions	210	-	199	-

The specific surface values obtained for sodium bentonite in Table 1.2 are within the typical value range 700-840 m^2/g (Mitchell and Soga, 2005).

1.2.3 Swelling tests and loading/unloading/reloading tests under isotropic conditions.

Swelling and loading/unloading/reloading tests under isotropic conditions were performed on powdered sodium and calcium bentonite using a flexible wall permeameter. Testing procedure, specimen preparation and test results are reported in this paragraph.

The powdered bentonites were deposited loosely in a dry state in a steel mold inside the permeameter. The bulk dry density was approximately equal to the gravimetric density (1 g/cm^3, typical of the dry bentonite contained in a geosynthetic clay liner). The flexible membrane inside the mold adhered to the specimen, so that, after removing the mold, the flexible wall permeameter was assembled completely without disturb the specimen, as reported in Fig. 1.5.

1.2.3.1 Swelling tests under isotropic conditions.

During swelling tests, the specimens were saturated with DW from both side (from top and bottom porous stone) with a constant effective confining stress, σ', of 10 kPa, under a constant back pressure, u_{BP}, of 515 kPa. During the test, the bulk volume of the specimen was monitored every half hour during the day, while, during the night, the specimen was left to swell for approximately 12 hours.

(a) **(b)**

Figure 1.5 – During specimen preparation the flexible membrane inside the mold adhered to the specimen (a) so that the flexible wall permeameter was assembled without disturbing the specimen (b). The specimen is light brown, the porous stones are dark brown.

The tests were stopped when the specimen volume ceased to increase.

The results of the swelling tests under isotropic conditions performed on sodium and calcium bentonite are reported in Fig. 1.6 in term of volume strain, ε_v, as a function of the time, t, and in Fig. 1.7 in term of void ratio, e, as a function of the time, t.

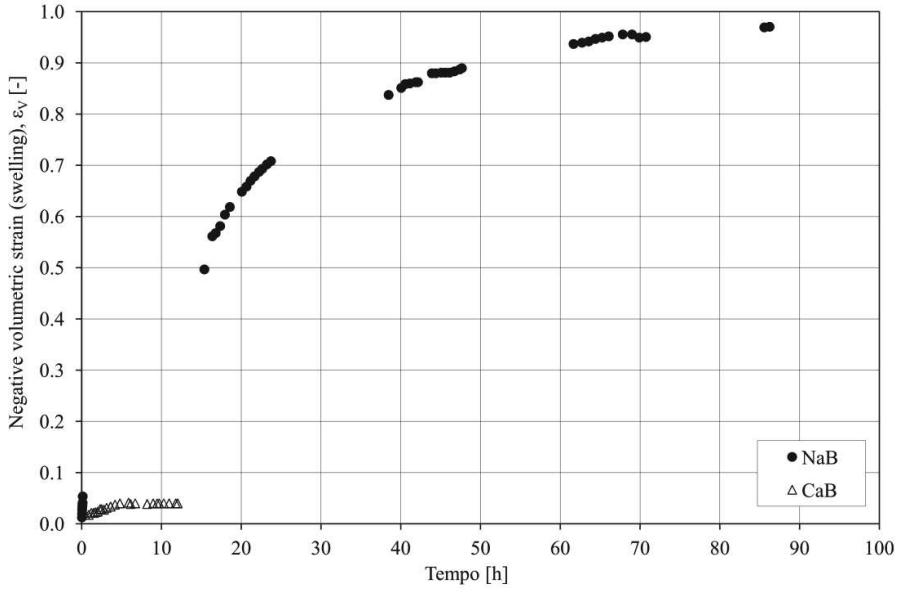

Figure 1.6 – Negative volumetric strain of sodium (NaB) and calcium (CaB) bentonite as a function of time during imbibitions with de-ionized water, DW.

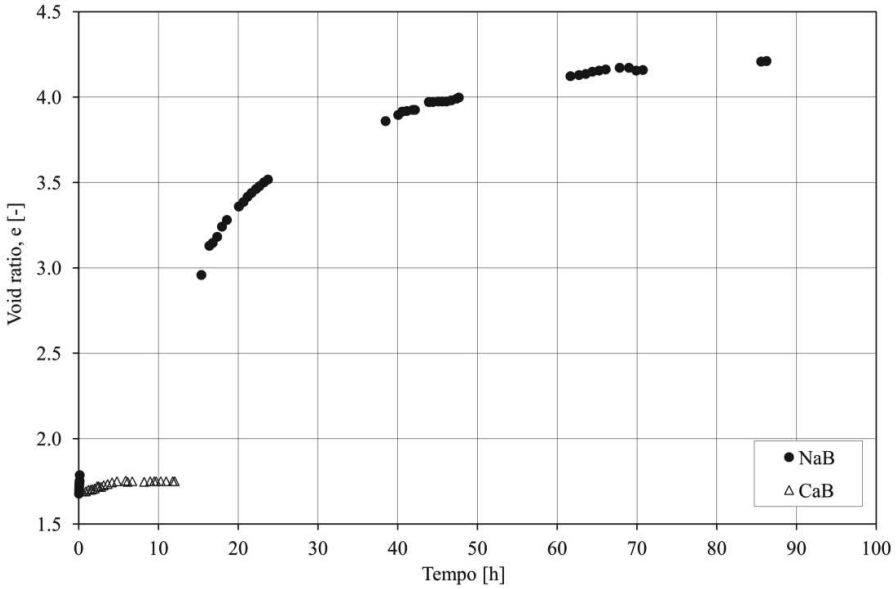

Figure 1.7 – Void ratio of sodium (NaB) and calcium (CaB) bentonite as a function of time during imbibitions with de-ionized water, DW.

The sodium bentonite specimen (NaB) doubled its volume during the hydration phase with DW. The final volumetric strain of NaB, measured in correspondence to the asymptote, was equal to approximately 100%, while the void ratio increased from the initial value of 1.68 to the final value of 4.20, corresponding to the asymptote. The calcium bentonite specimen (CaB) substantially did not swell during imbibitions. The final volumetric strain of CaB was equal to 4% and the void ratio increased from 1.68 to 1.75 during hydration.

1.2.3.2 Loading/unloading/reloading tests under isotropic conditions.

The specimen of sodium (NaB) and calcium (CaB) bentonite beforehand hydrated with de-ionized water, DW, for the swelling test (see paragraph 1.2.3.1) have been subjected to a loading/unloading test, without disassemble the flexible-wall permeater, with the aim to measure the average modulus of deformation under isotropic conditions during the loading phase and, after unloading, during the

reloading phase.During the test, the load was assigned to the specimen following the steps reported in Table 1.3 in terms of effective isotropic confining stress. The back pressure of the pore solution, consisting of DW, was maintained constant and equal to 515 kPa.

Table 1.3 – Steps for loading/unloading/reloading test.

	Effective isotropic confining stress, σ' [kPa]
Loading phase:	10
	27.5
	70
Unloading phase:	70
	27.5
	10
Reloading phase:	10
	27.5
	70

The results of the test performed on sodium and calcium bentonite are reported in Fig. 1.8 and in Fig. 1.9, respectively.Fig. 1.8 and Fig. 1.9 show the positive volumetric strain, during the loading and reloading phases, corresponded to bentonite consolidation, whereas the negative volumetric strain, during the unloading phase, corresponded to material swelling. The specimen deformation trend show an elasto-plastic behaviour, where the elastic deformation was regained during the unloading phase while the plastic deformation resulted unrecoverable.
The deformation modulus, K, under isotropic conditions has been defined as:

$$K = \frac{\Delta p'}{\Delta \varepsilon_v} = \frac{\Delta \sigma'}{\Delta \varepsilon_v} \qquad [1.6]$$

where ε_v is the volumetric strain and p' is the isotropic tensor, which, under isotropic conditions as in the studied test, results equal to the confining stress, σ'.

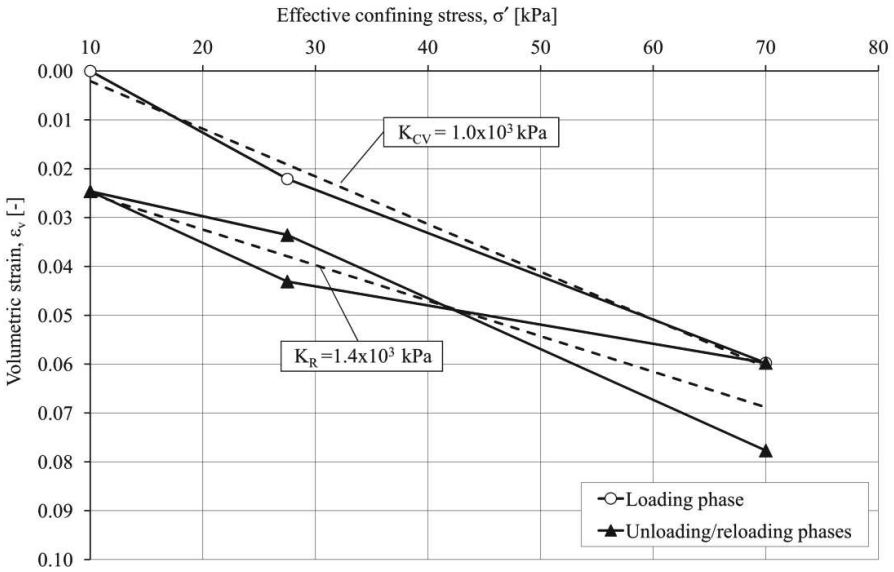

Figure 1.8 – Volumetric strain as a function of the effective confining stress during the loading, unloading and reloading phase of the test on sodium bentonite and evaluation of the deformation modulus.

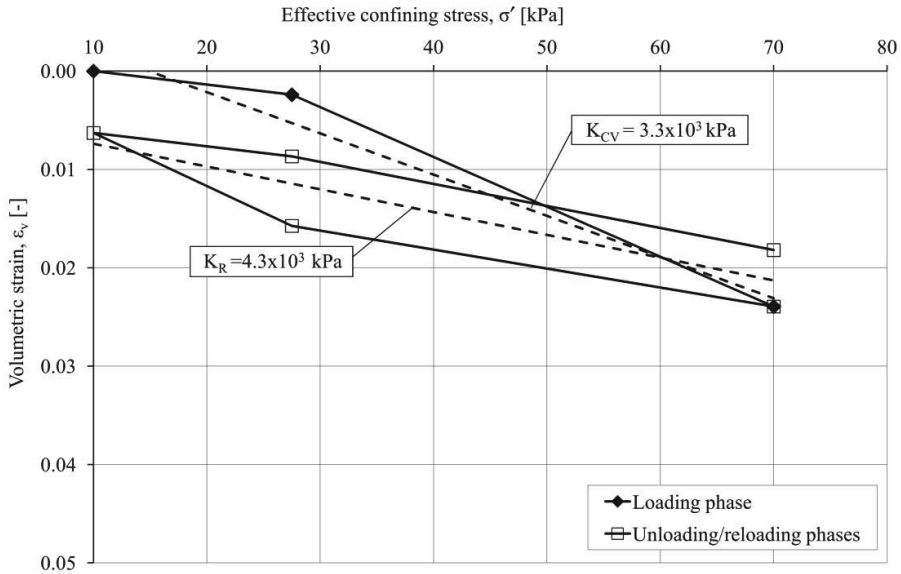

Figure 1.9 – Volumetric strain as a function of the effective confining stress during the loading, unloading and reloading phase of the test on calcium bentonite and evaluation of the deformation modulus.

The deformation modulus of sodium and calcium bentonite were calculated using Eq. 1.6 and resulted, for sodium bentonite, equal to $K_{CV} = 1.0 \cdot 10^3$ kPa (corresponding to the virgin compression curve) and $K_{CV} = 1.4 \cdot 10^3$ kPa (corresponding to the reloading curve) and, for calcium bentonite, equal to $K_{CV} = 3.3 \cdot 10^3$ kPa (corresponding to the virgin compression curve) and $K_{CV} = 4.3 \cdot 10^3$ kPa (corresponding to the reloading curve).

The test highlights that the bentonite degradation induced by cation exchange phenomenon, although worsens the swelling performance of sodium bentonite, produces an increase in mechanical properties of the material. The aggregated structure, which characterized calcium bentonite at microscopic scale, determines the higher stiffness of the material and the lower compressibility.

1.3 GEOSYNTHETIC CLAY LINERS (GCLs)

Geosynthetic clay liners, or GCLs, consist of a thin layer of dry sodium (or calcium) bentonite added to a layer or layers of geosynthetic. The geosynthetics are either geotextiles or a geomembrane (Bouazza, 2002). Bentonite is bounded with adhesive, needle-punching or stitch-bonding to the geotextiles on both sides, as reported in Figure 1.10.

Although stitch-bonding and needle-punching create small holes in the GCL, these holes are sealed when bentonite hydrates and swells.

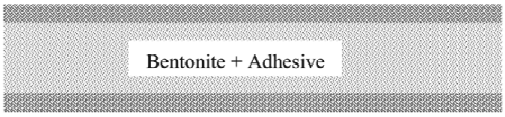

(a) Adhesive bound bentonite to upper and lower geotextiles

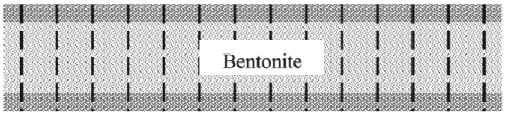

(b) Stitch bonded bentonite between upper and lower geotextiles

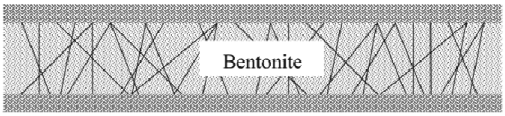

(c) Needle punched bentonite through upper and lower geotextiles

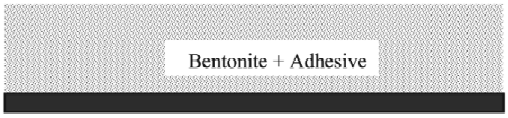

(d) Adhesive bound bentonite to a geomembrane

Figure 1.10 – Cross section of main quality of geosynthetic clay liners (after Daniel and Koerner, 1995).

The more up-to-date production of GCLs generally uses the needle-punching technology. This process causes some fibres form the top of geotextiles to extend through the bentonite and bottom geotextile, bonding the entire structure together (Von Maubeuge and Heerteen, 1994). The fibers that are punched through the bottom geotextile rely on natural entanglement and friction to keep the GCL together.

If GCL is considered as a replacement of the most common compacted clay liner (CCL), the main advantage of GCL-made sealing liner are the limited thickness, the good compliance with differential settlements of underlying soil waste, easy installation and low cost (Manassero et al. 2000). A qualitative comparison of GCLs and CCLs, provided by different authors referring to different criteria had been proposed by Manassero et al. (2000) and here reported in Figure 1.11.

The type of bentonite used in the GCL effects the permeability. Sodium bentonite (i.e. a soil composed by montmorillonite which presents mainly Sodium as exchangeable cation) is the predominant clay mineral component of the bentonite normally used and is a product of the weathering of volcanic ash deposited in a marine environment. Calcium montmorillonite (i.e. a montmorillonite which presents mainly Calcium as exchangeable cation) is the product of volcanic ash being deposited in a fresh water environment.

Hydrated sodium bentonite has a dispersed structure, a very high swelling potential and a very low permeability characteristic. However, a disadvantage of sodium bentonite is the potential for cation exchange of Sodium with Calcium (dominant in the pore water of many soils), which tends to neutralize the charges within the tactoids and, consequently, to increase tactoid dimension, with the associate reduction in swelling and increase in permeability.

The cation exchange produces a transformation of sodium bentonite into calcium bentonite and, consequently, a reduction in the repulsion forces between the lamellae and the formation of tactoids. The main effects of this phenomenon are a reduction in the swelling performances (see paragraph 1.2), which leads to the consolidation of the material and the expulsion of water, and an increase in hydraulic conductivity.

A landfill bottom barrier is required to ensure hydraulic and pollutant containment during the entire active life of a landfill (i.e. during the waste storage phase) and

over decades in the post-closure period. During this period, the barrier must guarantee performances according to the regulations in force and the cation exchange phenomenon can mean that this requirement is not guaranteed in long term conditions.

	Criterion	Equivalency of GCL to CCL			
Category	for Evaluation	GCL Probably Superior	GCL Probably Equivalent	GCL Probably Inferior	Site or Product Dependent
Construction Issues	Ease of Placement	X			
	Material Availability	X			
	Puncture Resistance			X	
	Quality Assurance	X			
	Speed of Construction	X			X
	Subgrade Condition	X			
	Water Requirements				X
	Weather Constraints				
Contaminant Transport Issues	*Attenuation Capacity*			X(1)	X
	Gas Permeability				X
	Solute Flux and Breakthrough Time	X(2)		X	
Hydraulic Issues	*Compatibility*	X(2)		X	
	Consolidation Water	X			
	Steady Flux of Water		X		
	Water Breakthrough Time				X
Physical/ Mechanical Issues	Bearing Capacity				X
	Erosion				X
	Freeze-Thaw	X			
	Settlement-Total		X		
	Settlement-Differential	X			
	Slope Stability				X
	Wet-Dry	X			

(1) Based only on total exchange capacity, TEC
(2) Only for GCLs with a geomembrane

Figure 1.11 – Equivalency between geosynthetic clay liners and compacted clay liners (after Daniel , 1995; Shackelford and Nelson, 1996).

Several authors (Jo et al. 2001; Petrov et al. 1997; Shackelford et al. 2000) have studied the behaviour of untreated sodium bentonite and GCLs in long term landfill

conditions and reported hydraulic performance and swelling ability degradation induced by the permeation of electrolyte solutions containing divalent cations.
The evidence of the strong degradation induced in the hydraulic performances of sodium bentonite by the cation exchange phenomenon highlights on one hand the need to study the temporal development of this phenomenon with the aim to compare that to the period in which landfill barrier performances have to be guaranteed, on the other hand the need to develop innovative materials aimed at improving GCL resistance to the degradation induced by the cation exchange phenomenon. Both objectives have been developed in the PhD research project:
(1) in chapter 6 a finite difference model is developed to study the diffusive flux of Calcium through a bentonite barrier, since the diffusive component of flux seems to give the higher contribution to cation exchange in bentonite layers subjected to a hydraulic gradient, i, typical of in situ conditions (i.e. $i < 30$);
(2) regarding the second point, both the influence of chemico-physical pre-treatments (i.e. pre-hydration, pre-consolidation and salt removal) and the influence of polymer addiction to the hydraulic performance of sodium bentonite, subjected to a Calcium advective flux, have been studied and reported in chapter 2.

In the last decade, new GCL applications, requiring their use for hydrocarbon containment, have found growing interest. In this particular area, the main GCL application is the secondary containment aimed at preventing subsoil dispersion of accidental oil spills through primary lining system (HDPE) from hydrocarbon storage tanks (underground or on surface).
As hydrocarbon containment is concerned, a reduction of the barrier efficiency (with respect to the hydraulic conductivity values commonly measured with water) can be expected due to the reactive nature of sodium bentonite. In fact petroleum products, that are characterized by dielectric constant values significantly lower than that of water, produces the formation of tactoids and consequently a decrease of the hydraulic containment performances of the barrier.
Both physical pre-treatments (i.e. pre-hydration) and polymer addiction have been developed during the PhD to limit the reduction of sodium bentonite efficiency when subjected to hydrocarbons. These contents are reported in chapter 4.

1.4 CLAY MEMBRANE BARRIERS

In the last decades, several research has focused on the potential benefits arising from the existence of semi-permeable membrane behaviour in bentonite and bentonite-based barrier materials (Malusis, 2001; Malusis and Shackelford, 2002a,b; Van Impe, 2002, Malusis et al. 2003; Manassero and Dominijanni, 2003; Shackelford at al., 2003; Henning, 2004; Lu et al., 2004; Dominijanni and Mannassero, 2005; Yeo et al., 2005; Kang and Shackelford, 2009; Kang and Shackelford, 2010; Dominijanni and Manassero, 2012a,b).

The electric interaction between the montmorillonite lamellae and the ions contained in the pore solution generates macroscopic phenomena that cannot be modelled with the classical constitutive equations of soil mechanics (Mitchell, 1993). For instance, when a bentonite layer is put in equilibrium with an electrolyte solution, swelling or shrinkage is observed depending on the salt concentration, without any apparent modification of the effective stresses. Moreover, if a bentonite layer is interposed between two electrolyte solutions with different salt concentrations, a volumetric flux of water can be observed, even in the absence of a hydraulic gradient.

The mechanical and transport behaviour of bentonites has more affinity with that of biological tissues, reverse-osmosis membranes, or polyelectrolyte gels than with that of sands or gravels, since clays are characterized by membrane behaviour.

Clay soils in general are semipermeable or permiselective porous media. The term "semipermeable" describes the ability of some materials to be permeable to only some components of a solution. Referring to a permeating solution constituted by a solvent and a single solute, a semipermeable membrane is "ideal" or "perfect" if is able to prevent completely the passage of the solute. However the ability to restrict the movement of solutes is only one of the so-called "osmotic properties" of clay soils. The movement of the permeating solution through a semipermeable membrane, for example, may be driven by a solute concentration gradient (chemico-osmosis) or by an electric potential gradient (electro-osmosis).

Nowadays, we know that all osmotic properties of semipermeable membranes are due to the ability of the solid skeleton to "interact" differently with the components

of the fluid phase. The simplest "interaction" is that to hinder the passage of molecules having size greater than the pore size (steric hindrance). For clays the main source of osmotic phenomena is recognized to be the electrostatic interaction between the ions in the pore solution and the solid skeleton, having generally a negative electric charge.

The materials characterized by similar properties are very common. The semipermeable membranes may be classified in three categories: (1) mineral membranes; (2) biological membranes; (3) synthetic membranes. Clay soils are an example of mineral semipermable membranes or, preferentially, semipermeable porous media, considering that: (i) they are characterized by a system of interconnected pores; (ii) they may have an appreciable thickness (Dominijanni, 2005). A lot of biological tissues, as well as cell membranes, articular cartilages or bones behave as semipermeable membranes. Polyelectrolyte gels and concrete are examples of synthetic semipermeable materials.

Clay membrane behaviour is quantified in terms of reflection coefficient, σ. The value of σ for a clay soil exhibiting no solute restriction is zero ($\sigma = 0$), corresponding to zero membrane efficiency, whereas the value of σ for clay soil exhibiting complete solute restriction is unity ($\sigma = 1$), corresponding to 100% membrane efficiency. In general, the value of σ for naturally occurring clay soils that exhibit membrane behaviour range from greater than zero to less than unity because of the variation in the pore sizes that exist in such soils (Shackelford, 2005).

Clay membrane behaviour is a function of several mechanical, physical and chemical factors, such as stress-strain properties of clay, boundary and initial salt concentrations, type of solute species (ions) and mineralogy of the soil (Shackelford et al., 2003). In general, the potential for the existence of membrane behaviour increases with (a) an increase in stress (decrease in porosity), (b) an increase in content of high activity clay minerals, particularly sodium montmorillonite, and (c) a decrease in the salt concentration in the pore water (Shackelford et al., 2003).

Both osmotic and swelling properties have been studied for the bentonite used in the laboratory activity of the PhD research programme. The results of these analyses are reported in chapter 3.

1.5 BENTONITE BASED BARRIERS

Compacted bentonite based barriers (i.e. sand or sand-like material + bentonite) have been used for hydraulic containment applications in cases where suitable natural clayey soils are not readily or economically available (e.g. Garlanger et al., 1987; Chapuis et al., 1992; O'Sadnick et al., 1995; Stern and Shackelford, 1998; Kaoser et al., 2006; Castelbaum and Shackelford, 2009). In most cases the use of sodium bentonite is chosen on the basis of the ability to achieve a relatively low hydraulic conductivity (i.e. $K \approx 10^{-9}$ m/s) upon permeation with DW using only a relatively small quantity of bentonite, generally < 20% by weight. The use of small quantities of bentonite decreases the cost of the raw material supply.

The low hydraulic conductivity values for compacted bentonite based barriers can be attributed primarily to the high swelling potential of sodium bentonites in the presence of water resulting in the formation of a relatively tight soil matrix (Howell and Shackelford, 1997).

During the development of the PhD, the reuse of incinerator slag, instead of the soil commonly used in soil-bentonite mixtures (i.e. sand), was evaluated for landfill capping purposes.

Nowadays, large quantities of bottom ashes from municipal solid waste incineration (MSWI BA), with mechanical properties that are appropriate for the construction of landfill covers, are increasingly becoming available, due to the spread of incineration plants.

Since MSWI BA generally has a similar particle size distribution to that of a sand, or at least to that of a sand-fine gravel mixture (Monteiro et al. 2008; Dominijanni et al., 2009; Xue et al. 2009), the possibility of mixing BA with sodium bentonite was considered aimed at decreasing the hydraulic conductivity of BAs. The aim of the research was to verify whether the high swelling potential of sodium bentonite, in the presence of water, can produce a low hydraulic conductivity soil matrix for compacted BA-bentonite mixtures, as typically is the case of compacted sand-bentonite layers. The results of this research are summarized in chapter 5.

REFERENCES

Bouazza, A. (2002). Geosynthetic clay liners. Review article. Geotextiles and Geomembranes, **20**, 3-17.

Castelbaum, D. and Shackelford, C.D. (2009). Hydraulic conductivity of bentonite slurry mixed sands. Journal of Geotechnical and Geoenvironmental Engineering, ASCE, **135**(12),1941-1956.

Chapuis, R.P., Lavoie, J., and Girard, D. (1992). Design, construction, performance, and repair of the soil-bentonite liners of two lagoons. Canadian Geotechnical Journal, **29** (4), 638-649.

Daniel, D.E., Koerner, R.M. (1995). Waste Containment Facilities: Guidance for Construction, Quality Assurance and Quality Control of Liner and Cover Systems. ASCE, New York.

Dominijanni, A. (2005). Osmotic properties of clay soils. PhD Dissertation. Politecnico di Torino, Torino, Italy.

Dominijanni, A., Manassero, M. (2005). Modeling osmosis and solute transport through clay membrane barriers. Waste containment and remediation (ASCE Geotechnical Special Publication No. 47), Alshawabkeh, A., Benson, C. H., Culligan, P. J., Evans, J. C., Gross, B. A., Narejo, D., Reddy, K. R., Shackelford, C. D., Zornberg, J. G. (Eds), ASCE, Reston, VA (CD version only).

Dominijanni, A., Genon, G., Luciani, P., Maggiorotto, M., Manassero, M, Marchese, F., Puma, S., Soldi, G.L., Zanetti, M.C. (2009). Landfilling and reuse of bottom ashes from refuse derived fuel and municipal solid waste incineration. Proceedings Sardinia 2009, Twelfth International Waste Management and Landfill Symposium, Cagliari, Italy; 5 - 9 October 2009.

Dominijanni, A., Manassero, M. (2012,a). Modelling the swelling and osmotic properties of clay soils. Part I: The phenomenological approach. International Journal of Engineering Science, **51**, 32-50.

Dominijanni, A., Manassero, M. (2012,b). Modelling the swelling and osmotic properties of clay soils. Part I: The physical approach. International Journal of Engineering Science, **51**, 51-73.

Farrar, D., M., Coleman, J., D., (1967). The correlation of surface area with other properties of nineteen British clay soils. Journal or Soil Science. **18**(1), 118-124.

Garlanger, J.E., Cheung, F.K., Bishar, S.T. (1987). Quality control testing for a sand-bentonite liner. Geotechnical Practice for Waste Disposal '87. R.D. Woods, ed. ASCE, Reston, Va. 488-499.

Guyonnet, D., Gaucher, E., Gaboriau, H., Pons, C.H., Clinard, C., Norotte, V., and Didier, G. (2005). Geosynthetic clay liner interaction with leachate: correlation between permeability, microstructure and surface chemistry. Journal of Geotechnical and Geoenvironmental Engineering, **131** (6), 740-749.

Henning, J. T. (2004). Chemico-osmotic efficiency of two real word slurry trench cutoff wall backfills. MS Thesis, Bucknell University, Lewisburg, Pennsylvania, USA.

Howell, J.L. and Shackelford, C.D. (1997). Hydraulic conductivity of sand admixed with processed clay mixtures. Proceedings, 14th International Conference on Soil Mechanics and Foundation Engineering, Hamburg, Germany, Sept. 6-12, 1997, A. A. Balkema, Rotterdam, The Netherlands, **1**, 307-310.

Jo H., Katsumi T., Benson C.H., Edil T.B. 2001. Hydraulic conductivity and swelling of non-prehydrated GCLs permeated with single species salt solutions. Journal of Geotechnical and Geoenvironmental Engineering, ASCE. **127**(7), 557–567.

Kang, J. B., Shackelford, C. D. (2009). Clay membrane testing using a flexible-wall cell under closed-system boundary conditions. Applied clay science, **44**, 43-58.

Kang, J. B., Shackelford, C. D. (2010). Membrane behaviour of compacted clay liners. Journal of geotechnical and geoenvironmental engineering, **136**(10), 1368-1382.

Kaoser, S., Barrington, S., Elektorowicz, M., and Ayadat, T. (2006). The influence of hydraulic gradient and rate of erosion on hydraulic conductivity of sand-bentonite mixtures. Soil and Sediment Contamination, **15**(5), 481-496.

Katsumi, T., Ishimori, H., Onikata, M., Fukagawa, R. (2008). Long-term barrier performance of modified bentonite materials against sodium and calcium permeant solutions. Geotextiles and Geomembranes, **26**, 14-30.

Lu, N., Olsen, H. W., Likos, W. (2004). Appropriate material properties for advective-diffusive solute flux in membran soil. Journal of geotechnical and geoenvironmental engineering, **130**(12), 1341-1346.

Luckham, P. F., Rossi, S. (1999). The colloidal and rheological properties of bentonite suspentions. Advances in colloid and interface science, **82**, 43-93.

Malusis, M.A. (2001). Membrane behaviour and coupled solute transport through a Geosynthetic Clay Liner. PhD Dissertation, Colorado State University, Fort Collins, Colorado, USA.

Malusis, M. A., Shackelford, C. D. (2002,a) Chemico-osmotic efficiency of a geosynthetic clay liner. Journal of geotechnical and geoenvironmental engineering, **128**(2), 97-106.

Malusis, M. A., Shackelford, C. D. (2002,b). Coupling effects during steady-state solute diffusion through a semipermeable clay membrane. Environmental science and technology, **36**(6), 1312-1319.

Malusis, M. A., Shackelford, C. D., Olsen, H. W. (2003). Flow and transport through clay membrane barriers. Engineering geology, **70**, 235-248.

Manassero, M., Benson, C., Bouazza, A. (2000). Solid waste containment systems. *In* Proceedings Int. Conference On Geological & Geotechnical Engeneering, Geoeng.2000, Melbourne, **1**, 520-642.

Manassero, M., Dominijanni, A. (2003). Modelling the osmosis effect on solute migration through porous media. Geotechnique, **53**(5), 481-492.

Mitchell, J. K. (1993). Fundamentals of soil behavior (2nd ed.). New York: Wiley.

Mitchell, J. K., Soga, K. (2005). Fundamentals of soil behaviour (3rd ed.) New York: Wiley & Sons.

Monteiro, R.C.C., Figueiredo, C.F., Alendouro, M.S., Ferro, M.C., Davim, E.J.R., Fernandes, M.H.V. (2008). Characterization of MSWI bottom ashes towards utilization as glass raw material. Waste Management, **28**, 1119-1125.

O'Sadnick, D.L., Simpson, B.E., and Kasel, G.K. (1995). Evaluation and performance of a sand-bentonite liner. Geoenvironment 2000, Y.B. Acar, and D.E. Daniel, eds, ASCE, Reston, Va., 688-701.

Petrov, R.J., Rowe, R.K. 1997. Geosynthetic clay liner (GCL) – chemical compatibility by hydraulic conductivity testing and factors impacting its performance. Canadian Geotechnical Journal **34**, 863–885.

Shackelford, C.D., Nelson, J.D. (1996). Geoenvironmental design considerations for tailings dams. *In* Proceedings Seismic and environmental design of earth dams, concrete dams and tailings dams. Santiago, Chile.

Shackelford, C. D., Benson, C. H., Katsumi, T., Edil, T., Lin, L. (2000). Evaluating the hydraulic conductivity of GCLs permeated with nonstandard liquids. Geotextiles and Geomembranes, **18**(2-4) 133–162.

Shackelford, C. D., Malusis, M. A., Olsen, H. W. (2003). Clay membrane behaviour for geoenvironmental containment. Soil and rock America conference 2003 (*in* Proceedings of the joint 12th Panamerican Confernce on Soil Mechanics and Geotechnical Engineering and the 39th U.S. Rock Symposium), Culligan, P. J., Einstein, H. H., and Whittle, A. J. (Eds), Verlag Glückauf GMBH, Essen, Germany, **1**, 767-774.

Shackelford, C. D. (2005). Environmental issues in geotechnical engineering. 16th International conference on soil mechanics and geotechnical engineering, **1**, Osaka, Japan, September 12-16, Millpress, Rotterdam, Netherlands, 95-122.

Shainberg, I., Bresler, E., and Klausner, Y. (1971). Studies on Na/Ca montmorillonite systems. 1. The swelling pressure. Soil Science, **111** (4), 214-219.

Stern, R. T., Shackelford, C. D. (1998). Permeation of sand-processed clay mixtures with calcium chloride solutions. Journal of Geotechnical and Geo-environmental Engineering, **124** (3), 231-241.

Van Impe P. O. (2002). Consolidation, contaminant transport and chemico-osmotic effects in liner materials. PhD Dissertation, Ancona University, Ancona, Italy.

Von Maubeuge, K.P., Heerten, G. (1994). Needle punched geosynthetic clay liners. *In* Proceedings of the Eighth GRI Conference, Philadelphia, USA, 129–207.

Xue, Y., Hou, H., Zhu, S., Zha, J. (2009). Utilization of municipal solid waste incineration ash in stone mastic asphalt mixture: pavement performance and environmental impact. Construction and Building Materials **23**, 989-996.

Yeo, S. S., Shackelford, C. D., Evans, J. C. (2005). Membrane behaviour of model soil-bentonite backfills. Journal of geotechnical and geoenvironmental engineering, **131**(4).

Chapter 2

CONTAINMENT PERFORMANCE OF NATURAL AND POLYMER-MODIFIED BENTONITE BARRIERS SUBJECTED TO PHYSICAL PRE-TREATMENTS

This chapter reports the contents of a Paper:

Puma, S., Dominijanni, A., Manassero, M.

Titled: **The role of physical pretreatments on the hydraulic conductivity of natural and polymer modified sodium bentonites.**

(Submitted in November 2012 to the journal *Geotextiles and Geomembranes*).

In revision.

THE ROLE OF PHYSICAL PRETREATMENTS ON THE HYDRAULIC CONDUCTIVITY OF NATURAL AND POLYMER MODIFIED SODIUM BENTONITES.

by

Sara Puma*, Andrea Dominijanni** and Mario Manassero***

* *Corresponding Author*

Dipartimento di Ingegneria Strutturale, Edile e Geotecnica [Department of Structural, Geotechnical and Building Engineering], Politecnico di Torino, Corso Duca degli Abruzzi 24, 10129 Torino – ITALY; Ph: +39-331-2045926, Fax: +39-011-090-7699, e-mail: sara.puma@polito.it

** Dipartimento di Ingegneria Strutturale, Edile e Geotecnica [Department of Structural, Geotechnical and Building Engineering], Politecnico di Torino, Corso Duca degli Abruzzi 24, 10129 Torino – ITALY; e-mail: andrea.dominijanni@polito.it

*** Dipartimento di Ingegneria Strutturale, Edile e Geotecnica [Department of Structural, Geotechnical and Building Engineering], Politecnico di Torino, Corso Duca degli Abruzzi 24, 10129 Torino – ITALY; e-mail: mario.manassero@polito.it

2.1 ABSTRACT

The role of physical pretreatments, such as pre-hydration, pre-consolidation and salt removal, applied to sodium and polymer modified bentonites, has been analyzed in this paper. Moreover, the effect of the presence or absence of needling across the bentonite layer has been studied.

All these variables have been shown to influence the hydraulic performances of bentonite through hydraulic conductivity evaluation in both short and long term conditions. Physical pretreatments, in fact, influence the swelling behaviour of bentonite and its response to the cation exchange phenomenon.

The hydraulic conductivity tests, performed on specimens containing natural bentonite, have shown that the presence of needling deteriorates the hydraulic performances of a material to a great extent particularly in long term conditions, while the pre-consolidation process greatly improve the long term behaviour.

The specimen subjected to salt removal ($K = 0.8 \cdot 10^{-11}$ m/s) in short term conditions showed a better hydraulic performance than the other specimens, whose hydraulic conductivity value appeared almost equal to $1.5 - 2.0 \cdot 10^{-11}$ m/s.

The tests performed on polymer modified specimens showed conductivity values in short term conditions that were approximately one order of magnitude lower than those obtained on natural specimens. During the permeation with water and Calcium solution, the polymer was solubilised and removed from the specimen by the volumetric flux. Spectroscopy results also highlighted the absence of the polymer in the exhumed specimens and confirmed its complete solubilisation during the hydraulic conductivity test.

2.2 KEYWORDS

Bentonite,
Hydraulic conductivity,
Needling,
Physical pre-treatments,
Pre-consolidation,
Salt removal.

2.3 INTRODUCTION

Geosynthetic clay liners (GCLs) are the most common manufactured barriers used in landfill applications. GCLs generally contain a thin layer of sodium bentonite (dry thickness of between 5 and 10 mm), needled between two geotextiles or glued to a geomembrane, which ensures excellent containment performances, in the short term, regarding both volumetric flux and contaminant advective transport. The excellent performance of GCLs has to be attributed, in the absence of a glued geomembrane, to the sodium bentonite characteristics (Shackelford et al. 2000).

Bentonite is a clay soil that usually contains at least 70% of the three layered (2:1) clay mineral montmorillonite. Isomorphic substitution in montmorillonite usually results in the replacement of a portion of the trivalent aluminium (Al^{3+}) in the crystalline structure with a divalent metal, such as magnesium (Mg^{2+}), and this causes a permanent negative surface charge. This electric charge per unit solid volume can be expressed as $F \cdot \overline{c}_{sk,0}$, where F is Faraday's constant (96,485 $C \cdot mol^{-1}$) and $\overline{c}_{sk,0}$ is the molar concentration of the solid skeleton electric charge, which is assumed to have unitary valence (i.e. $z_{sk} = -1$).

Montmorillonite crystals consist of parallel-aligned elementary alumino-silicate lamellae, which are approximately 10 Å thick and 1000-2000 Å wide, and this crystalline structure determines a very high specific surface (≈ 760 $m^2 \cdot g^{-1}$). Dominijanni and Manassero (2012) have shown that $\overline{c}_{sk,0}$ is proportional to the effective specific surface of the solid particles and decreases when the montmorillonite lamellae aggregate to form tactoids.

Due to the permanent negative charge and the very high specific surface, a large quantity of water penetrates between the bentonite lamellae during imbibitions, determining a dispersed structure of individual platelets or small tactoids, which are characterized by considerable swelling behaviour. Moreover, the hydrated and swollen material shows very low hydraulic conductivity to permeation with water and diluted aqueous solutions.

Since the swelling ability of sodium bentonite is induced by the negative electric

charge of the platelets, it is influenced to a great extent by the electrical characteristics of the pore solution, such as the cation concentration and valence in the pore solution, and, as a consequence, by the chemical composition of the landfill leachate and of the water contained in the soil surrounding the barrier. The main problem concerning the use of sodium bentonite as a sealing material is in particular represented by the cation exchange of Sodium with Calcium, which is dominant in the pore water of many soils. The cation exchange produces a transformation of sodium bentonite into calcium bentonite and, consequently, a reduction in the repulsion forces between the lamellae, the formation of tactoids and a decrease in the molar concentration of the electric charge of the solid skeleton ($\overline{c}_{sk,0}$). The most obvious effects of this phenomenon are a reduction in the swelling pressure, which leads to the consolidation of the material and the expulsion of water, and an increase in hydraulic conductivity.

A landfill bottom barrier is required to ensure hydraulic and pollutant containment during the entire active life of a landfill (i.e. during the waste storage phase) and over decades in the post-closure period. During this period, the barrier must guarantee performances according to the regulations in force and the cation exchange phenomenon can mean that this requirement is not guaranteed in long term conditions.

Several authors (Jo et al. 2001; Petrov et al. 1997; Shackelford et al. 2000) have studied the behaviour of untreated sodium bentonite and GCLs in long term landfill conditions and reported good hydraulic performance and swelling ability degradation induced by the permeation of electrolyte solutions containing divalent cations.

Many recent studies have been aimed at improving the chemical resistance of sodium bentonite through the addition of large organic molecules, such as polymers, that join to the lamella surface and maintain a wide inter-particle distance, even in the presence of strong electrolyte and divalent pore solutions (Schroeder 2001; Kolstad et al. 2004, Katsumi et at. 2008; Di Emidio 2010; Scalia et al. 2011).

In this work, physical pretreatments, such as pre-hydration, pre-consolidation and salt removal, have been applied to sodium and polymer modified bentonite

specimens. Moreover, the effects of the presence or absence of needling across the specimen have been studied. All these variables can influence the swelling behaviour of bentonite and its response to the cation exchange phenomenon. Hydraulic conductivity tests have been performed to assess how these factors may affect the hydraulic performance of the specimens in both short and long term landfill conditions.

2.4 MATERIAL AND SPECIMEN PREPARATION

Natural, pre-treated and polymer modified bentonite materials have been used in this study. The natural specimens were: a commercial geosynthetic clay liner, *GCL*, and a sodium bentonite specimen, *NaB*, made up of the powdered material (the same contained in the GCL), prepared in a dry state, without needling or geotextiles. The laboratory pre-treated specimens were: a natural bentonite specimen subjected to a pre-hydration and a pre-consolidation process, *C-NaB*, and a bentonite specimen, deprived of soluble salts and then subjected to pre-hydration and pre-consolidation, *SQ-C-NaB*. The laboratory polymer modified specimens were: a polymer modified bentonite specimen, *NS-NaB*, made up of powdered modified material, prepared in a dry state, without needling or geotextiles, and a polymer modified bentonite specimen subjected to a pre-hydration and pre-consolidation process, *NS-C-NaB*.
The main features of the tested materials, the pre-treatments and the polymer modification procedures are described in this paragraph. The main characteristics of the specimens are reported in Table 2.1.

Table 2.1. Main characteristics of the tested specimens.

Specimen ID	Needling	Loose preparation	Pre-hydration + pre-consolidation	Salt removal	Polymer modification
GCL	√	√			
NaB		√			
C-NaB			√		
SQ-C-NaB			√	√	
NS-NaB		√			√
NS-C-NaB			√		√

2.4.1 Materials

The GCL used in this study is reinforced (needle-punched) and contains powdered sodium bentonite, encapsulated between a non-woven polypropylene geotextile and a woven polypropylene geotextile. The GCL is characterized by a thickness of 6 mm and an average bentonite mass per unit area of 5000 g/m^2 (12% average water content).

The powdered bentonite, tested in loose and consolidated specimens, is the same that was used for the production of the previously mentioned GCL. The bentonite is characterized by a cation exchange capacity (CEC, measured using the methylene blue adsorption method) of 105 meq/100g.

The mineralogical composition, evaluated through the x-ray diffraction analysis reported in Figure 2.1, shows a bentonite that is primarily composed of smectite (> 98%) with traces of calcite, quartz, mica and gypsum.

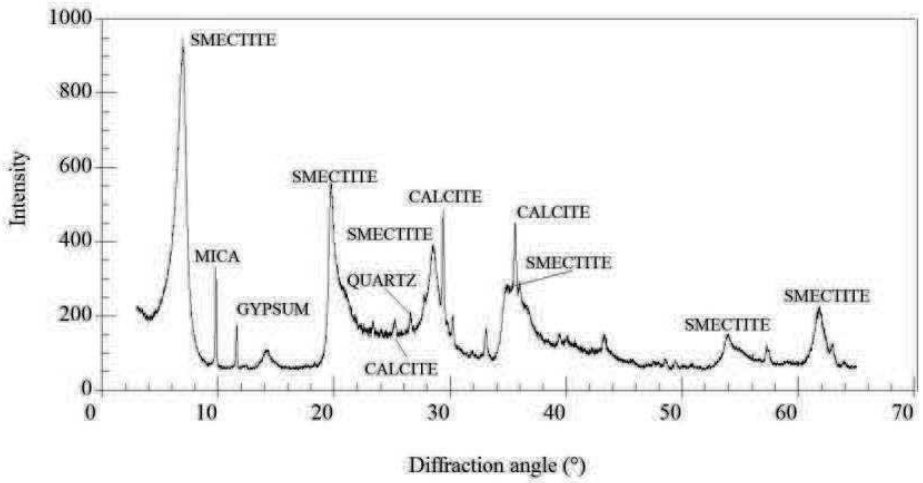

Figure 2.1 - Mineralogical composition of the natural bentonite.

The bentonite is characterized by a liquid limit (LL) of 525% with deionised water and 113% with a 0.5 M NaCl solution.

The swelling behaviour of the natural bentonite (NaB) is reported in Figure 2.3, in terms of swell index as a function of the NaCl concentration. Turbid samples ('T' in the graph) do not present a precise interface between the settled bentonite and the

upper clear solution. In these cases, bentonite forms a stable suspension and it is not possible to evaluate a value of SI. As a consequence, a conventional value of SI of 100 mL/2g has been assigned to the turbid solutions. The results highlight that the stability of bentonite suspensions decreases when the electrolyte concentration increases: the material behaves as a stable suspension for very low molarity values and for deionised water, while swelling behaviour is inhibited for a higher NaCl concentration than 0.5 M.

2.4.2 Permeant liquids

Calcium and Sodium solutions were prepared with dehydrated calcium chloride and sodium chloride (ACS reagent, purity ≥ 99%) and de-ionized water (DW). The calcium solution had the purpose of simulating in situ sodium bentonite degradation due to cation exchange phenomenon. A 250 mM $CaCl_2$ solution was assumed for this application in order to induce the degradation process in an acceptable time. The DW (pH = 6.95; EC at 20 °C = 0.6 mS/m) consisted of tap water processed through a series of activated carbon filters, a reverse osmosis process and, finally, a UV lamp (Elix Water Purification system).

2.4.3 Soluble salt removal

One of the specimens tested in this study (the 'squeezed and compacted specimen', or SQ-C-NaB), was obtained by submitting natural sodium bentonite to a process that had the aim of removing the soluble salts, mainly sodium, which are naturally present inside the material, due to its marine origin. The treatment prevents soluble salts from interfering with the swelling ability of sodium bentonite.

Several authors (Malusis et al. 2001; Malusis and Shackelford 2002a, 2002b; Shackelford and Lee 2003; Yeo et al. 2005; Kang and Shackelford 2009; Di Emidio 2010) have used the *'flushing'* method to remove soluble salts. This method consists of an initial permeation phase, performed before measuring the actual hydraulic conductivity, which requires a long period (i.e. from months to a year), because of the low bentonite hydraulic conductivity.

In this study, the *'squeezing'* method has been used with the aim of reducing the salt removal time. The *'squeezing'* method consists of a series of consecutive phases of

powder bentonite hydration with DW, at a higher water content than the liquid limit, and drained consolidation, performed in a consolidometer under a maximum load of 500 kPa. The drained solution is sampled daily and the EC is monitored to evaluate the soluble salt concentration in the bentonite pore water. After the *'squeezing'* process, the material is oven dried at 105 °C and pulverized once again. When a 5 L consolidometer is used, the above procedure can produce about 500 g of dry powder squeezed bentonite, characterized by a lower EC value than 50 mS/m, corresponding to a lower NaCl solution molarity than 5 mM, in 40-50 days. The results of the EC monitoring during the squeezing process are reported in Figure 2.2.

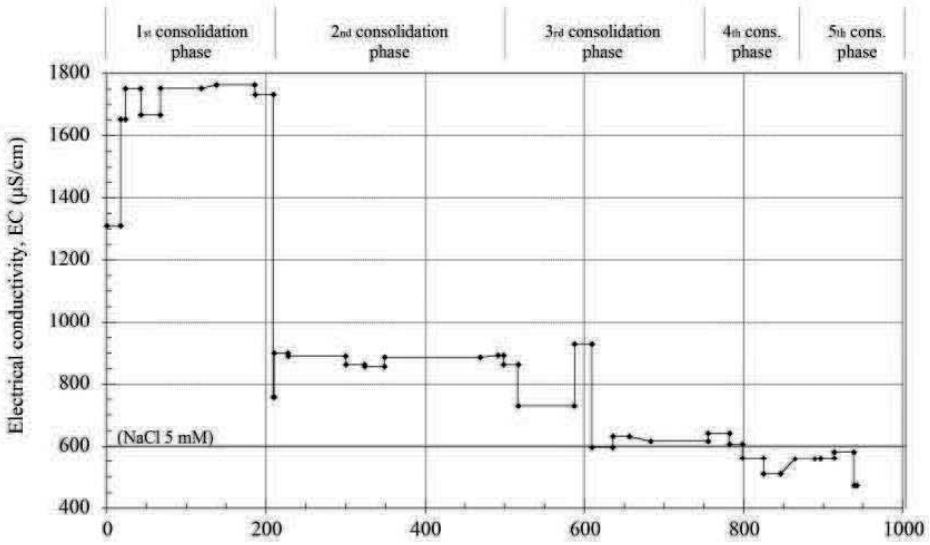

Figure 2.2 - Electrical conductivity monitoring during the squeezing process.

2.4.4 Polymer modification

Two of the specimens tested in this study were polymer modified. The modified material mainly consists of sodium montmorillonite prepared by adding 10% of an organic polymer named Nanosponge, NS, [F. Trotta, W. Tumiatti, R. Vallero. Italian Patent: MI2004A000614]. In order to obtain modified bentonite, the materials were dried separately at 60°C and then mixed in the dry state.

Two polymer modified specimens were obtained: a 'modified powder specimen', or NS-NaB, constituted by the powdered modified material, prepared in a dry state,

without needling or geotextiles, and a 'modified compacted specimen', or NS-C-NaB, subjected to a pre-hydration and pre-consolidation process.

Polymer modification induces a variation in the index properties of the material. The LL value of the 10% nanosponge-bentonite mixture results in 367% for DW and 135% for the 0.5 M NaCl solution.

The swell index trend obtained for the polymer modified bentonite is reported in Figure 2.3 as a function of the NaCl concentration.

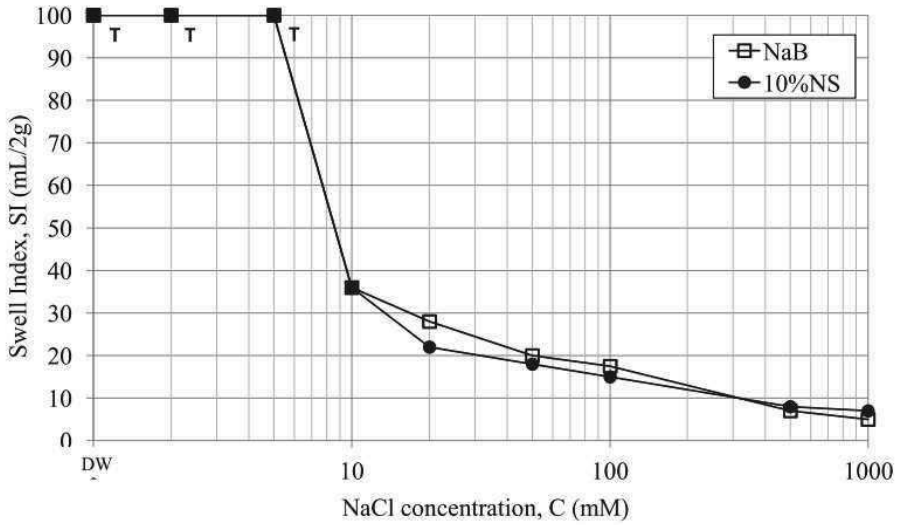

Figure 2.3 - Swell index as a function of the NaCl concentration, for natural and polymer modified bentonite.

The swelling behaviour of the modified material was similar to that obtained for natural bentonite: stable suspensions were obtained for solutions characterized by a lower molarity value than 5 mM while, for higher molarities than 0.5 M, the swelling was completely inhibited.

2.4.5 Pre-hydration and pre-consolidation

Pre-hydrated and pre-consolidated specimens were prepared from the powdered materials (the same materials that constitute the loose samples) through saturation with DW, at a lower water content than the LL value, and then by means of static

consolidation, performed in a compaction mould or in a oedometer, which allowed excess water release.

The loose specimens (NaB, NS-NaB) were used to analyze the effect of the absence of needling on the hydraulic performance of natural (or modified) bentonite, while the consolidated specimens were used to study the influence of the great modification induced by the static drained consolidation of the saturated material on the bentonite microstructure. This consolidation, in fact, produced alignment of the lamellae of a clayey soil in a face-to-face fabric.

2.5 EXPERIMENTAL METHODS AND TESTING PROCEDURES

The hydraulic conductivity tests performed in this study allow the barrier performances to be quantitatively evaluated in both short and long term landfill conditions. The former was simulated by permeating the specimens using DW, while the latter was obtained by subjecting the specimens, after permeation with DW, to a 250 mM $CaCl_2$ solution. The tests were performed accordingly to ASTM D 5887 and ASTM D 5084 for the GCL and the bentonite specimens, respectively, using flexible wall permeameters and the "falling head" method.

The GCL specimen was prepared according to the procedure described in ASTM D 5887, while the other loose and consolidated specimens were prepared using the following procedures:

- Loose specimens: the powdered materials were deposited loosely in a dry state in a steel mold inside the permeameter. The bulk dry density was approximately equal to the gravimetric density (1 g/cm^3 for natural and modified bentonite) in order to simulate the initial conditions of the bentonite in a GCL. The flexible membrane inside the mold adhered to the specimen, so that, after removing the mold, the flexible wall permeameter could be assembled completely. The specimen was saturated for 48 h and then permeated, so that a hydration phase with DW could be conducted before testing.
- Pre-hydrated and pre-consolidated specimen: the powdered materials were saturated at a lower water content than the LL value and then statically consolidated

in a compaction mold (C-NaB and NS-C-NaB) or in an oedometer (SQ-C-NaB), to allow the excess water to be released. Since the high swelling pressure that develops in the hydrated bentonite specimens contrasts the consolidation and reduces consolidation process rate, the porosity reached for the compacted specimens, in an acceptable time for the laboratory scheduling (i.e. 3-4 weeks), was higher than that obtained for loose specimens in initial dry conditions. As a consequence, the initial bulk dry density of the consolidated specimens was lower than the dry density of the bentonite in the GCL. The compacted specimens were then placed inside the permeameter and after the swelling volumetric strain had been fully stabilized under constant isotropic stress (this phase takes approximately 48 h), the permeation was started.

The specimens had a 101.6 mm diameter, except for SQ-C-NaB, which had a diameter of 70.0 mm, and an initial height approximately equal to 6 mm and 10-13 mm for the GCL and bentonite specimens, respectively. The tests were performed using a maximum hydraulic gradient of 500, a confining stress of between 28 and 50 kPa, depending on the test, following two consecutive stages: first the specimens were permeated with DW, in order to evaluate their short term behaviour, and then with a 250 mM $CaCl_2$ solution, in order to evaluate the long-term landfill conditions. The termination criteria of the second stage was established on the basis of the simultaneous achievement of the following targets: (1) completion of the consolidation phase induced by cation exchange, (2) achievement of steady state hydraulic conductivity, (3) specimen permeation with a higher calcium mass than that necessary for complete saturation of the cation-exchange centres (calculated on the basis of the CEC value measured using the methylene blue adsorption method). Targets (1) and (2) are analogous to those indicated in many other studies (Dunn and Mitchell 1984; Peirce and Witter 1986; Bowders 1988; Daniel 1994; Shackelford 1994; Shackelford et al. 2000). These authors recommended that the tests should not be terminated until steady hydraulic conductivity is achieved, the outflow/inflow ratio is approximately unitary and at least one or two PVs of flow have passed through the specimen. Moreover, when the electrolyte solution has been permeated, Bowders (1988), Daniel (1994) and Shackelford (1994) recommend that the chemical equilibrium should be established before a test is terminated. In this study,

chemical equilibrium establishment corresponds to cation exchange completion, which is controlled indirectly through targets (1) and (3). It was not possible to verify the attainment of the chemical equilibrium, as suggested by Shackelford et al. (1999) (i.e. monitoring of effluent/influent EC and pH, which should fall within 1.0 ± 0.1), because it was not possible to sample the outflow with the necessary frequency. However, as illustrated by Shackelford et al. (2005), through very long hydraulic conductivity tests, chemical equilibrium is reached very quickly (few PV) for bentonite specimens permeated with higher Calcium Chloride concentration than 50 mM, because a high Calcium concentration results in a rapid exchange with Sodium. In this study, the specimens were permeated with a very high $CaCl_2$ concentration (i.e. 250 mM) and, consequently, targets (1) and (3) can be considered adequate for the monitoring of chemical equilibrium.

2.6 RESULTS

2.6.1 Natural bentonite specimens

The data concerning the initial characteristics of the natural specimens and the test procedure parameters are listed in Table 2.2.

Table 2.2 - Initial specimen characteristics and test parameters (where σ' is the effective stress acting on the specimen, i_{MAX} is the maximum hydraulic gradient used in the test, D and L are the diameter and length of the specimen, respectively, V_B is the total volume of the bentonite, M_B is the dry mass of the bentonite and e_0 is the initial void ratio of the specimen).

Specimen ID	σ' [kPa]	i_{MAX} [-]	D [mm]	L [mm]	V_B [cm^3]	M_B [g]	e_0 [-]*
GCL	28	500	101.6	6.0	40.54	37.0	1.93
NaB	50	500	101.6	10.0	81.07	80.7	1.66
C-NaB	50	500	101.6	14.0	113.50	80.7	2.73
SQ-C-NaB	28-50	500	70.0	11.1	42.66	35.1	2.22

*G_S is assumed equal to 2.65 (Dominijanni & Manassero 2006)

The comparison between the results obtained from the hydraulic conductivity tests performed on the GCL and the NaB specimens (made of by the same material contained in the GCL, but prepared in a dry state without needling or geotextiles) is

presented in Figure 2.4 as a function of the pore volumes of flow, PV. A comparison of the data underlines the influence of needling and geotextiles on the hydraulic performance of the GCL.

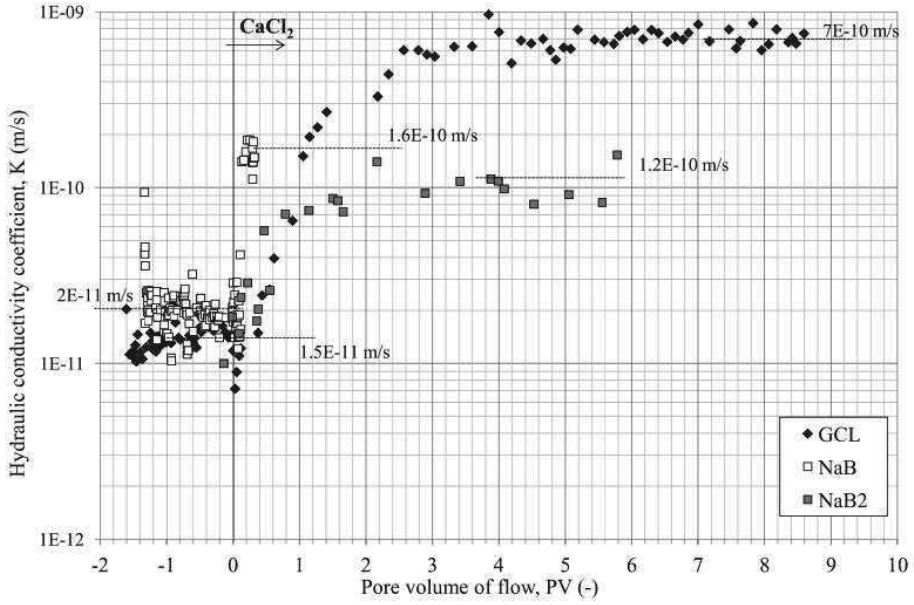

Figure 2.4 - Hydraulic conductivity, as a function of the pore volume of flow, for the GCL, NaB and NaB2 specimens.

Since the results of the first test with NaB were affected by clogging of the porous stones, during the permeation with the 250 mM $CaCl_2$ solution, a second test was performed, referred to as NaB2 in the graph. Clogging developed after the permeation of 0.4 PV of $CaCl_2$ solution and the results obtained after clogging have not been presented in the graph. The second test was conducted by hydrating the specimen with DW and directly starting the permeation with the $CaCl_2$ solution. The results obtained from NaB and NaB2 are very similar.

The hydraulic conductivity value obtained with DW was approximately equal for the GCL and NaB specimens: $K = 1.5 \cdot 10^{-11}$ m/s for the GCL and $K = 2.0 \cdot 10^{-11}$ m/s for the NaB. On the contrary, the permeation with the 250 mM $CaCl_2$ solution produced a greater increase in hydraulic conductivity in the case of GCL ($K = 7.0 \cdot 10^{-10}$ m/s) than in the case of NaB-NaB2 ($K = 1.2 \div 1.6 \cdot 10^{-10}$ m/s).

The relative volumetric strain, $\delta\varepsilon_v = \frac{\delta e}{1+e_0} = \frac{e-e_0}{1+e_0}$ (positive for swelling), of the GCL and the NaB specimens is plotted in Figure 2.5 as a function of PV.

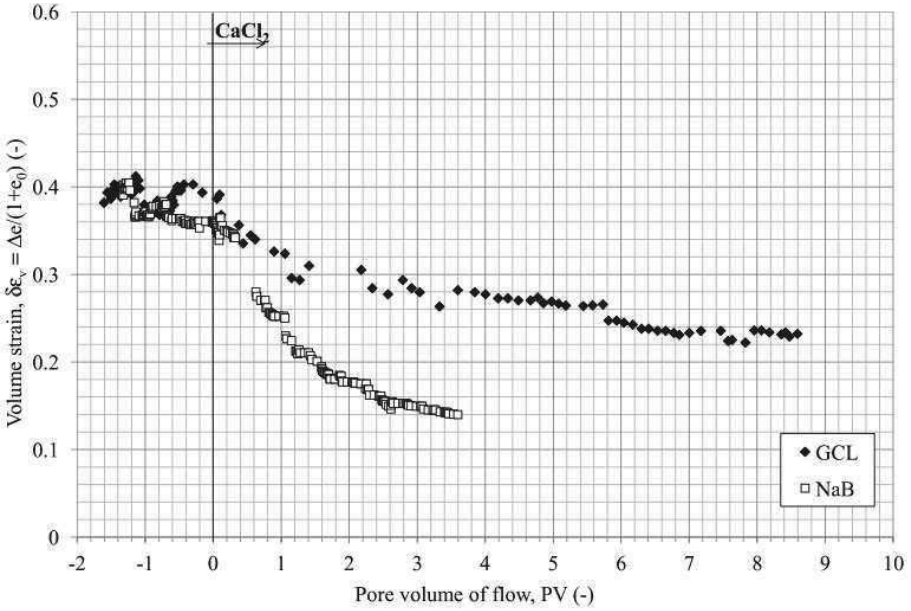

Figure 2.5 - Relative volume strain of GCL and NaB during the hydraulic conductivity test.

The $\delta\varepsilon_v$ of the GCL was calculated referring to the volume of the bentonite layer, under the hypothesis that the geotextile volume was approximately constant during the test since the effective confining stress was constant.

Both specimens presented a positive volumetric strain (swelling), during hydration, of $\delta\varepsilon_v = 0.36$ and $\delta\varepsilon_v = 0.38$ for NaB and GCL, respectively. The specimen volume was approximately stable during the permeation with DW and started to decrease when the specimens were permeated with the $CaCl_2$ solution, due to the compression effect induced by the reduction in the swelling pressure. NaB presented higher sensibility to the bulk volume reduction induced by the cation exchange phenomenon: at the end of the consolidation phase NaB had a residual volumetric strain of $\delta\varepsilon_v = 0.14$, while it was equal to $\delta\varepsilon_v = 0.24$ for the GCL.

The data obtained in these tests highlight that the presence of needling across a GCL sample does not hinder the swelling during hydration and does not influence the hydraulic conductivity of bentonite to DW. During the permeation with the calcium chloride solution, the presence of needling induced lower hydraulic performances: the hydraulic conductivity was 7 times higher than that measured on NaB. This result can be explained by the formation of preferential flow pathways in correspondence to the holes produced by needling, where macro-voids can develop during the consolidation phase. The formation of internal macro-voids, instead of a homogeneous consolidation, can also explain the lower reduction of the bulk volume measured for the GCL than for the NaB specimen.

The results obtained from the tests on C-NaB and SQ-C-NaB are presented in Figure 2.6 in terms of hydraulic conductivity coefficient as a function of PV.

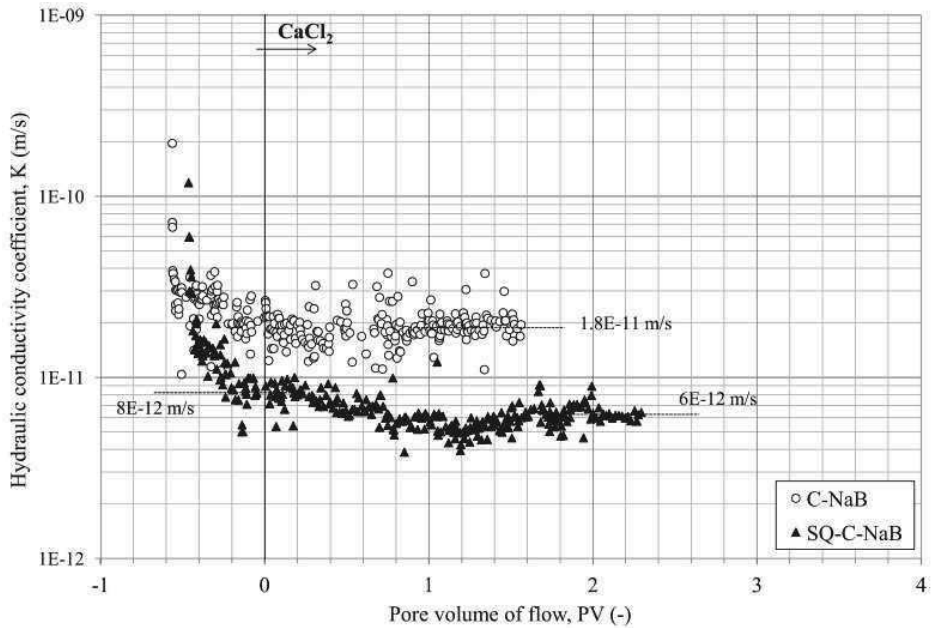

Figure 2.6 - Hydraulic conductivity, as a function of the pore volume of flow, for the C-NaB and SQ-C-NaB specimens.

The graph in Figure 2.6 has the purpose of showing the role of the pre-hydration and pre-consolidation process (C-NaB) and that of the salt removal process (SQ-C-NaB) on the hydraulic performances of bentonite.

The hydraulic conductivity measured on C-NaB during the permeation with DW was equal to that obtained for the NaB specimen, $K = 2.0 \cdot 10^{-11}$ m/s, and it can, therefore, be stated that pre-hydration and pre-consolidation processes do not influence the hydraulic performances of bentonite permeated with 'standard' liquids.

The salt removal process, carried out on SQ-C-NaB before pre-hydration and pre-consolidation, produced a considerable reduction in the hydraulic conductivity value, measured with DW, that it was halved ($K = 0.8 \cdot 10^{-11}$ m/s at $\sigma'_v = 50$ kPa).

The permeation phase with the 250 mM $CaCl_2$ solution did not produce any perceptible variation in hydraulic conductivity in the case of C-NaB. The conductivity value, in fact, remained approximately stable during the whole permeation phase, and, at the end of the test, was equal to $K = 1.8 \cdot 10^{-11}$ m/s. This value is one order of magnitude lower than that obtained for NaB.

Moreover, the hydraulic conductivity value monitored for SQ-C-NaB during $CaCl_2$ circulation decreased from $K = 0.8 \cdot 10^{-11}$ m/s to $K = 0.6 \cdot 10^{-11}$ m/s.

The trends of relative the volumetric strain, $\delta\varepsilon_v$, measured during the permeation of C-Nab and SQ-C-NaB, are plotted in Figure 2.7 as a function of PV.

The results highlight more swelling during the saturation phase for C-NaB than for SQ-.C-NaB and for the other specimens reported in Figure 2.5. Confined swelling requires a force of repulsion that separates the bentonite particles and increases the volume of the specimen as the water content increases. This force, called swelling pressure, appears to be greater for specimens subjected to consolidation pressure, which produces parallel particle orientation.

In the case of parallel orientation, swelling occurs primarily in the plane perpendicular to the flat surface of the particles, and induces anisotropic behaviour: horizontal swelling can only be computed for a few percent of the vertical swelling. A random particle configuration, such as that of a NaB specimen, should lead to a more homogeneous swelling.

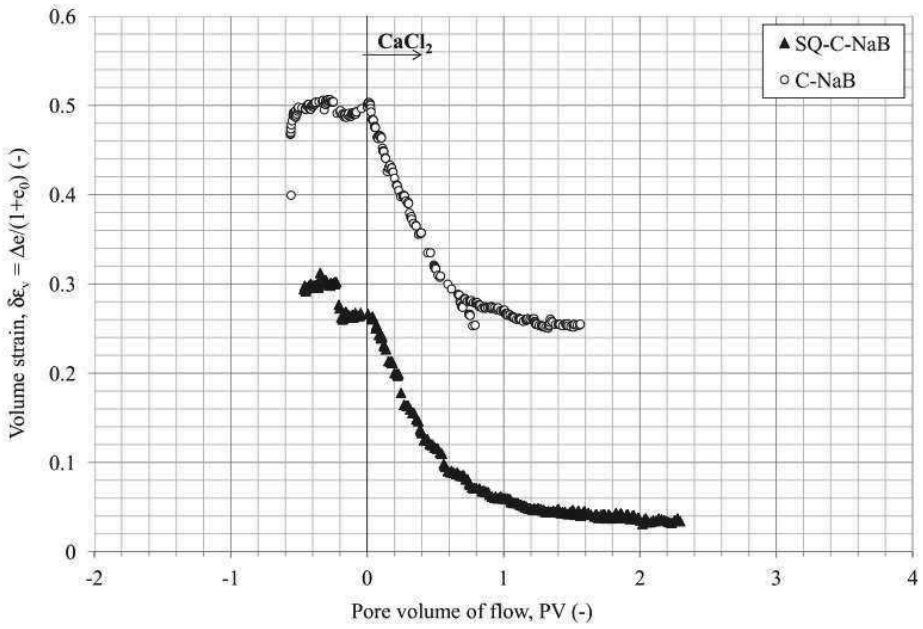

Figure 2.7 - Relative volume strain of C-NaB and SQ-C-NaB during the hydraulic conductivity test.

Anomalous behaviour appears from a comparison of the C-NaB and the SQ-C-NaB specimens. SQ-C-NaB was expected to swell as much as C-NaB during saturation, or even more, due to the higher swelling pressure induced by the absence of soluble salt between the bentonite lamellae. Instead, SQ-C-NaB showed a lower volumetric strain than C-NaB. The different pre-consolidation method that was used can explain this behaviour: SQ-C-NaB was in fact consolidated in the oedometer while C-NaB and NS-C-NaB were consolidated in the compaction mold.

2.6.2 Polymer modified specimens

The data concerning the initial characteristics of the modified specimens and the test procedure parameters are listed in Table 2.3.

Table 2.3 -Initial specimen characteristics and test parameters (for more information on the parameters see Table 2.2).

Specimen ID	σ′ [kPa]	i_{MAX} [-]	D [mm]	L [mm]	V_B [cm^3]	M_B [g]	e_0 [-]*
NS-NaB	50	500	101.6	10.0	81.07	80.8	1.66
NS-C-NaB	50	500	101.6	10.0	81.07	81	1.65

*G_S is assumed equal to 2.65 (Dominijanni & Manassero 2006)

The hydraulic conductivity results, obtained from the tests performed on the polymer modified specimen, NS-NaB and NS-C-NaB, are reported in Figure 2.8.

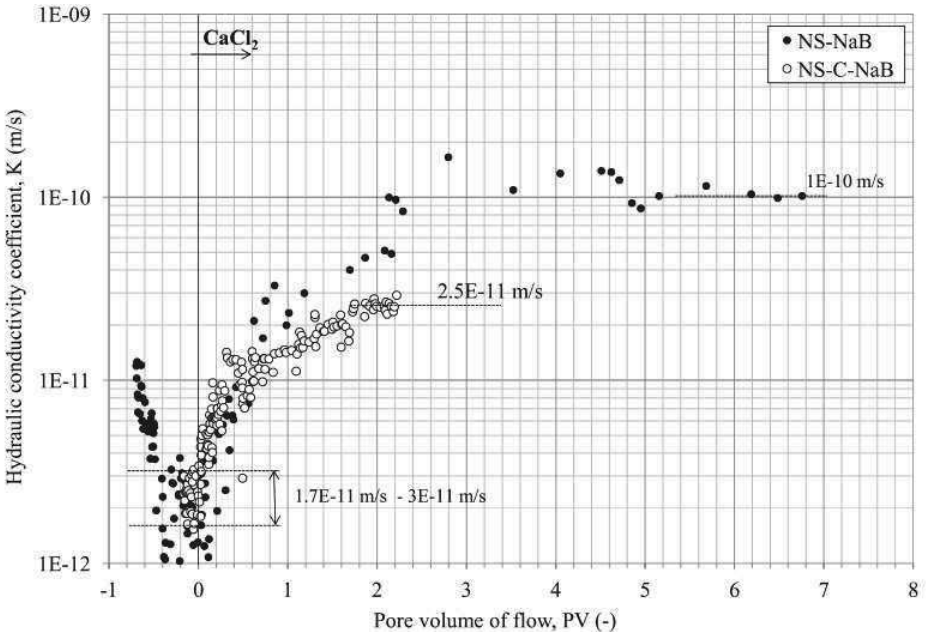

Figure 2.8 - Hydraulic conductivity, as a function of the pore volume of flow, for the NS-NaB and NS-C-NaB specimens.

The hydraulic conductivity values measured with DW on both specimens were extremely low, within the $1.7 \cdot 10^{-12}$ m/s and $3 \cdot 10^{-12}$ m/s range, a value approximately one order of magnitude lower than those obtained by permeating natural bentonite specimens (GCL, NaB and C-NaB) with DW. The permeameter used for the tests at these conductivity values was not accurate enough to define a single value of

hydraulic conductivity. For this reason, a range of values was chosen in order to characterize the hydraulic behaviour of the modified material with DW. However, no difference in hydraulic conductivity of NS-NaB and NS-C-NaB was shown in the tests performed with DW.

When the modified specimens were subjected to the 250 mM $CaCl_2$ solution, an immediate increase in hydraulic conductivity was registered for both specimens as well as a subsequent achievement of the steady state conductivity value of $1 \cdot 10^{-10}$ m/s and $2.5 \cdot 10^{-11}$ m/s for NS-NaB and NS-C-NaB, respectively. These values are similar to those obtained for the natural specimens.

The trend of relative volumetric strain, $\delta\varepsilon_v$, measured during the permeation of the modified specimens, is plotted as a function of PV in Figure 2.9 and compared with the data obtained for the corresponding natural specimens.

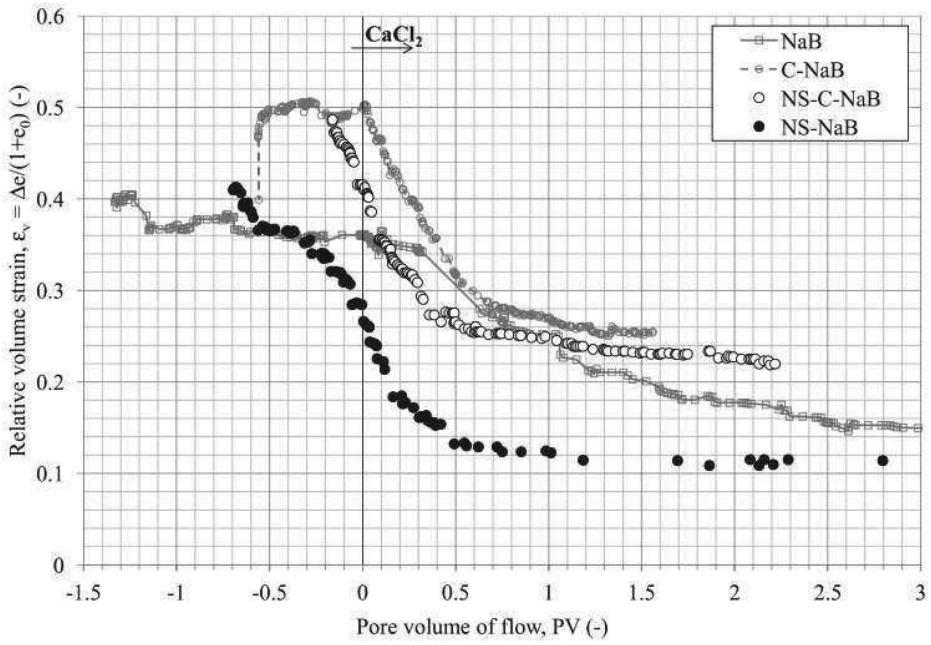

Figure 9 - Relative volumetric strain, as a function of the pore volume of flow, for the NS-NaB and NS-C-NaB specimens and comparison with the results obtained for the corresponding natural bentonite specimens.

The relative volumetric strain induced by the saturation phase (swelling) was approximately equal for the natural and modified specimens: $\delta\varepsilon_v = 0.4$ for the loose specimens (NaB and NS-NaB) and $\delta\varepsilon_v = 0.5$ for the saturated and statically consolidated specimens (C-NaB and NS-C-NaB). The residual strain of the specimens after consolidation was slightly lower for the modified specimens than for the natural ones. An important point is that the consolidation phase of the modified samples starts during permeation with DW. During this phase, the consolidation is not induced by a decrease in the internal swelling pressure caused by the cation exchange phenomenon but instead precedes it. The consolidation of the modified specimens, during the permeation with DW, can be explained by the polymer solubilisation and its subsequent removal from the specimens by the permeant solution. This possibility was subsequently confirmed in the FTIR test, i.e. the Fourier Transform Infrared Spectroscopy test, performed on the NS-C-NaB specimen exhumed from the permeameter at the end of the test and on a natural bentonite sample used for comparison purposes. The results of the spectroscopy, reported in Figure 2.10, highlight the absence of the polymer in the exhumed specimen and confirm its complete solubilisation.

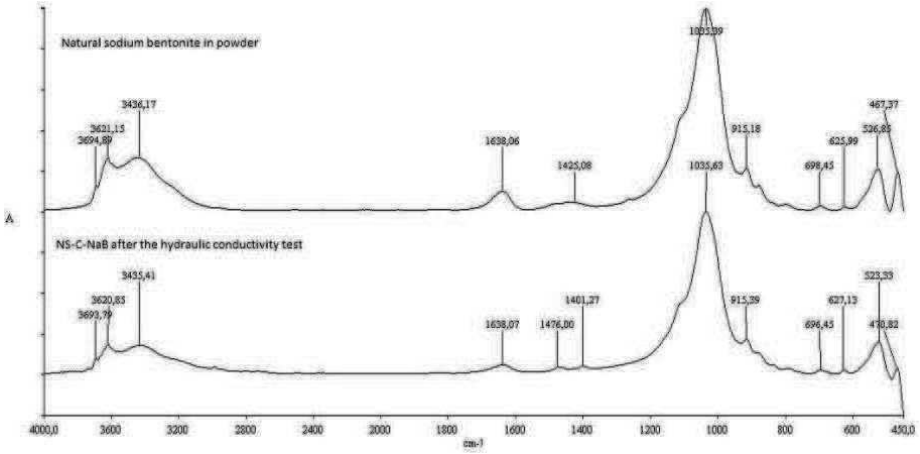

Figure 2.10 - FTIR test results obtained for the NS-C-NaB specimen exhumed from the permeameter and a natural sodium bentonite sample for comparison purposes.

During the permeation with the $CaCl_2$ solution, the consolidation phenomenon, registered through the specimen volume monitoring shown in Figure 2.9, was induced by both polymer solubilisation and a reduction in swelling pressure induced by cation exchange phenomenon.

2.6.3 Termination criteria

The hydraulic conductivity tests were aimed at evaluating the hydraulic behaviour of different bentonite specimens in short and long term conditions. By "short term" we mean those conditions that represent the state of the bentonite layer in the first period of usage in a landfill barrier, while by "long term" we mean those typical conditions of a bentonite layer that emerge after years of use as a sealing layer in a landfill. The hydraulic conductivity value, corresponding to the hydraulic performance of the specimen in the first part of the test performed with DW, was assumed equal to the steady state conductivity value, i.e. the asymptote reached after a short transient phase.

Other, more complicated considerations should be made on the termination criteria of the second stage. In the second part of the test, in fact, the long transient phase of the hydraulic conductivity parameter was caused by the slow cation exchange phenomenon, which started to act when the first Calcium ion was injected into the specimen, and stopped when all the exchange active centres were saturated with Calcium ions.

The tests performed in this study were aimed at individuating the conductivity value of the specimen in a completely exchanged state. To this aim, the termination criteria of the second phase of the tests were established as: (1) the completion of the consolidation phase induced by cation exchange, which achievement was reached for all the specimens in the graphs that report the relative volumetric strain trend as a function of PV, i.e. Figures 2.5, 2.7 and 2.9; (2) steady state hydraulic conductivity achievement, which was reached for all the specimens, as highlighted in the graphs in Figures 2.4, 2.6 and 2.8; and, finally, (3) a higher permeation with calcium mass than that necessary for complete saturation of the cation-exchange centres.

The calculation procedure conducted to obtain the theoretical value of the solution PV necessary to bestow the correct Calcium mass to each specimen is reported below.

As in Dominijanni and Manassero (2005), the molar concentration of the solid skeleton electric charge, with reference to the average pore volume of the specimen during consolidation, can be defined as a function of the cation exchange capacity and the void ratio:

$$c_{sk} = \frac{c_{sk,0}}{e_{ave(cons)}} = \frac{\phi_x \cdot CEC \cdot G_S \cdot \rho_w}{e_{ave(cons)}} \tag{2.1}$$

where: ϕ_x is the fixed charge coefficient, CEC is the cation exchange capacity, expressed in meq/g, G_S is the specific gravity of the bentonite (assumed equal to 2.65, as proposed by Dominijanni and Manassero 2006), ρ_w is the water density, which is equal to 1 g/cm^3, and $e_{ave(cons)}$ is the average void ratio during the consolidation phase, calculated as:

$$e_{ave(cons)} = \frac{e_{i(cons)} + e_{f(cons)}}{2} \tag{2.2}$$

The fixed charge coefficient, ϕ_x, is an adjustable parameter that accounts for all the uncertainties of the model and is expected to be less than 1 (Dominijanni and Manassero, 2005). In this case, it was set equal to 1 to obtain a prudential estimate of the pore volume necessary for the complete exchange of calcium with sodium.

Since Calcium has a double valence in the $CaCl_2$ compound, the Calcium concentration that saturates the fixed charge of the bentonite specimen can be expressed as follows:

$$C_{Ca,exc} = \frac{c_{sk}}{2} \tag{2.3}$$

and the corresponding Calcium molar mass can be obtained by multiplying the void volume of the specimen, $V_{v,ave(cons)}$:

$$M_{Ca,exc} = C_{Ca,exc} \cdot V_{v,ave(cons)} \quad (2.5)$$

Finally, the 250 mM $CaCl_2$ solution pore volume theoretically required to provide the Calcium mass, $M_{Ca,exc}$, is obtained as:

$$PV_{Th} = \frac{C_{Ca,exc}}{0.25M} \quad (2.6)$$

The calculation results are reported in Table 2.4.

Table 2.4 - Calculation results for the third termination criterion.

Specimen ID	$e_{ave,exp}$ [-]	c_{sk} [M]	$C_{Ca,exc}$ [M]	M_{Ca} [mol]	V_{sol} [cm^3]	PV_{th} [-]	PV_{exp} [-]
GCL	2.48	1.12	0.561	0.019	77	2.24	10.00
NaB	2.26	1.23	0.616	0.042	170	2.46	6.00
C-NaB	4.13	0.67	0.336	0.042	169	1.34	1.56
SQ-C-NaB	2.70	1.03	0.514	0.018	73	2.06	2.29
NS-NaB	2.17	1.28	0.604	0.043	170	2.56	6.76
NS-C-NaB	2.64	1.05	0.552	0.042	167	2.2	2.21

2.7 DISCUSSIONS AND CONCLUSIONS

Except for SQ-C-NaB, i.e. the specimen subjected to the salt removal process, the hydraulic conductivity to DW of the natural bentonite specimens (GCL, NaB, C-NaB) was approximately the same and the values ranged between $1.5 \cdot 10^{-11}$ m/s and $2 \cdot 10^{-11}$ m/s. These results highlight that physical pre-treatments or the presence/absence of needling do not influence the hydraulic performance of bentonite layers in short term condition, i.e. during permeation with DW.

The SQ-C-NaB specimens showed a higher hydraulic performance with DW than the other specimens: the hydraulic conductivity value was $K = 0.8 \cdot 10^{-11}$ m/s. The salt removal process, or squeezing procedure, reduced the cation concentration in the pore solution and, as a consequence, enhanced the repulsion between the montmorillonite lamellae and the exfoliation of the tactoids. The resulting montmorillonite lamellae configuration was more dispersed and homogeneous in order to justify the hydraulic conductivity reduction.

Further studies are required to investigate whether the low hydraulic conductivity value, obtained for SQ-C-NaB, can be univocally associated to the squeezing procedure or whether it can be induced by pre-consolidation stress and, consequently, by the initial void ratio, e_0, which is lower for the SQ-C-NaB specimen than for the C-NaB specimen.

Hydraulic conductivity tests with natural bentonite specimens have shown that both physical pre-treatments and the presence/absence of needling have a great influence on the hydraulic performance of a the material, particularly in long term conditions, i.e. during permeation with the 250 mM $CaCl_2$ solution.

Strong Calcium solutions are known to affect the hydraulic conductivity of natural bentonite. In particular, the performed hydraulic conductivity tests highlighted the negative impact induced by needling on GCL hydraulic performances when permeated with the 250 mM $CaCl_2$: the hydraulic conductivity value of the NaB specimen ($K = 1.2 – 1.6 \cdot 10^{-10}$ m/s), made up of the powdered material contained in the GCL, prepared in a dry state as in the industrial production of GCL, but devoid of needling and geotextiles, was 7 times lower than that obtained for the GCL sample ($K = 7.0 \cdot 10^{-10}$ m/s).

Neither C-NaB nor SQ-C-NaB, which were pre-hydrated and pre-consolidated specimens, showed any conductivity value variation during the consolidation phase induced by cation exchange phenomenon, a result that was in contrast to the trend registered for loose specimens (GCL and NaB). The hydraulic conductivity value obtained from the SQ-C-NaB specimen even seemed to decrease during permeation with $CaCl_2$: the final value was equal to $K = 0.6 \cdot 10^{-11}$ m/s.

During hydration, the consolidated specimens swelled more than the loose specimens, due to the face-to-face fabric induced by the drained consolidation pre-treatment. The charged montmorillonite lamellae, in fact, manifested a higher repulsion force when the two charged surface were aligned parallel. It follows that, during the imbibitions phase, the specimens previously subjected to consolidation absorbed a greater amount of water in the interlamellae space and, consequently, swelled more.

The SQ-C-NaB specimen showed anomalous swelling behaviour: it was in fact expected to swell like C-NaB, or even more, due to the higher swelling pressure

induced by the soluble salt removal pre-treatment. Further studies are necessary to assess whether that lower swelling behaviour was induced by the salt removal process or by the higher stress subjected during the pre-consolidation phase.

The tests performed on polymer modified specimens showed conductivity values to DW that were approximately one order of magnitude lower than those obtained for natural specimens ($1.7 \cdot 10^{-12}$ m/s - $3 \cdot 10^{-12}$ m/s), highlighting an excellent result with regard to the use of the polymer Nanosponge. Unfortunately, during the permeation with water and the Calcium solution, the polymer was solubilised and removed from the specimen by the volumetric flux. The final hydraulic conductivity values registered for NS-NaB and NS-C-NaB, at the end of the $CaCl_2$ stage, were similar to those obtained with the respective natural bentonite specimens (NaB and C-NaB). The results of the spectroscopy substantially highlight the absence of the polymer in the exhumed C-NaB specimen and confirm its complete solubilisation during the hydraulic conductivity test.

ACKNOWLEDGEMENTS

The polymer selection and chemical analysis, which were essential for this study, were conducted with the help of Prof. Francesco Trotta and Dr. Marco Zanetti of the Chemistry faculty at the University of Turin.

REFERENCES

Bowders, J. 1988. Discussion of Termination criteria for clay permeability testing. Journal of Geotechnical Engineering, **114**(8), 947–949. doi: 10.1061/(ASCE)0733-9410(1988)114:8(947)

Daniel, D. 1994. State-of-the-art: Laboratory hydraulic conductivity tests for saturated soils. Hydraulic conductivity and waste contaminant transport in soil. STP 1142, D. Daniel and S. Trautwein, eds., ASTM, West Conshohocken, 30–78.

Di Emidio G. 2010. Hydraulic and chemico-osmotic performance of polymer treated clays. PhD Thesis, Ghent University.

Dominijanni, A. & Manassero, M. 2012. Modelling the swelling and osmotic properties of clay soils. Part II: The physical approach. International Journal of Engineering Science **51**, 51-73. doi:10.1016/j.ijengsci.2011.11.001

Dominijanni, A., Manassero, M., and Vanni, D., 2006. Micro/macro modeling of electrolyte transport through semipermeable bentonite layers. In Proceedings of the 5th International Congress on Environmental Geotechnics, 26th-30th June, 2006, Cardiff, Wales, UK, Thomas, H.R., Ed., Thomas Telford, London, Volume II: 1123-1130.

Dunn, R. & Mitchell, J. 1984. Fluid conductivity testing of fine-grained soils. Journal of Geotechnical Engineering, **110**(11), 1648–1665. doi: 10.1061/(ASCE)0733-9410(1984)110:11(1648)

Malusis, M.A. & Shackelford, C.D. 2002a. Chemico-osmotic efficiency of a geosynthetic clay liner. Journal of Geotechnical and Geoenvironmental Engineering **128**(2), 97–106. doi:10.1061/(ASCE)1090-0241(2002)128:2(97)

Malusis, M.A. & Shackelford, C.D. 2002b. Coupling effects during steady-state solute diffusion through a semipermeable clay membrane. Environmental Science and Technology **36**(6), 1312–1319. doi: 10.1021/es011130q

Malusis, M.A., Shackelford, C.D. & Olsen, H.W. 2001. A laboratory apparatus to measure chemico-osmotic efficiency coefficients for clay soils. Geotechnical Testing Journal **24**, 229-242. doi: 10.1520/GTJ11343J

Jo H., Katsumi T., Benson C.H., Edil T.B. 2001. Hydraulic conductivity and swelling of non-prehydrated GCLs permeated with single species salt solutions. Journal of Geotechnical and Geoenvironmental Engineering, ASCE **127**(7) 557–567. doi: 10.1061/(ASCE)1090-0241(2001)127:7(557)

Kang, J.-B. & Shackelford, C.D. 2009. Clay membrane testing using a flexible-wall cell under closed-system boundary conditions. Applied Clay Science **44**, 43-58. doi: 10.1016/j.clay.2009.01.006

Katsumi T., Ishimori H., Onikata M., Fukagawa R. 2008. Long-term barrier performance of modified bentonite materials against sodium and calcium permeant solutions. Geotextiles and Geomembranes **26**, 14–30. doi: 10.1016/j.geotexmem.2007.04.003

Kolstad D.C., Benson C.H., Edil T.B., Jo H.Y. 2004. Hydraulic conductivity of a dense prehydrated GCL permeated with aggressive inorganic solutions. Geosynthetics International **11** (3), 233–241. doi: 10.1680/gein.2004.11.3.233

Peirce, J. & Witter, K. 1986. Termination criteria for clay permeability testing. Journal of Geotechnical Engineering, **112**(9), 841–854. doi: 10.1061/(ASCE)0733-9410(1986)112:9(841)

Petrov R.J. and Rowe R.K. 1997. Geosynthetic clay liner (GCL) – chemical compatibility by hydraulic conductivity testing and factors impacting its performance. Canadian Geotechnical Journal **34**, 863–885.

Scalia J., Benson C.H., Edil T.B., Bohnhoff G.L., Shackelford C.D. (2011). Geosynthetic clay liners containing bentonite polymer nanocomposite. *In* GeoFrontiers 2011, ASCE, 2001–2009.

Shackelford, C. (1994). Waste–soil interactions that alter hydraulic conductivity. ASTM STP 1142, ASTM, Philadelphia, 111–168.

Shackelford, C.D. & Lee, J.-M. 2003. The destructive role of diffusion on clay membrane behavior. Clays and Clay Minerals **51**(2), 186–196. doi: 10.1346/CCMN.2003.0510209

Shackelford, C., Malusis, D., Majeski, M., and Stern, R. 1999. Electrical conductivity breakthrough curves. Journal of Geotechnical and Geoenvironmental Engineering, **125**(4), 260–270. doi: 10.1061/(ASCE)1090-0241(1999)125:4(260)

Shackelford C., Benson C., Katsumi T., Edil T., and Lin L. 2000. Evaluating the hydraulic conductivity of GCLs permeated with nonstandard liquids. Geotextiles and Geomembranes, **18**(2-4) 133–162. doi: 10.1016/S0266-1144(99)00024-2

Schroeder C., Monjoie A., Illing P., Dosquet D., Thorez J. 2001. Testing a factory-prehydrated GCL under several conditions. *In* Proceedings Sardinia 2001 8th International Waste Management and Landfill Symposium, CISA, Cagliari, Italy, 187–196.

Yeo, S.-S., Shackelford, C.D. & Evans, J.C. 2005. Membrane behaviour of model soil-bentonite backfill mixtures. Journal of Geotechnical and Geoenvironmental Engineering **131**(4), 418-429. doi: 10.1061/(ASCE)1090-0241(2005)131:4(418)

Chapter 3

OSMOTIC AND SWELLING PROPERTIES OF BENTONITE BARRIERS

This chapter reports the contents of the Paper:

Dominijanni, A., Manassero, M., Puma, S. (2013).

Géotechnique **63**, No. 3, 191-205 [http://dx.doi.org/10.1680/geot.SIP13.P.010].

Titled: **Coupled chemical-hydraulic-mechanical behaviour of bentonites.**

(Manuscript received 29 February 2012; revised manuscript accepted 22 October 2012).

Other contents are reported at the end of the chapter, regarding the results and comments to further osmotic tests, which have not been included in the Paper, and the design of a new apparatus to measure both the swelling pressure and the reflection coefficient.

COUPLED CHEMICAL-HYDRAULIC-MECHANICAL BEHAVIOUR OF BENTONITES

by

Andrea Dominijanni*, Mario Manassero** and Sara Puma***

* *Corresponding Author*
Dipartimento di Ingegneria Strutturale, Edile e Geotecnica [Department of Structural, Geotechnical and Building Engineering], Politecnico di Torino, Corso Duca degli Abruzzi 24, 10129 Torino – ITALY; Ph: +39-011-090-7705, Fax: +39-011-090-4899, e-mail: andrea.dominijanni@polito.it

** Dipartimento di Ingegneria Strutturale, Edile e Geotecnica [Department of Structural, Geotechnical and Building Engineering], Politecnico di Torino, Corso Duca degli Abruzzi 24, 10129 Torino – ITALY; Ph: +39-011-090-4820, Fax: +39-011-090-4899, e-mail: mario.manassero@polito.it

*** Dipartimento di Ingegneria Strutturale, Edile e Geotecnica [Department of Structural, Geotechnical and Building Engineering], Politecnico di Torino, Corso Duca degli Abruzzi 24, 10129 Torino – ITALY; Ph: +39-011-090-7705, Fax: +39-011-090-4899, e-mail: sara.puma@polito.it

3.1 ABSTRACT

The common use of bentonites, which are clay soils characterized by a high specific surface and a permanent negative electric charge on their solid skeleton, as hydraulic and contaminant barriers for landfill and soil remediation applications, including the final disposal of nuclear waste, needs to be supported by adequate theoretical modelling of their mechanical behaviour and transport properties, in order to assess the expected performance in the long term. To this aim, a theoretical approach has been proposed in order to derive constitutive equations for their coupled chemical-hydraulic-mechanical behaviour. The phenomenological parameters that govern the transport of electrolyte solutions through bentonites, i.e. the hydraulic conductivity, the reflection coefficient, which is also called the chemico-osmotic efficiency coefficient, and the osmotic effective diffusion coefficient, have been measured through laboratory tests on a bentonite with porosity of 0.81, over a range of sodium chloride concentrations in the pore solution that varied from 5 mM to 100 mM. The relevance of the osmotic phenomena has been shown to decrease when the salt concentration increases. The obtained results have been interpreted by assuming that the microscopic deviations of the pore solution state variables from their average values are negligible. In this way, it is possible to interpret the macroscopic behaviour on the basis of the physical and chemical properties of the bentonite mineralogical components.

3.2 KEY-WORDS

Chemical properties,
clays,
constitutive relations,
expansive soils,
laboratory tests,
pore pressures.

3.3 INTRODUCTION

The term “bentonite” is commonly used to indicate a clay soil with a high content (> 70%) of montmorillonite, a mineral of the smectite group. Montmorillonite particles are thin lamellae that are characterized by a high specific surface (defined as the surface per unit weight) and a permanent negative electric charge. Bentonite is used in hydraulic and contaminant barriers, because of its low hydraulic conductivity, k, to permeation with water and dilute aqueous solutions (k typically $\leqslant 3 \cdot 10^{-11}$ m/s). Geosynthetic clay liners (GCLs), which consist of a thin layer of bentonite (~ 5- to 10-mm thick) sandwiched between two geotextiles, are examples of such barriers. GCLs are currently used in bottom and cover landfill barriers to limit water infiltration and contaminant migration.

Owing to its physical and chemical properties, the macroscopic mechanical behaviour and transport properties of bentonite cannot be modelled through classical soil mechanics approaches (Manassero and Dominijanni, 2003). In fact, bentonite swells or shrinks in response to changes in the chemical composition of the pore solution. Moreover, when a hydraulic pressure gradient, or a solute concentration gradient, is applied to it, both a volumetric flux and a diffusive solute mass flux occur, as in semipermeable membranes. For this reason, a theoretical approach that accounts for the electric interaction that occurs between the solid skeleton of the bentonite and the ions contained in the pore solution is proposed in the first part of this paper. The experimental determination of the swelling pressure and the transport properties of a natural sodium bentonite is described in the second part. The obtained results have been interpreted with the proposed theoretical model, in which the microscopic properties of the bentonite have been linked to the observed macroscopic behaviour.

3.4 THEORY

Montmorillonite lamellae are characterized by a negative electric charge, due to the isomorphic substitution of a portion of the tetravalent silicon (Si^{4+}) and the trivalent aluminium (Al^{3+}) in their crystalline structure, with metals, such as magnesium (Mg^{2+}), which have a lower valence. This electric charge per unit solid volume can be expressed as $F \cdot \overline{c}_{sk,0}$, where F is Faraday's constant (96,485 $C \cdot mol^{-1}$) and $\overline{c}_{sk,0}$ is the molar concentration per unit solid volume of the solid skeleton electric charge, which is assumed to have unit valence (i.e. $z_{sk} = -1$). $\overline{c}_{sk,0}$ represents the moles of solid skeleton electric charge per volume of solids and, in order to be compared with the ion concentrations of the pore solution, it needs to be divided by the void ratio, e, which represents the pore volume per volume of solids. Dominijanni and Manassero (2012b) have shown that $\overline{c}_{sk,0}$ is proportional to the effective specific surface of the solid particles and decreases when the montmorillonite lamellae aggregate to form the so-called tactoids.

If the pore solution contains a single salt that is completely dissociated with the following stoichiometric reaction:

$$(\text{Cation})_{z_1}^{\nu_1} (\text{Anion})_{z_2}^{\nu_2} \rightarrow \nu_1 (\text{Cation})^{z_1} + \nu_2 (\text{Anion})^{z_2}$$

where z_1 and z_2 are the electrochemical valences of the cation and the anion, and ν_1 and ν_2 are the stoichiometric coefficients of the cation and the anion, respectively, the following condition has to be satisfied in order to preserve electroneutrality within a saturated porous medium, even in the presence of the solid skeleton electric charge:

$$z_1 \overline{c}_1 + z_2 \overline{c}_2 = \frac{\overline{c}_{sk,0}}{e} \tag{3.1}$$

where $\overline{c}_1$ and $\overline{c}_2$ are the molar concentrations of the cation and the anion, respectively, and e is the void ratio.

As a consequence, the solid skeleton electric charge influences the distribution of the ions contained in the pore solution. This phenomenon is known as the ion-partition effect and is expected to be more relevant for porous media characterized by higher solid skeleton charge concentrations.

3.4.1 Equilibrium conditions

When an electrically charged porous medium is placed in contact with an external bulk solution that contains the same ions that are present in the pore solution, a thermodynamic equilibrium condition is reached, after a certain period of time, in which the water chemical potential and the ion electrochemical potentials between the two solutions are equal. The external bulk solution can be considered as a "chemical thermometer" in order to evaluate the equilibrium conditions of the porous medium (Coussy, 2004). The electroneutrality condition in the external solution is given by:

$$z_1 c_1 + z_2 c_2 = 0 \tag{3.2}$$

where c_1 and c_2 are the molar concentrations of the cation and the anion that are contained in the bulk solution.

It is convenient to define the salt concentration, c_s, of the external solution as follows:

$$c_s = \frac{c_1}{\nu_1} = \frac{c_2}{\nu_2} \tag{3.3}$$

Using Eq. (3.3), the electroneutrality condition, Eq. (3.2), provides the relation between the electrochemical valences and the stoichiometric coefficients:

$$z_1 \nu_1 + z_2 \nu_2 = 0 . \tag{3.4}$$

As a result, the equilibrium condition can be characterized by the following state variables of the external bulk solution: the absolute temperature, T, the hydraulic pressure (referenced to the atmospheric pressure, as is usual in soil mechanics), u,

and the salt concentration, c_s. The corresponding variables of the pore solution can be evaluated from the following conditions:

$$\overline{T} = T \tag{3.5}$$

$$\overline{\mu}_w = \mu_w \tag{3.6}$$

$$\overline{\mu}_i^{ec} = \mu_i^{ec} \qquad i = 1,2 \tag{3.7}$$

where $\overline{T}$ and T are the absolute temperature in the pore solution and in the external bulk solution, respectively; $\overline{\mu}_w$ and μ_w are the water chemical potential in the pore solution and in the external bulk solution, respectively; $\overline{\mu}_i^{ec}$ and μ_i^{ec} are the electrochemical potentials of the i-th ion in the pore solution and in the external bulk solution, respectively.

The water chemical potential, μ_w, and the ion electrochemical potentials, μ_i^{ec}, of the external solution can be related to the hydraulic pressure, u, and the salt concentration, c_s, for a dilute solution, as follows (Katchalsky and Curran, 1965; Dominijanni and Manassero, 2012a):

$$\mu_w = \mu_w^0(T) + \frac{(u - \Pi)}{c_w} \tag{3.8}$$

$$\mu_i^{ec} = \mu_i + z_i F\varphi = \mu_i^0(T) + RT\ln(\nu_i c_s) + z_i F\varphi \qquad i = 1,2 \tag{3.9}$$

where μ_w^0 and μ_i^0 are integration constants that only depend on the absolute temperature T; c_w is the water molar concentration; $\Pi = RT\sum_{i=1}^{2}\nu_i c_s$ is the osmotic pressure; μ_i is the chemical potential of the i-th ion; R is the universal gas constant ($8.314\ J\cdot mol^{-1}\cdot K^{-1}$); and φ is the electric potential.

The state variables in the external bulk solution can be measured easily, whereas it is very difficult to determine the corresponding variables in the pore solution. Moreover, the relations obtained by linking the chemical potentials to the state variables of the pore solution are more uncertain, due to the interaction with the

solid skeleton charge, which alters the ion concentration distribution near the solid particles. The simplest assumption that can be adopted involves using analogous relations to Eqs. (3.8) and (3.9) as they are also considered valid for the pore solution. This assumption, which was first proposed by Donnan (1911), neglects the microscopic deviations of the ion concentrations from their average values that are induced by the electric potential distribution within the pores. If this approximation is accepted, the water chemical potential, $\overline{\mu}_w$, and the ion electrochemical potentials, $\overline{\mu}_i^{ec}$, of the pore solution can be expressed as follows:

$$\overline{\mu}_w = \overline{\mu}_w^0(T) + \frac{(\overline{u} - \overline{\Pi})}{\overline{c}_w} \tag{3.10}$$

$$\overline{\mu}_i^{ec} = \overline{\mu}_i + z_i F\overline{\varphi} = \overline{\mu}_i^0(T) + RT\ln(\overline{c}_i) + z_i F\overline{\varphi} \qquad i = 1,2 \tag{3.11}$$

where $\overline{\mu}_w^0$ and $\overline{\mu}_i^0$ are integration constants that only depend on the absolute temperature T; $\overline{c}_w$ is the molar concentration of the water in the pore solution, which can be taken equal to the molar concentration of the water in the external bulk solution, i.e. $\overline{c}_w \cong c_w$; $\overline{\Pi} = RT\sum_{i=1}^{2}\overline{c}_i$ is the osmotic pressure of the pore solution; $\overline{\mu}_i$ is the chemical potential of the i-th ion in the pore solution; and $\overline{\varphi}$ is the electric potential in the pore solution.

The hydraulic pressure of the pore solution, $\overline{u}$, and the ion partition factors, Γ_i, defined as the ratio between the ion concentration of the pore solution and the ion concentration of the external bulk solution, can therefore be expressed on the basis of Eqs. (3.6) and (3.7), and using Eqs. (3.8)-(3.11), as follows:

$$\overline{u} = u + (\overline{\Pi} - \Pi) \tag{3.12}$$

$$\Gamma_i = \frac{\overline{c}_i}{c_i} = \frac{\overline{c}_i}{\nu_i c_s} = \exp\left(-z_i \frac{F}{RT}\overline{\psi}\right) \qquad i = 1,2 \tag{3.13}$$

where $\overline{\psi} = \overline{\varphi} - \varphi$ is the electric potential of the porous medium, which is also called Donnan's potential.

On the basis of this approach, the hydraulic pressure of the pore solution is different from the hydraulic pressure of the external solution that is in equilibrium with it. The pressure difference between the pore solution and the external solution is called the swelling pressure, u_{sw}, and is given by:

$$u_{sw} = \overline{\Pi} - \Pi \,. \tag{3.14}$$

Eqs. (3.12) and (3.13) for i = 1.2, together with Eq. (3.1), constitute a set of four equations that can be solved to find the four unknown variables: the hydraulic pressure, $\overline{u}$, the ion concentrations, $\overline{c}_i$ for i = 1.2, and the electric potential, $\overline{\psi}$.

When the ion electrochemical valences are both unitary, such as for NaCl, Eq. (3.13) implies that

$$\Gamma_1 = \Gamma_2^{-1} \,. \tag{3.15}$$

Inserting Eq. (3.15) into Eq. (3.1) results in the following equation:

$$\Gamma_2^{-1} - \Gamma_2 - \frac{\overline{c}_{sk,0}}{e \cdot c_s} = 0 \,, \tag{3.16}$$

which has a positive solution of the following form:

$$\Gamma_2 = -\frac{\overline{c}_{sk,0}}{2 \cdot e \cdot c_s} + \sqrt{\left(\frac{\overline{c}_{sk,0}}{2 \cdot e \cdot c_s} \right)^2 + 1} \tag{3.17}$$

and

$$\Gamma_1 = \Gamma_2^{-1} = \frac{\overline{c}_{sk,0}}{2 \cdot e \cdot c_s} + \sqrt{\left(\frac{\overline{c}_{sk,0}}{2 \cdot e \cdot c_s} \right)^2 + 1} \,. \tag{3.18}$$

On the basis of Eqs. (3.17) and (3.18), the swelling pressure can be expressed as follows:

$$u_{sw} = RTc_s\left(\Gamma_1 + \Gamma_2 - 2\right) = 2RTc_s\left[\sqrt{\left(\frac{\overline{c}_{sk,0}}{2\cdot e\cdot c_s}\right)^2 + 1} - 1\right]. \tag{3.19}$$

Change in equilibrium

When the hydraulic pressure and/or the salt concentration are changed in the external bulk solution, a new equilibrium condition is restored in the porous medium after a sufficiently long period of time. In order to evaluate this new condition, the change in the free energy per unit initial (undeformed) volume of the porous medium, $\Im_V$, can be determined by assuming that it is a function of the macroscopic strain tensor, $\boldsymbol{\varepsilon}$, and the concentration of each fluid component (Dormieux et al., 2003). A second assumption that can be made refers to the reversible mechanical behaviour of the solid constituents: in such a case, the intrinsic dissipation, due to the solid skeleton strains, is zero (Dormieux et al. 2003; Dominijanni and Manassero, 2012a). On the basis of these assumptions, the increment in free energy per unit initial volume, under isothermal conditions, can be expressed as follows:

$$d\Im_V = \boldsymbol{\sigma} : d\boldsymbol{\varepsilon} + \sum_{k=w,1}^{2} \overline{\mu}_k \frac{d(e\cdot\overline{c}_k)}{1+e_0} \tag{3.20}$$

where $\boldsymbol{\sigma}$ is the total stress tensor and e_0 is the initial void ratio.

In Eq. (3.20), the chemical potentials of the pore solution, $\overline{\mu}_i$, can be substituted by the electrochemical potentials, $\overline{\mu}_i^{ec}$, since the adding term given by

$$F\cdot\overline{\varphi}\left\{\frac{d\left[e\cdot(z_1\overline{c}_1 + z_2\overline{c}_2)\right]}{1+e_0}\right\} = F\cdot\overline{\varphi}\cdot\frac{d\overline{c}_{sk,0}}{1+e_0}$$

is null, if the solid skeleton charge, $\overline{c}_{sk,0}$, is assumed constant.

Then, applying Eqs. (3.6) and (3.7), the water chemical potential and the ion electrochemical potentials in the pore solution can be substituted by the

corresponding potentials in the external solution. If the electroneutrality condition, Eq. (3.2), is taken into account, the ion electrochemical potentials of the bulk solution can be substituted by the ion chemical potentials. As a result, $d\Im_V$ can be expressed using the readily available chemical potentials of the external bulk solution, instead of the chemical potentials of the pore solution. If the analysis is restricted to a unidimensional geometry, Eq. (3.20) becomes:

$$d\Im_V = \sigma \cdot d\varepsilon + \sum_{k=w,1}^{2} \mu_k \frac{d(e \cdot \overline{c}_k)}{1+e_0}. \tag{3.21}$$

The free energy of the solid skeleton, which accounts for the interaction with the fluid phase, $\Im_V^{sk}$, can be derived by subtracting, from $\Im_V$, the free energy of the fluid phase that is given as a function of the specific free energies of the components of the external bulk solution, F_k (k = w,1,2):

$$\Im_V^{sk} = \Im_V - \frac{e}{1+e_0} \sum_{k=w,1}^{2} (\overline{c}_k \cdot F_k). \tag{3.22}$$

The free energy change, due to the interaction between the solid skeleton charge and the ions in the pore solution, is included in $\Im_V^{sk}$ because the specific free energy of the equilibrium bulk solution is subtracted from $\Im_V$, instead of the specific free energy of the pore solution.

Using the following thermodynamic relations:

$$\mu_k = F_k + \frac{u_k}{c_k} \qquad k = w,1,2 \tag{3.23}$$

$$d\mu_k = \frac{du_k}{c_k} \qquad k = w,1,2 \tag{3.24}$$

$$dF_k = -u_k d\left(\frac{1}{c_k}\right) \qquad k = w,1,2 \tag{3.25}$$

where u_k represents the partial pressure of the k-th component of the bulk solution, the change in $\Im_V^{sk}$ can be expressed as follows:

$$d\Im_V^{sk} = \sigma \cdot d\varepsilon + \sum_{k=w,1}^{2} \frac{u_k}{1+e_0} d\left(\frac{e \cdot \overline{c}_k}{c_k} \right). \tag{3.26}$$

Observing that $\overline{c}_w \cong c_w$ and

$$u_w = u - \Pi, \tag{3.27}$$

where the osmotic pressure represents the sum of the ion partial pressures,

$$\Pi = \sum_{i=1}^{2} u_i, \tag{3.28}$$

the increment $d\Im_V^{sk}$ can be expressed as follows:

$$d\Im_V^{sk} = \sigma \cdot d\varepsilon + (u - \Pi) \frac{de}{1+e_0} + \sum_{i=1}^{2} \frac{u_i}{1+e_0} d\left(\frac{e \cdot \overline{c}_i}{c_i} \right). \tag{3.29}$$

For infinitesimal strains, assuming that the solid component is incompressible,

$$d\varepsilon = -\frac{de}{1+e_0} \tag{3.30}$$

and, as a consequence, Eq. (3.29) can be expressed as follows:

$$d\Im_V^{sk} = \left[\sigma - (u - \Pi) \right] \cdot d\varepsilon + \sum_{i=1}^{2} \frac{u_i}{1+e_0} d\left(\frac{e \cdot \overline{c}_i}{c_i} \right) \tag{3.31}$$

In order to derive the mechanical constitutive equations, it is convenient to work with the Gibbs free energy, $\mathcal{G}_V^{sk}$, which is the following Legendre transform of $\Im_V^{sk}$:

$$\mathcal{G}_V^{sk} = \left[\sigma - (u - \Pi) \right] \cdot \varepsilon + \sum_{i=1}^{2} \frac{e}{1+e_0} u_i \frac{\overline{c}_i}{c_i} - \Im_V^{sk}. \tag{3.32}$$

Taking into account Eqs. (3.31) and (3.24), the infinitesimal increment in $\mathcal{G}_V^{sk}$ is given by:

$$\begin{aligned} d\mathcal{G}_V^{sk} &= \varepsilon \cdot \left[d\sigma - (du - d\Pi) \right] + \sum_{i=1}^{2} \frac{e \cdot \overline{c}_i}{1+e_0} d\mu_i = \\ &= \varepsilon \cdot \left[d\sigma - (du - d\Pi) \right] + \left[\frac{e \cdot (\overline{c}_1 + \overline{c}_2)}{1+e_0} \right] \frac{1}{\nu_1 + \nu_2} d\mu_s \end{aligned} , \tag{3.33}$$

where $d\mu_s$ is the salt chemical potential increment, which is defined as follows:

$$d\mu_s = \nu_1 \cdot d\mu_1 + \nu_2 \cdot d\mu_2 = \frac{1}{c_s} d\Pi . \tag{3.34}$$

The function $\mathcal{G}_V^{sk}$ can be considered to depend on the variables $\left[\sigma - (u - \Pi) \right]$ and μ_s; therefore the simplest constitutive equations that can be inferred are:

$$d\varepsilon = \beta_{vv} \cdot \left[d\sigma - (du - d\Pi) \right] + \beta_{vs} \cdot d\mu_s \tag{3.35}$$

$$\frac{d\left[e \cdot (\overline{c}_1 + \overline{c}_2) \right]}{(\nu_1 + \nu_2)(1+e_0)} = \beta_{sv} \left[d\sigma - (du - d\Pi) \right] + \beta_{ss} \cdot d\mu_s \tag{3.36}$$

Symmetry of the coefficients, i.e. $\beta_{vs} = \beta_{sv}$, can be demonstrated by considering $\mathcal{G}_V^{sk}$ as a continuous function of the variables $\left[\sigma - (u - \Pi) \right]$ and μ_s (Dominijanni and Manassero, 2012a).

Eq. (3.35) can also be expressed in the following form:

$$d\sigma - du - du_{sw} = M \cdot d\varepsilon \tag{3.37}$$

where $M = \frac{1}{\beta_{vv}}$ is the one-dimensional elastic modulus of the porous medium and du_{sw} represents the swelling pressure increment, which is given by:

$$du_{sw} = -\varpi \cdot d\Pi , \tag{3.38}$$

where $\varpi = 1 + \frac{\beta_{vs}}{\beta_{vv} \cdot c_s}$ is the swelling coefficient (Dominijanni and Manassero 2012a).

Since it is known, from experimental observations, that the swelling pressure tends to zero when $c_s \to \infty$, the swelling pressure, u_{sw}, can be obtained as follows:

$$u_{sw} = \int_{\Pi}^{\infty} \varpi \cdot d\Pi . \tag{3.39}$$

The effective stress principle can be restored, on the basis of Eq. (3.37), if the effective stress increment, $d\sigma'$, is defined as follows:

$$d\sigma' = d\sigma - du - du_{sw} \tag{3.40}$$

The classical definition of effective stress, $d\sigma' = d\sigma - du$, corresponds to the particular case for which $du_{sw} = 0$, i.e. $\varpi = 0$ and $\beta_{vs} = -\beta_{vv} \cdot c_s$.

Adopting Donnan's assumptions and using Eq. (3.14), the swelling coefficient can be expressed as follows:

$$\varpi = 1 - \frac{d\bar{\Pi}}{d\Pi} . \tag{3.41}$$

Dominijanni and Manassero (2012b) have demonstrated that Eq. (3.41) can also be expressed in the following form:

$$\varpi = 1 - \frac{d\bar{\Pi}}{d\Pi} = 1 - \frac{\nu_1 + \nu_2}{\nu_1 \Gamma_2 + \nu_2 \Gamma_1} \Gamma_1 \Gamma_2 . \tag{3.42}$$

3.4.2 Transport equations

If clay is interposed between two reservoirs with different hydraulic pressures or ion concentrations, a pore solution volumetric flux, q, and an ion mass flux, J_i, relative

to the solid skeleton, are generated. In order to derive appropriate flux equations, the linear momentum balance equations of the fluid components can be developed on the basis of a number of assumptions. If only unidimensional problems are considered and inertial effects are neglected, these equations can be expressed as follows (Ehlers, 2002; Dominijanni and Manassero, 2010):

$$-\frac{\partial(n\cdot\overline{u}_w)}{\partial x}+f_w=m_w \tag{3.43}$$

$$-\frac{\partial(n\cdot\overline{u}_i)}{\partial x}+f_i=m_i \qquad i=1,2 \tag{3.44}$$

where n is the porosity, x is the spatial coordinate, f_w is the external force per unit volume acting on the water, m_w is the momentum supply of water, f_i is the external force per unit volume acting on the i-th ion and m_i is the momentum supply of the i-th ion.

The external forces are gravity, which can be considered to only act on the solvent (i.e. water) in the x direction, and the electric force, which is proportional to the electric potential gradient:

$$f_w=n\cdot\rho_w\cdot g \tag{3.45}$$

$$f_i=-n\cdot\overline{c}_i\cdot z_i\cdot F\cdot\frac{\partial\overline{\varphi}}{\partial x} \qquad i=1,2 \tag{3.46}$$

where ρ_w is the water density and g is the gravity acceleration.

The momentum supply of the fluid components can be expressed as follows:

$$m_k=-\overline{u}_k\nabla n+m_k^E \qquad k=w,1,2 \tag{3.47}$$

where m_k^E represents the extra-momentum supply of the k-th fluid component, which can be associated with the friction between the porous medium components that move with different velocities.

If the extra-momentum supply is associated with the frictional force per unit volume exchanged with the other components of the porous medium, it can be assumed to be equal to the sum of the binary interactions:

$$m_w^E = m_{w,sk}^E + \sum_{i=1}^{2} m_{w,i}^E \tag{3.48}$$

$$m_i^E = m_{i,w}^E + m_{i,j}^E + m_{i,sk}^E \qquad i,j = 1,2;\ i \neq j \tag{3.49}$$

where w is the water, sk the solid skeleton, and i and j are the i-th and j-th ions. The friction between the ions and between the ions and the solid skeleton can be considered negligible for a dilute solution compared to the friction between the ions and the solvent:

$$m_{i,j}^E\ ;\ m_{i,sk}^E << m_{i,w}^E \qquad i,j = 1,2;\ i \neq j$$

$$m_i^E \cong m_{i,w}^E \qquad i = 1,2 \tag{3.50}$$

Moreover, on the basis of the assumption of binary interaction, it can be assumed that

$$m_{w,i}^E = -m_{i,w}^E \qquad i = 1,2\,. \tag{3.51}$$

For the friction forces per unit volume, the following constitutive equations can be adopted:

$$m_{w,sk}^E = \alpha \cdot n \cdot (v_w - v_{sk}) = \alpha \cdot q \tag{3.52}$$

$$m_{i,w}^E = -m_{w,i}^E = \beta_i \cdot n \cdot \overline{c}_i \cdot (v_i - v_w) \qquad i = 1,2 \tag{3.53}$$

where α and β_i are friction coefficients, while v_w, v_{sk} and v_i are the water, solid skeleton and i-th ion velocities, respectively.

The factors n and $(v_w - v_{sk})$ in Eq. (3.52), as well as $n \cdot \overline{c}_i$ and $(v_i - v_w)$ in Eq. (3.53), have been picked out as an indication of the fact that $m_{w,sk}^E = 0$ if $n = 0$ or

$(v_w - v_{sk}) = 0$, and $m^E_{i,w} = 0$ if $n \cdot \bar{c}_i = 0$ or $(v_i - v_w) = 0$. However, this does not mean that the friction coefficients α and β_i are independent of n, $\bar{c}_i$ and the relative velocities.

Taking into account these constitutive assumptions, and using the thermodynamic relation that relates the chemical potentials to the partial pressure

$$d\bar{\mu}_k = \frac{d\bar{u}_k}{\bar{c}_k} \qquad k = w, 1, 2, \tag{3.54}$$

the following flux equations can be derived from Eqs. (3.43) and (3.44):

$$q = n(v_w - v_{sk}) = -\frac{n}{\alpha}\left(\bar{c}_w \frac{\partial \bar{\mu}_w}{\partial x} - \rho_w g + \sum_{i=1}^{2} \bar{c}_i \frac{\partial \bar{\mu}_i^{ec}}{\partial x} \right) \tag{3.55}$$

$$J_i = n\bar{c}_i (v_i - v_{sk}) = q\bar{c}_i - n\frac{D_i}{RT}\bar{c}_i \frac{\partial \bar{\mu}_i^{ec}}{\partial x} \qquad i = 1, 2 \tag{3.56}$$

where $D_i = \frac{RT}{\beta_i}$ represents the macroscopic diffusion coefficient of the i-th ion.

At this point, it is convenient to introduce the concept of a virtual external bulk solution that is in thermodynamic equilibrium with the pore solution at the generic position x within the porous medium (Dormieux et al., 1995; Yaroshchuk, 1995). The virtual solution coincides with the real bulk solutions in contact with the porous medium at the boundaries. The thermodynamic potentials in Eqs. (3.55) and (3.56) can be substituted with the corresponding potentials of this virtual solution, using Eqs. (3.6) and(3.7). This leads to a formulation that does not depend on the determination of the pore solution variables. Therefore, Eqs. (3.55) and (3.56) can be expressed as follows:

$$q = -\frac{n}{\alpha}\left(\frac{\partial u}{\partial x} - \frac{\partial \Pi}{\partial x} - \rho_w g + RT \sum_{i=1}^{2} \Gamma_i \frac{\partial c_i}{\partial x} + F \frac{\bar{c}_{sk,0}}{e} \frac{\partial \varphi}{\partial x} \right) \tag{3.57}$$

$$J_i = q\Gamma_i c_i - nD_i\Gamma_i \frac{\partial c_i}{\partial x} - z_i \Gamma_i c_i \frac{nD_i}{RT} F \frac{\partial \varphi}{\partial x} \qquad i = 1, 2. \tag{3.58}$$

If an external electric current is not applied to the porous medium, the electric potential derivative in Eqs. (3.57) and (3.58) can be eliminated by means of the condition of electric current, I_e, equal to zero:

$$I_e = F\sum_{i=1}^{2} z_i J_i = 0 . \tag{3.59}$$

The resulting flux equations can be expressed as follows:

$$q = -\frac{k}{\gamma_w}\left(\frac{\partial u}{\partial x} - \omega\frac{\partial \Pi}{\partial x}\right) \tag{3.60}$$

$$J_s = (1-\omega)qc_s - nD_\omega^* \frac{\partial c_s}{\partial x} \tag{3.61}$$

where

$$k = \frac{n\cdot\gamma_w}{\alpha\left[1+\frac{RT}{\alpha}\frac{(\Gamma_1-\Gamma_2)^2\nu_1\nu_2 c_s}{\nu_1\Gamma_2 D_2+\nu_2\Gamma_1 D_1}\right]} = \text{hydraulic conductivity;} \tag{3.62}$$

$$\omega = 1-\frac{\nu_1 D_2+\nu_2 D_1}{\nu_1\Gamma_2 D_2+\nu_2\Gamma_1 D_1}\Gamma_1\Gamma_2 = \text{reflection coefficient;} \tag{3.63}$$

$$J_s = \frac{J_1}{\nu_1} = \frac{J_2}{\nu_2} = \text{salt molar flux} \tag{3.64}$$

$$D_\omega^* = (1-\omega)\cdot D_s = \text{osmotic effective diffusion coefficient;} \tag{3.65}$$

$$D_s = \frac{(\nu_1+\nu_2)D_1 D_2}{\nu_1 D_2+\nu_2 D_1} = \text{macroscopic salt diffusion coefficient.} \tag{3.66}$$

Dominijanni and Manassero (2012b) have demonstrated that, if the microscopic deviations of the variables from their average values are assumed to be negligible, the macroscopic ion diffusion coefficients, D_i, result to be equal to the ion effective diffusion coefficients, D_i^*:

$$D_i = D_i^* = \tau_m D_{i,0} \qquad i = 1,2 \tag{3.67}$$

$$D_s = D_s^* = \frac{(\nu_1 + \nu_2) D_1^* D_2^*}{\nu_1 D_2^* + \nu_2 D_1^*} = \tau_m \frac{(\nu_1 + \nu_2) D_{1,0} D_{2,0}}{\nu_1 D_{2,0} + \nu_2 D_{1,0}} = \tau_m D_{s,0} \tag{3.68}$$

where τ_m is the dimensionless matrix tortuosity factor that accounts for the tortuous nature of the actual diffusive pathway through the porous medium (Malusis and ShacKelford, 2002b), $D_{i,0}$ is the free (aqueous) solution diffusion coefficient of the i-th ion, D_s^* is the salt effective diffusion coefficient and $D_{s,0}$ is the free solution diffusion coefficient of the salt.

An interesting observation is that the reflection coefficient, ω, results to be equal to the swelling pressure coefficient, ϖ, when the ion free solution diffusion coefficients are equal.

When the solid skeleton electric charge is equal to zero, the ion partition coefficients, Γ_i, are equal to 1 and Eqs. (3.60) and (3.61) reduce to the Darcy equation and the classical advective-diffusion equation, respectively.

The osmotic effective diffusion coefficient, D_ω^*, results to be related to the reflection coefficient, ω, through Eq. (3.65), so that $D_\omega^* = 0$ when $\omega = 1$. As a result, the condition $\omega = 1$ implies a null salt flux through the porous medium, which, in this case, can be said to act as a "perfect" or "ideal" barrier.

If Eq. (3.65) is compared with the expression of D_ω^* proposed by Malusis and Shackelford (2002b) and Malusis et al. (2012):

$$D_\omega^* = \tau_r D_s^* \tag{3.69}$$

where τ_r is the restrictive tortuosity factor, τ_r results to be given by:

$$\tau_r = (1 - \omega) \frac{D_s}{D_s^*} . \tag{3.70}$$

Moreover, if the hypotheses implied by Eq. (3.68) are adopted, the expression of τ_r reduces to:

$$\tau_r = (1-\omega)\,. \tag{3.71}$$

The coefficient k can be measured, under steady state conditions, using traditional permeameters. Malusis et al. (2001) developed a testing apparatus to determine ω and D^*_ω. This apparatus is able to impose the condition of no-volumetric flux (q = 0) through a soil sample in contact with two external solutions, maintained at constant salt concentrations, so that the global or averaged values of the coefficients can be measured. The global values of ω and D^*_ω are defined as follows (Auclair et al., 2002):

$$\omega_g = \frac{1}{\Delta c_s}\int_{c_b}^{c_t} \omega \cdot dc_s \tag{3.72}$$

$$D^*_{\omega g} = \frac{1}{\Delta c_s}\int_{c_b}^{c_t} D^*_\omega \cdot dc_s \tag{3.73}$$

where c_t and c_b represent the salt concentration at the top and the bottom boundaries of the clay sample, respectively, and $\Delta c_s = c_t - c_b$ is their difference. These coefficients can be determined by means of the following relations under steady state conditions:

$$\omega_g = \left(\frac{\Delta u}{\Delta \Pi}\right)_{q=0} \tag{3.74}$$

$$D^*_{\omega g} = \frac{L}{n}\left(\frac{J_s}{\Delta c_s}\right)_{q=0} \tag{3.75}$$

where $\Delta u = u_t - u_b$ and $\Delta \Pi = \Pi_t - \Pi_b$ represent the differences between the hydraulic pressure and the osmotic pressure at the boundaries of the clay sample, and L is the length of the sample.

It is interesting to observe that the relationship between D^*_ω and ω is also maintained between their corresponding global values: in fact, inserting Eq. (3.65) into Eq. (3.73) with $D_s = D^*_s$ leads to:

$$D^*_{\omega g} = (1-\omega_g)\cdot D^*_s = (1-\omega_g)\cdot \tau_m \cdot D_{s,0}\,. \tag{3.76}$$

In the case of a salt constituted by monovalent ions, inserting Eq. (3.63) into Eq. (3.72) and using Eqs. (3.17) and (3.18), the following expression of ω_g is obtained:

$$\omega_g = 1+\frac{\overline{c}_{sk,0}}{2\cdot \Delta c_s \cdot e}\left[Z_2 - Z_1 - (2t_1-1)\cdot \ln\left(\frac{Z_2+2t_1-1}{Z_1+2t_1-1}\right)\right] \tag{3.77}$$

where

$$t_1 = \frac{D_{1,0}}{D_{1,0}+D_{2,0}} = \text{cation transport number,} \tag{3.78}$$

$$Z_1 = \sqrt{1+\left(\frac{2\cdot c_t \cdot e}{\overline{c}_{sk,0}}\right)^2}\,, \tag{3.79}$$

$$Z_2 = \sqrt{1+\left(\frac{2\cdot c_b \cdot e}{\overline{c}_{sk,0}}\right)^2}\,. \tag{3.80}$$

3.5 MATERIALS AND METHODS

3.5.1 Materials

The powdered bentonite tested in this study is an Indian sodium bentonite that is used for the production of a needle-punched GCL. The bentonite is characterized by a cation exchange capacity (CEC, measured using the methylene blue adsorption method) of 105 meq/100g. The mineralogical composition, evaluated through x-ray diffraction analysis, indicates a bentonite that is primarily composed of smectite (> 98%) with traces of calcite, quartz, mica and gypsum.

The bentonite is characterized by a liquid limit (LL) of 525% and a hydraulic conductivity of $8 \cdot 10^{-12}$ m/s, measured at a 27.5 kPa confining effective stress using de-ionized water as the permeant liquid.

Sodium solutions were prepared with sodium chloride (ACS reagent, purity ≥ 99%) and de-ionized water (DW). The sodium solutions were prepared at different molarity values, in the 5 mM to 100 mM range, with the aim of investigating the effect of the monovalent cations on the osmotic behaviour of the bentonite. The DW (pH = 6.95; EC at 20 °C = 0.6 mS/m) consisted of tap water processed through a series of activated carbon filters, a reverse osmosis process and, finally, a UV lamp (Elix Water Purification system). Moreover, the DW was deaerated prior to use. The electrical conductivity (EC) measured at 20 °C for the NaCl solutions ranged from 60.5 mS/m to 1.1 mS/m.

3.5.1.1 Bentonite preparation.

Prior to the osmotic property determination, the bentonite was submitted to a process with the aim of removing the soluble salts, mainly sodium, which are naturally present inside the material, due to its marine origin. The treatment prevents soluble salts from interfering with the determination of the osmotic properties.

Previous studies (Malusis et al., 2001; Malusis and Shackelford, 2002a, 2002b; Shackelford and Lee, 2003; Yeo et al., 2005; Kang and Shackelford, 2009; Di Emidio 2010) have used the *'flushing'* method to remove soluble salts. This method consists of an initial permeation phase, performed under back pressure, which

requires a long period of time (i.e. from months to a year), because of the low bentonite hydraulic conductivity.

In this study, the *'squeezing'* method has been used with the aim of reducing the salt removal time. The *'squeezing'* method consists of a series of consecutive phases of powder bentonite hydration with DW, at a higher water content than the liquid limit, and drained consolidation, performed in a consolidometer under a maximum load of 500 kPa. Moreover, the drained solution is sampled daily and the EC is monitored to evaluate the soluble salt concentration in the bentonite pore water. After the *'squeezing'* process, the material is oven dried at 105 °C and pulverized once again. When a 5 L consolidometer is used, the above procedure can produce about 500 g of squeezed dry powder bentonite, characterized by a lower EC value than 50 mS/m, in 40-50 days. The results of the EC monitoring during the squeezing process are reported in Fig. 3.1.

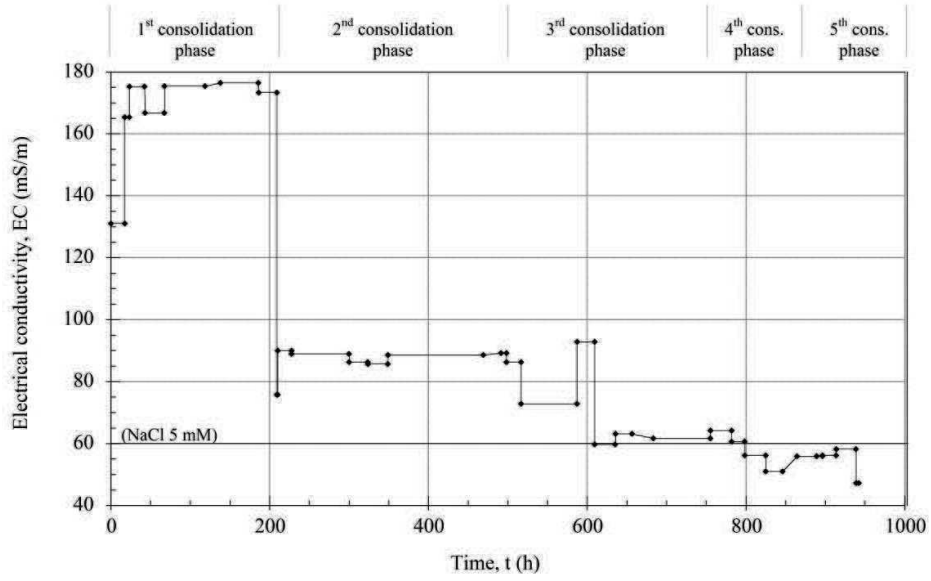

Figure 3.1 - Electrical conductivity as a function of time during the squeezing process.

The specimen for the chemico-osmotic test is prepared by rehydrating the squeezed bentonite with DW at a lower water content than the liquid limit value and then by

statically compacting the material in a compaction mould, while allowing the excess water to be released.

Dry powder bentonite is required for the swelling pressure test.

3.5.2. Testing apparatus and procedures

3.5.2.1 Chemico-osmotic test.

The testing apparatus used to measure the global reflection coefficient and the global osmotic effective diffusion coefficient is described in detail in Malusis et al. (2001). The main components of the apparatus, shown in Fig. 3.2, include the osmotic cell, the flow-pump system, the pressure transducer, which is used to measure the differential pressure that develops across the specimen during the test, and the data acquisition system.

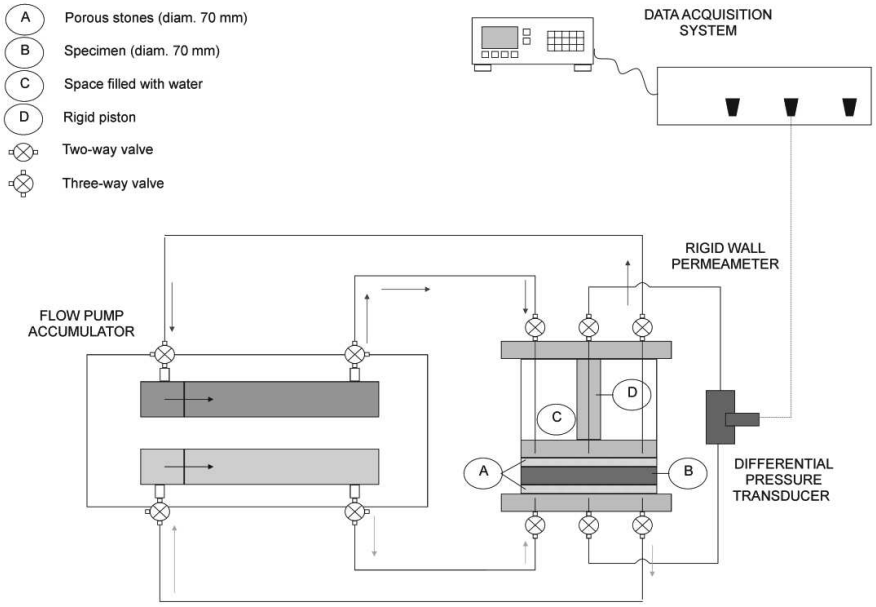

Figure 3.2 - Schematic view of the chemico-osmotic test apparatus. More details on this apparatus can be found in Malusis et al. (2001).

The cell consists of a modified rigid wall permeameter, in which the top piston and the bottom pedestal are equipped with three ports each: two enable the different

solutions to circulate through the top (NaCl solution) and the bottom (DW) porous stones with the aim of establishing a constant concentration gradient across the specimen. The third port is installed in both the top piston and the bottom pedestal to allow the differential pressure across the specimen to be measured.

The flow-pump system, which consists of a dual-carriage syringe pump and two stainless steel accumulators (Model 33 - Twin syringe pump, produced by Harvard, Holliston, MA), prevents the volumetric flux through the specimen by simultaneously injecting into and withdrawing from the porous stones the same volume of solution. In order to obtain this result, the syringes have to move at the same rate.

The test was performed according to the procedure proposed by Malusius et al. (2001): a solution containing a known electrolyte concentration (NaCl) was circulated in the top porous stone, while DW was circulated in the bottom porous stone. The concentration difference across the specimen was maintained constant by continuously infusing the two liquids at the boundaries of the specimen.

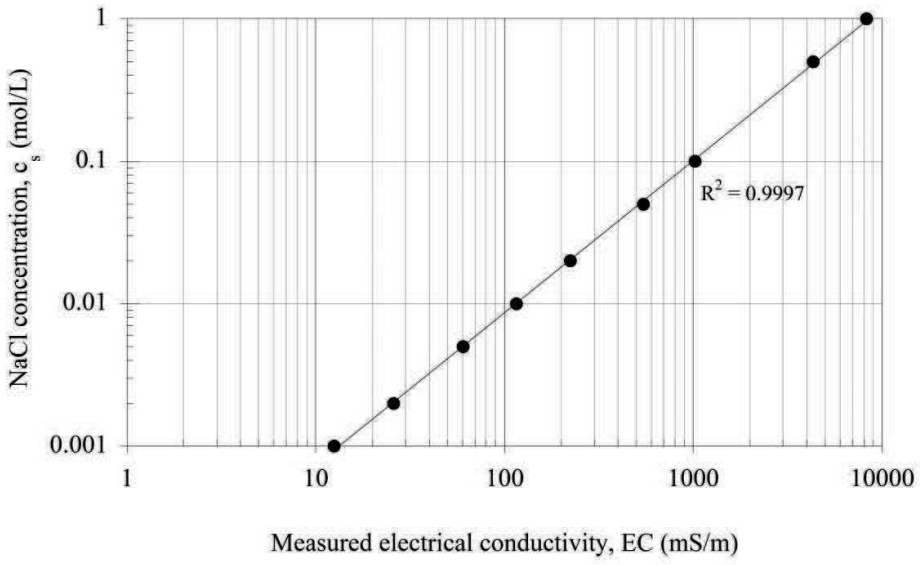

Figure 3.3 - Calibration of the sodium chloride concentration with electrical conductivity. R^2 is the coefficient of determination of the regression line.

Since the specimen was preliminary squeezed with DW to remove the soluble salts, the EC of the electrolyte solutions in the flux exiting from the porous stones at the steady state was induced solely by the contributions of Cl^- and Na^+ ions. Moreover, the calibration reported in Fig. 3.3 shows that the relation between the EC and solution molarity was linear over the concentration range examined in the study. As a consequence, the EC of the withdrawn fluxes (i.e. from the top and bottom porous stones, respectively) was monitored by sampling the solution contained in the pistons, and the NaCl molar concentration was derived using a linear relation. Since the volumetric flux through the specimen was hindered, the global reflection coefficient could be calculated using Eq. (3.74).

The diffusive solute flux through the specimen was calculated for the n-th sampling interval as follows

$$J_s^n = \frac{\sum_{m=1}^{n}\left(c_s^m \cdot \Delta V^m\right)}{A_S \cdot \Delta t^n} = \frac{\Delta Q^n}{\Delta t^n} \tag{3.81}$$

where c_s^n is the solute molar concentration measured by sampling the solution coming out from the bottom porous stone, ΔV^m is the volume of the solution circulating in the porous stones in the Δt^m interval, A_S is the cross-section of the specimen and ΔQ^n is the cumulative salt molar mass per unit area that passed through the specimen. The global osmotic effective diffusion coefficient, $D_{\omega g}^*$, is calculated at the steady state as follows:

$$D_{\omega g}^* = \frac{\Delta Q}{\Delta t} \cdot \frac{L}{n \cdot \left(c_{t,avg} - c_{b,avg}\right)} \tag{3.82}$$

where $c_{t,avg}$ and $c_{b,avg}$ are the average top and bottom salt concentrations, respectively.

3.5.2.2 Swelling pressure test.

The swelling pressure apparatus, shown in Fig. 3.4, primarily consists of a stainless steel oedometer cell, a NaCl solution supply tank that is placed above the pressure panel, a displacement transducer connected to the cell top piston, which is used to measure the axial strains of the specimen, a load cell and a data acquisition system.

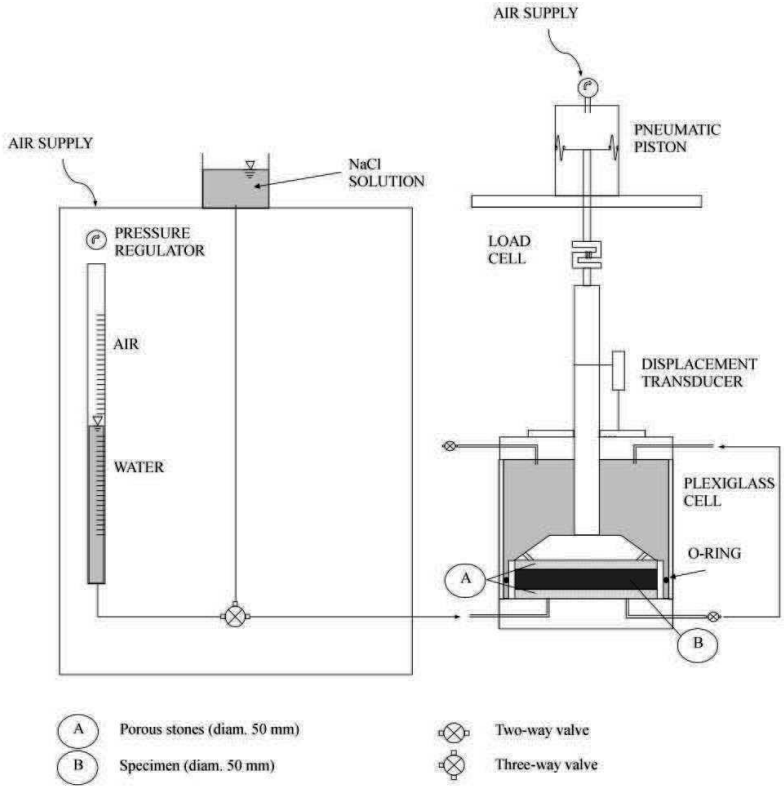

Figure 3.4 - Schematic view of the swelling pressure apparatus.

The swelling pressure apparatus consists of a rigid cell that confines the sample (i.e. the oedometer), which allows access to the water through both porous stones. The cell is connected to a pressure panel that allows the specimen to be back-pressurized. The rigid piston above the upper porous stone is connected to the load cell, which

measures the pressure that has to be applied in order to hinder the axial strain of the specimen.

The test procedure requires a known amount of dry material to be dusted inside the oedometer ring, the cell to be assembled and a NaCl solution to be supplied. The specimen, which is characterized by an initial dry height of 5 mm, is allowed to swell to 10 mm. The piston is then blocked, the sample is back-pressured and the steady state swelling pressure is recorded after a short transitional phase.

Since the bentonite that is initially dusted inside the oedometer is dry, the pressure increases for a number of days, during the hydration phase, and the steady state swelling pressure is reached when hydration has been completed.

3.6 RESULTS

3.6.1 Chemico-osmotic test results.

The chemico-osmotic test was performed using the oven dried squeezed material, rehydrated with DW and then statically compacted, in a drained compaction mould, at a porosity, n, equal to 0.81 (e = 4.26). After the preparation phase, the 17 mm thick specimen was transferred to the cell for the osmotic test.

After assembling the cell, DW was circulated through the top piston and the bottom pedestal for two weeks in order to establish a steady baseline differential pressure, before a concentration gradient was applied to the specimen. A source concentration of NaCl then was injected into the top porous stone, while DW was continuously circulated in the bottom porous stone.

A multiple-stage chemico-osmotic test was performed by sequential circulation of chemical solutions containing 5.16, 10.27, 20.24, 51.94 and 109.31 mM NaCl concentrations at a constant flow rate of 0.05 mL/min.

The EC values of the salt mass fluxes withdrawn from the top and the bottom porous stones, measured during the testing stages, are shown in Fig. 3.5 (a+b).

The measured values depend on the NaCl concentrations imposed at the boundaries of the specimen: the EC values progressively increase during the test as the NaCl concentration of the injected solution in the top porous stone rises. The trends of the electrical conductivity of the flux withdrawn from the top porous stone, $EC_{t,exit}$, and the electrical conductivity of the flux withdrawn from the bottom porous stone, $EC_{b,exit}$, both show that a steady state has been reached for each stage.

Moreover, the difference between the EC values measured in the flux withdrawn from the top porous stone ($EC_{t,exit}$) and the EC values of the solutions injected into the same stone ($EC_{t,ref}$) is due to the loss in NaCl mass induced by the diffusion through the bentonite from the top to the bottom boundary.

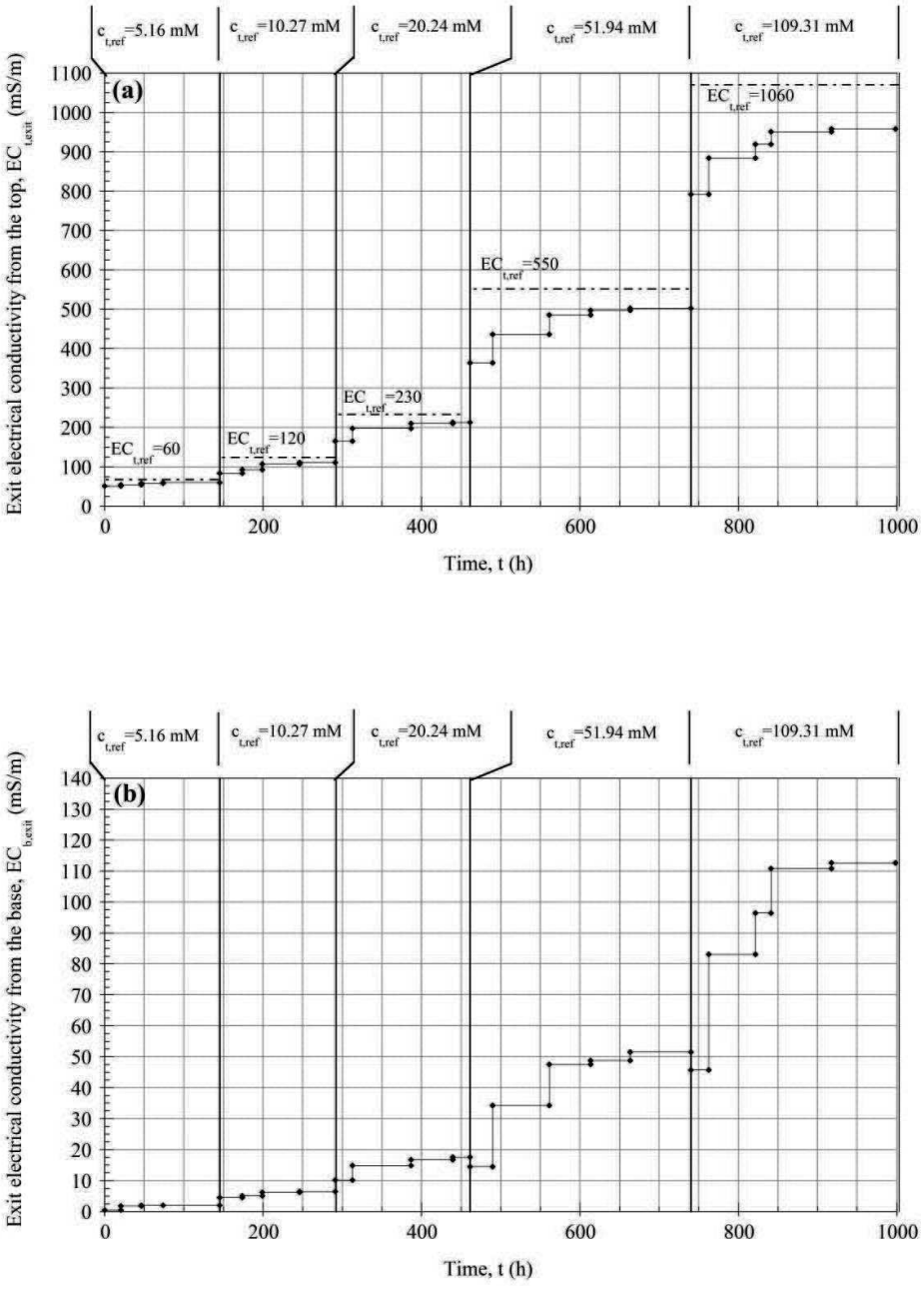

Figure 3.5 - Electrical conductivity of the salt flux flux withdrawn from the top porous stone (a) and the bottom porous stone (b) as a function of time during the multiple-stage chemico-osmotic test.

The global reflection coefficient values, ω_g, obtained during the multiple-stage chemico-osmotic test, are shown in Fig. 3.6 as a function of time.

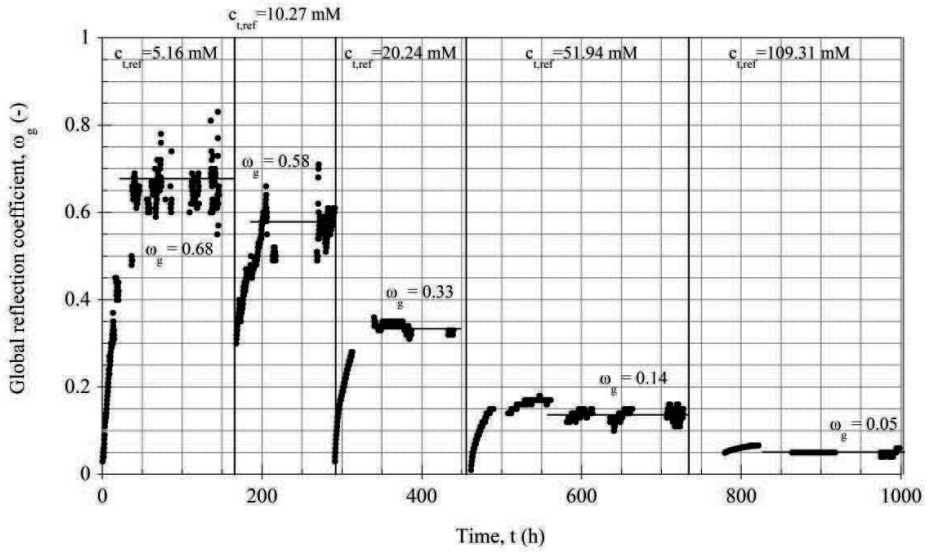

Figure 3.6 - Global reflection coefficient as a function of time during the multiple-stage chemico-osmotic test.

The ω_g values are determined using Eq. (3.74), on the basis of the differential pressure, Δu, measured during the test with a time step of 10 min, and the osmotic pressure, $\Delta\Pi$, calculated from the average of the top and bottom NaCl concentrations. The steady state values of the variables are reported in Table 3.1 for each concentration stage. The NaCl concentrations were derived from the measured EC using the linear calibration reported in Fig. 3.3.

As far as the EC measurements are concerned, the trend of the global reflection coefficient shows that a steady state has been reached for each stage. The steady state ω_g values tend to decrease as the salt concentration in the top porous stone increases. The recorded values range from 68%, for a 5.16 mM NaCl source concentration, to 5%, for a 109.31 mM NaCl source concentration. The global reflection coefficient can be assumed approximately null for higher molarities.

Table 3.1 - Steady state values of the variables involved in the multiple-stage chemico-osmotic test, where: $c_{t,exit}$ and $c_{b,exit}$ are the NaCl concentrations of the flux withdrawn from the top and the bottom porous stones, respectively; $c_{t,avg}$ and $c_{b,avg}$ are the NaCl average concentrations in the top and the bottom porous stones, respectively; Δu is the hydraulic pressure difference between the top and the bottom specimen boundaries, measured by the differential transducer; $\Delta\Pi$ is the osmotic pressure difference; ω_g is the global reflection coefficient and $D^*_{\omega g}$ is the global osmotic effective diffusion coefficient.

$c_{t.ref}$	$c_{t.exit}$ (mM)	$c_{b.exit}$ (mM)	$c_{t.avg}$ (mM)	$c_{b.avg}$ (mM)	Δu (kPa)	$\Delta\Pi$ (kPa)	ω_g (-)	$D^*_{\omega g}$ (m^2/s)
5.16 mM	5.12	0.83	5.14	0.42	15.65	23.02	0.68	-
10.27 mM	9.61	0.85	9.94	0.43	26,87	46.33	0.58	$2.54 \cdot 10^{-10}$
20.24 mM	18.93	1.45	19.58	0.72	30.32	91.89	0.33	$3.52 \cdot 10^{-10}$
51.94 mM	47.39	4.39	49.67	2.19	32.38	231.30	0.14	$4.19 \cdot 10^{-10}$
109.31 mM	97.18	9.78	103.24	4.89	23.96	479.21	0.05	$4.60 \cdot 10^{-10}$

The cumulative molar mass per unit area, Q, of the NaCl that migrated through the specimen during the multiple-stage test is reported in Fig. 3.7. The values of the global osmotic effective diffusion coefficient, $D^*_{\omega g}$, which have been obtained from the Q measurements shown in Fig. 7, are reported in Table 3.1.

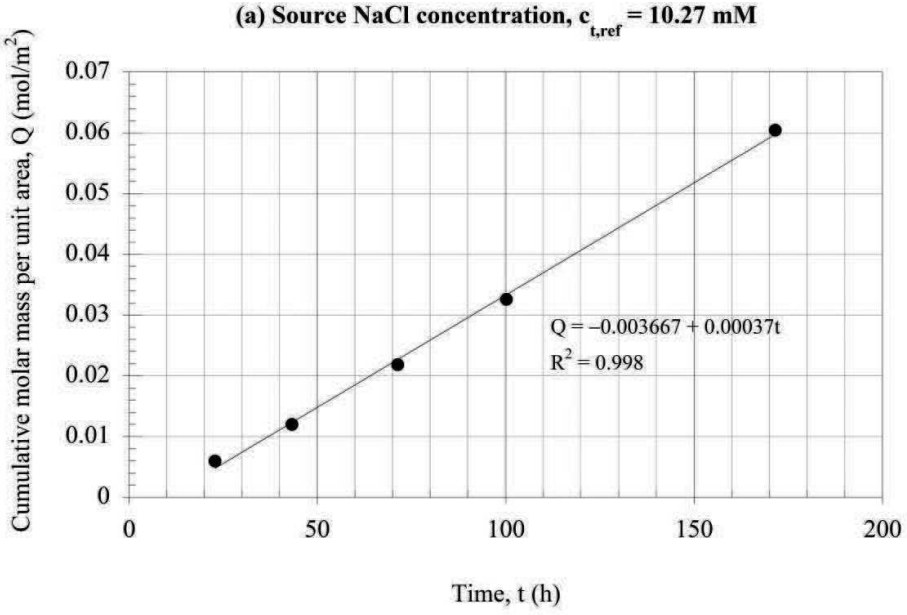
(a) Source NaCl concentration, $c_{t,ref}$ = 10.27 mM
Cumulative molar mass per unit area, Q (mol/m^2)
0.07
0.06
0.05
0.04
0.03
0.02
0.01
0
0
50
100
150
200
Time, t (h)
Q = –0.003667 + 0.00037t
R^2 = 0.998

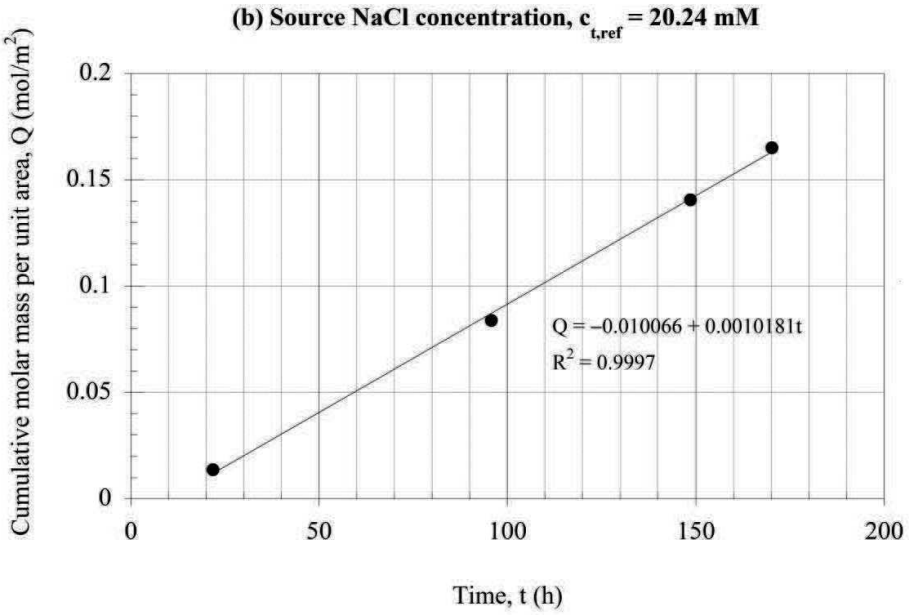
(b) Source NaCl concentration, $c_{t,ref}$ = 20.24 mM
Cumulative molar mass per unit area, Q (mol/m^2)
0.2
0.15
0.1
0.05
0
0
50
100
150
200
Time, t (h)
Q = –0.010066 + 0.0010181t
R^2 = 0.9997

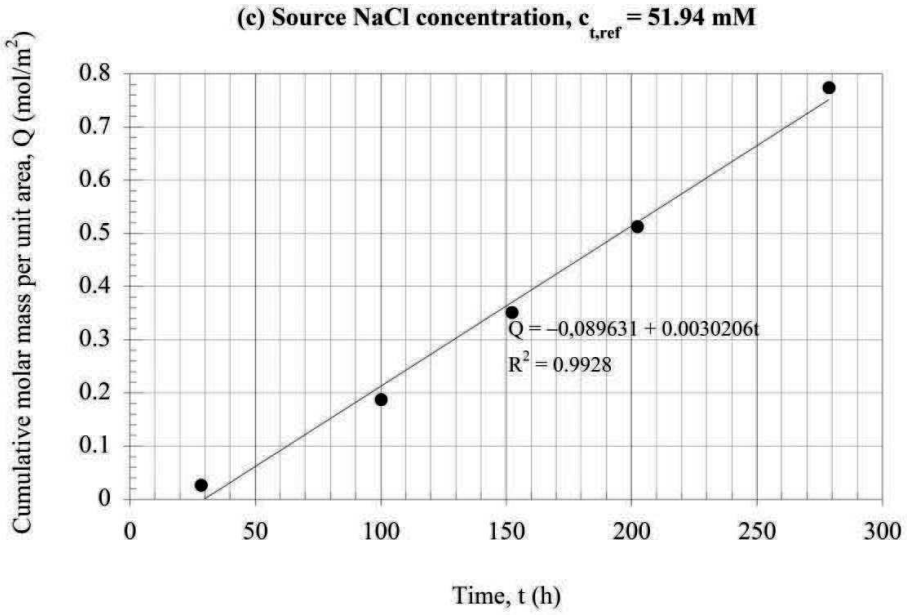

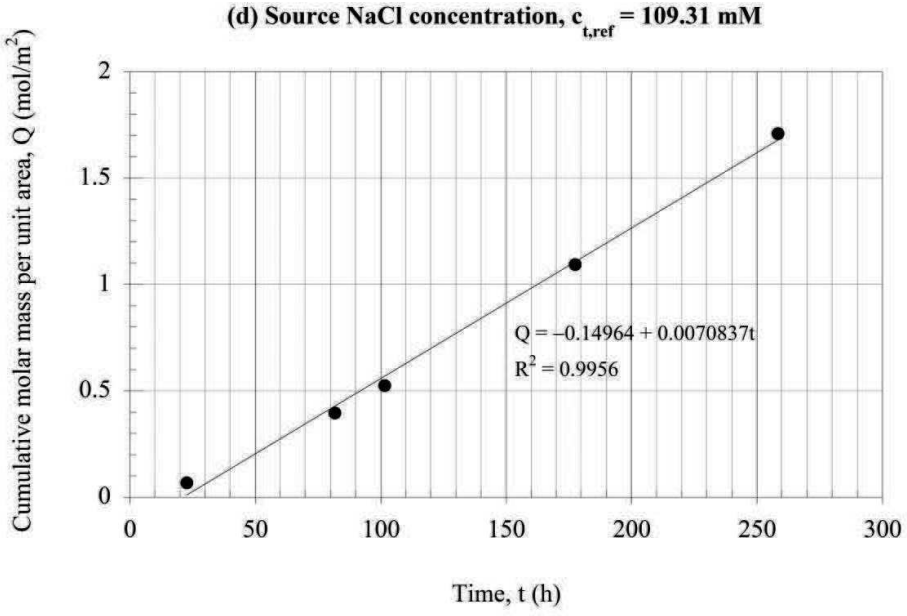

Figure 3.7 - Cumulative molar mass of NaCl per unit area as a function of time during the multiple-stage chemico-osmotic test. (a) $c_{t,ref} = 10$ mM, (b) $c_{t,ref} = 20$ mM, (c) $c_{t,ref} = 50$ mM, (d) $c_{t,ref} = 100$ mM.

3.6.2 Swelling pressure test results

The swelling pressure test was performed using dry specimens, prepared with the squeezed oven dried bentonite and characterized by an initial dry height of 5 mm, which were allowed to swell to 10 mm during hydration. The final hydrated volume of the specimens corresponded to n = 0.81.

The test was performed by hydrating five different specimens with five different NaCl solutions, characterized by increasing concentrations, i.e. 5, 10, 20, 50 and 100 mM. After hydration, the specimen volume change was inhibited and the value of the swelling pressure was recorded after a short transitional phase.

The swelling pressure trend is reported in Fig. 3.8 for each test as a function of time. Since, during the tests, the load cell was unloaded until the specimen swelled to 10 mm, the initial swelling/hydration phase of the dry material (from 5 to 10 mm) was characterized by null swelling pressure values.

All the tests show that the swelling pressure increases for approximately 15-20 h, during the controlled hydration phase (i.e. when the volumetric strain is inhibited), and that the equilibrium swelling pressure is reached when the hydration phase is completed. Moreover, in the tests with lower NaCl concentrations (i.e. for 5 and 10 mM NaCl equilibrium solutions), the specimens were successively back-pressurized to 300 kPa. The obtained results show that the swelling pressure value does not change after back-pressurization.

In the test performed using the 100 mM NaCl solution, the bentonite specimen did not rise to 10 mm, as it stopped at a height of 9.5 mm, and the load cell was never loaded during the test. For this reason, the swelling pressure for this test was taken equal to zero.

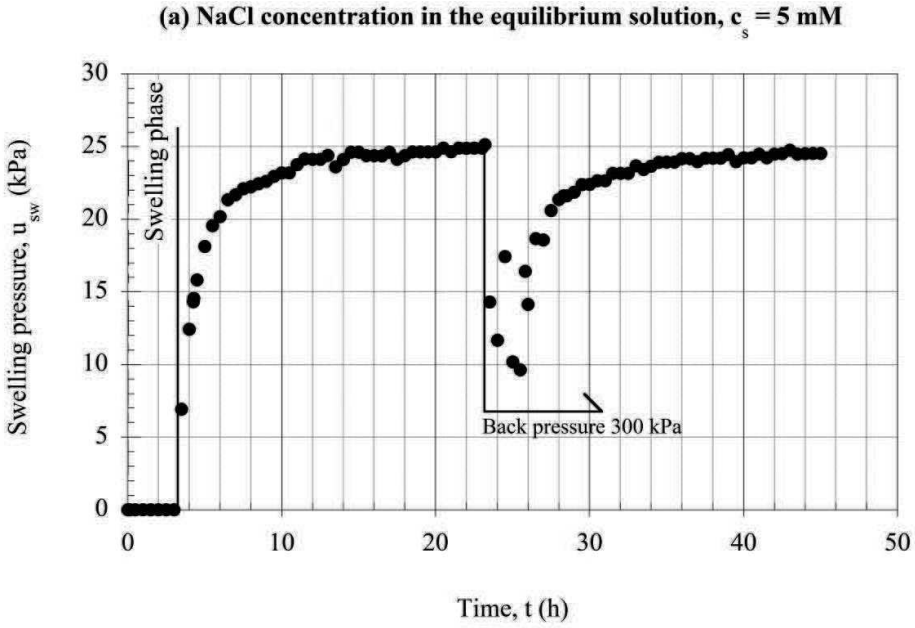
(a) NaCl concentration in the equilibrium solution, c_s = 5 mM
Swelling pressure, u_{sw} (kPa)
Swelling phase
Back pressure 300 kPa
Time, t (h)
0
5
10
15
20
25
30
0
10
20
30
40
50

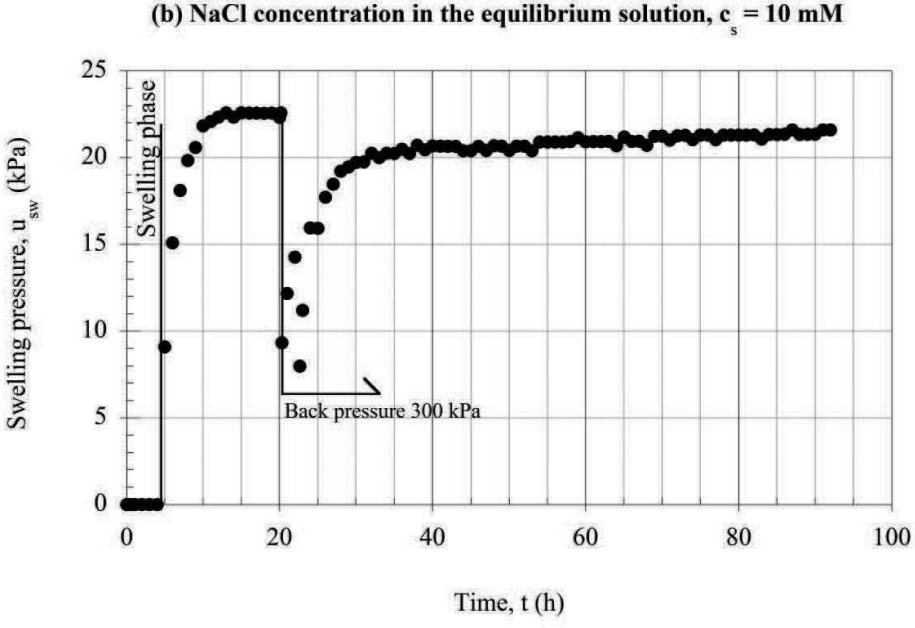
(b) NaCl concentration in the equilibrium solution, c_s = 10 mM
Swelling pressure, u_{sw} (kPa)
Swelling phase
Back pressure 300 kPa
Time, t (h)
0
5
10
15
20
25
0
20
40
60
80
100

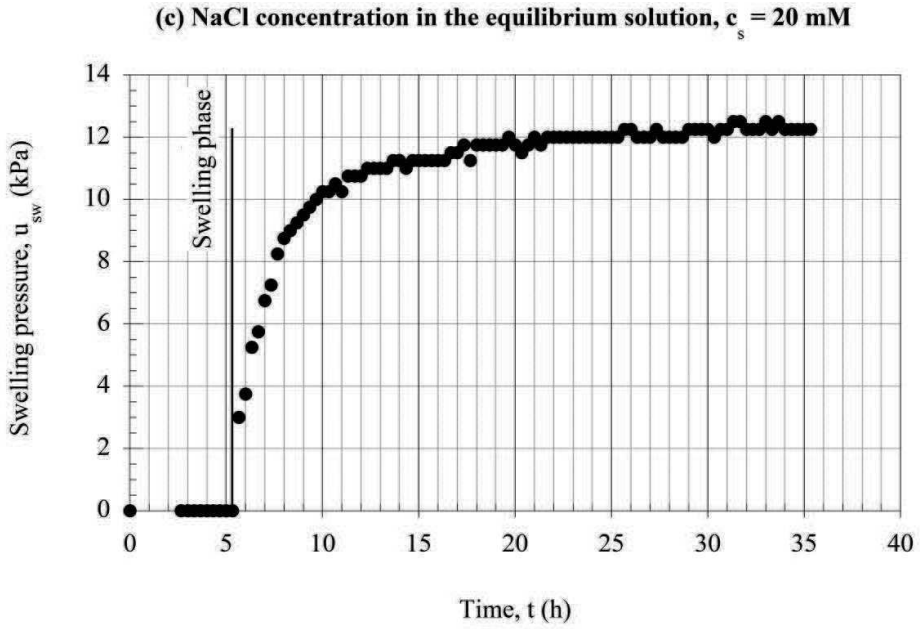

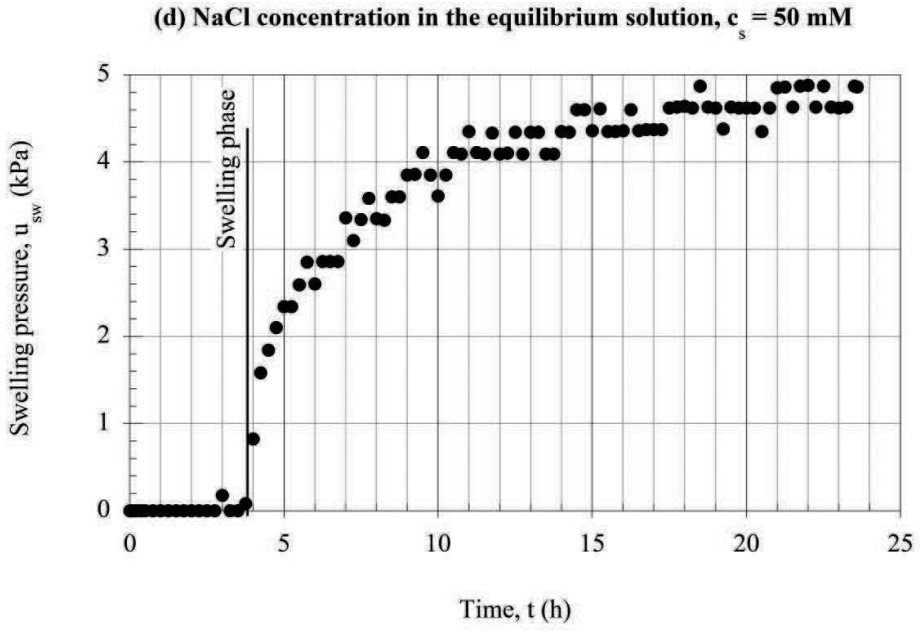

Figure 3.8 - Swelling pressure as a function of time. (a) $c_s = 5$ mM, (b) $c_s = 10$ mM, (c) $c_s = 20$ mM, (d) $c_s = 50$ mM.

3.7 INTERPRETATION OF THE TEST RESULTS

The experimental results can be related to the physical and chemical properties of the tested bentonite under the assumption that the microscopic deviations of the state variables from their average values are negligible. In such a case, both the global reflection coefficient and the swelling pressure depend on the solid skeleton electric charge through Eqs. (3.19) and (3.77). Therefore, from the best fitting of the theoretical curves with the experimental data of both tests, a value of $\overline{c}_{sk,0}$ equal to 90 mM was found. The obtained theoretical curves are reported in Figs. 3.9 and 3.10, together with the experimental data.

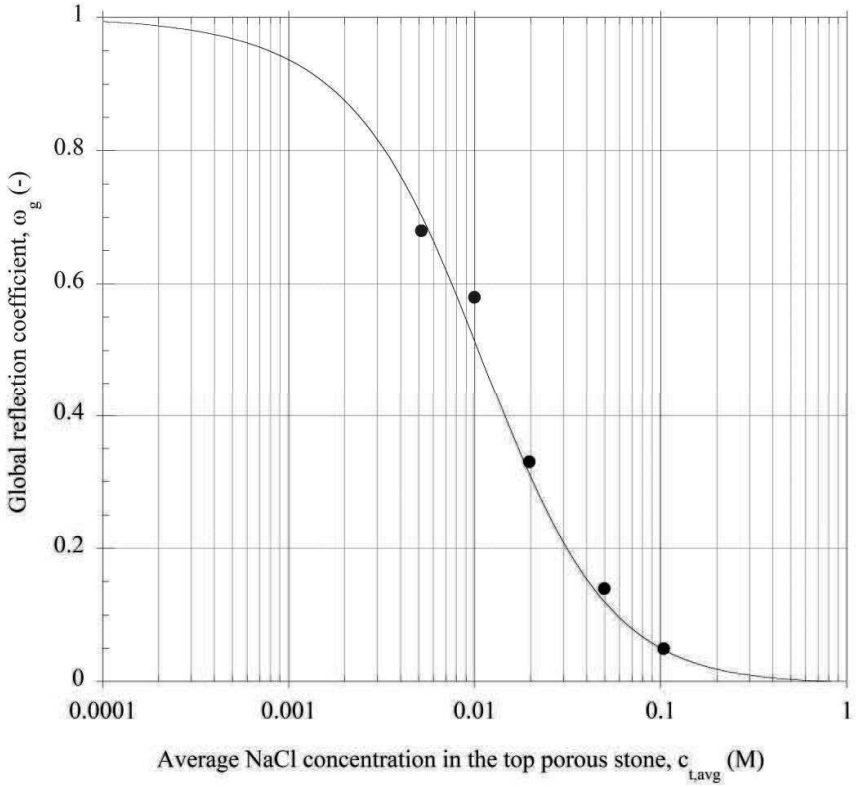

Figure 3.9 - Global reflection coefficient, ω_g, as a function of the average NaCl concentration at the top boundary of the bentonite specimen, with the best fitting theoretical curve, obtained for $\overline{c}_{sk,0} = 90\ \mathrm{mM}$ in Eq. (3.77) (continuous line).

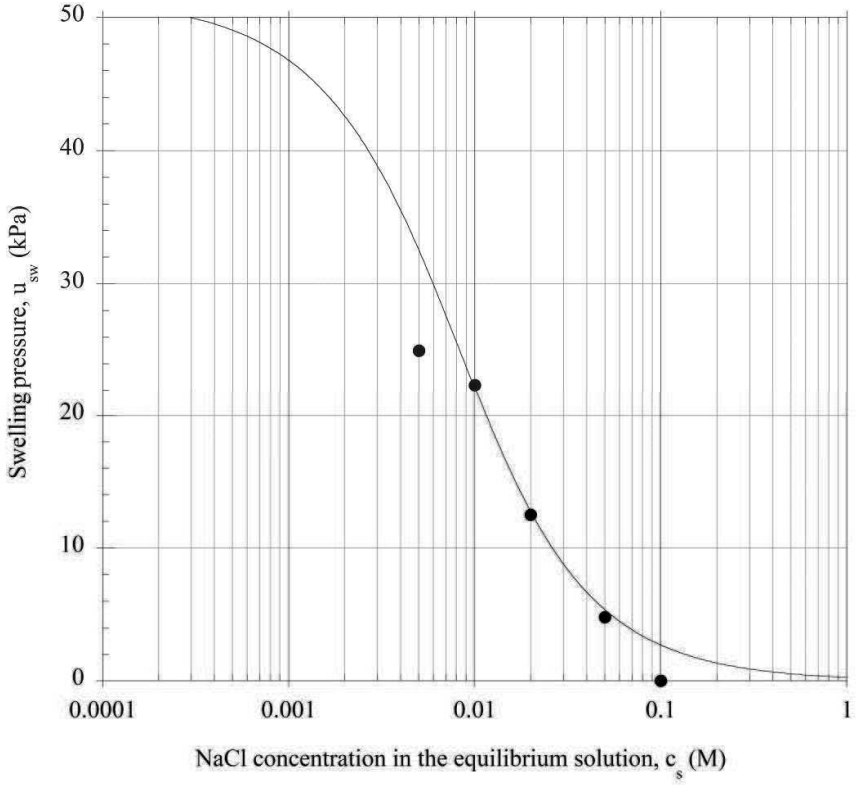

Figure 3.10 - Swelling pressure, u_{sw}, as a function of the NaCl equilibrium concentration, with the best fitting theoretical curve, obtained for $\bar{c}_{sk,0} = 90$ mM in Eq. (3.19) (continuous line).

The salt concentration at the top boundary was taken equal to $c_{t,avg}$ to determine ω_g, while the salt concentration at the bottom boundary was considered equal to zero, i.e. $c_b \cong c_{b,avg} \cong 0$. The sodium transport number was calculated from the sodium and chloride free-solution diffusion coefficient values (Shackelford and Daniel, 1991): $D_{Na,0} = 13.3 \cdot 10^{-10}$ m^2/s, $D_{Cl,0} = 20.3 \cdot 10^{-10}$ m^2/s.

In Fig. 3.11, the experimental reflection coefficient data were also fitted with the empirical semi-log linear curve proposed by Shackelford et al. (2003) and Malusis et al. (2003):

$$\omega_g = A + B \cdot \log(c_{t,avg}) \tag{3.83}$$

where A and B are the regression parameters. The value of the coefficient of determination R^2 close to one confirms the ability of this empirical curve to fit the ω_g experimental data, as it was found by Malusis et al. (2003) for the Kemper and Rollins (1966) and Malusis and Shackelford (2002a) data. However, the regression parameters A and B should be intended as functions of the soil porosity (Malusis et al., 2003) and of the bottom boundary condition (i.e. $c_{b,avg}$). The advantage of interpreting the experimental data with the proposed theoretical model is that, when the single unknown parameter, $\overline{c}_{sk,0}$, has been calibrated on a restricted experimental data set, the global reflection coefficient values can be estimated for different soil porosities and boundary conditions through Eq.(3.77).

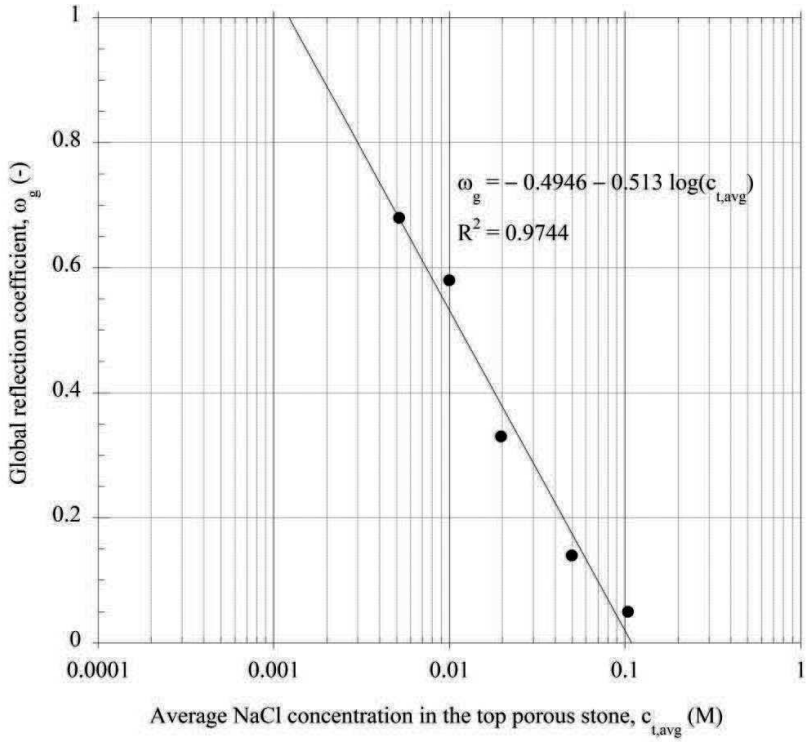

Figure 3.11 - Semi-log linear regression of the measured global reflection coefficients versus average NaCl concentration at the top boundary of the bentonite specimen.

The tortuosity factor was determined by plotting the measured values of $D^*_{\omega g}$ as a function of the corresponding values of the complement to 1 of ω_g, i.e. $(1-\omega_g)$ and finding the intercept of the linear regression with the ordinate axis at $(1-\omega_g)=1$, i.e. $\omega_g = 0$ (Fig. 3.12). The tortuosity factor in Eq. (3.76) is in fact given by:

$$\tau_m = \left(\frac{D^*_{\omega g}}{D_{s,0}} \right)_{\omega_g = 0} \tag{3.84}$$

where $D_{s,0}$ is the NaCl free solution diffusion coefficient, which is equal to $16 \cdot 10^{-10}$ m^2/s (Shackelford and Daniel, 1991).

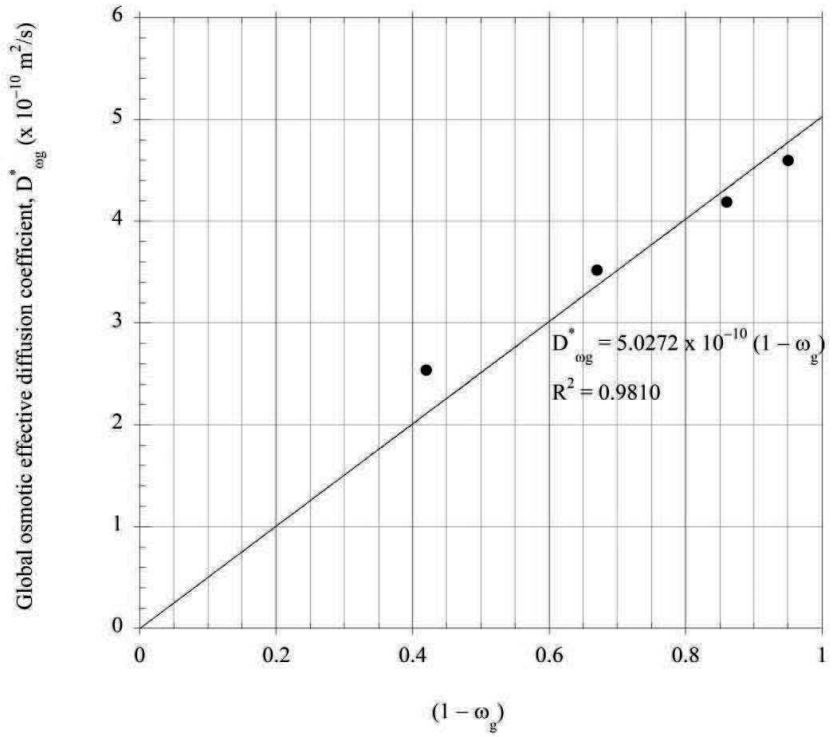

Figure 3.12 - Global osmotic effective diffusion coefficient, $D^*_{\omega g}$, as a function of the complement to 1 of the global reflection coefficient, ω_g, with the theoretical linear relation given by Eq. (3.76) (continuous line).

A value of τ_m equal to 0.31 was obtained from the data plotted in Fig. 3.12. The resulting theoretical curve of $D^*_{\omega g}$ is reported in Fig. 3.13 as a function of the top boundary salt concentration.

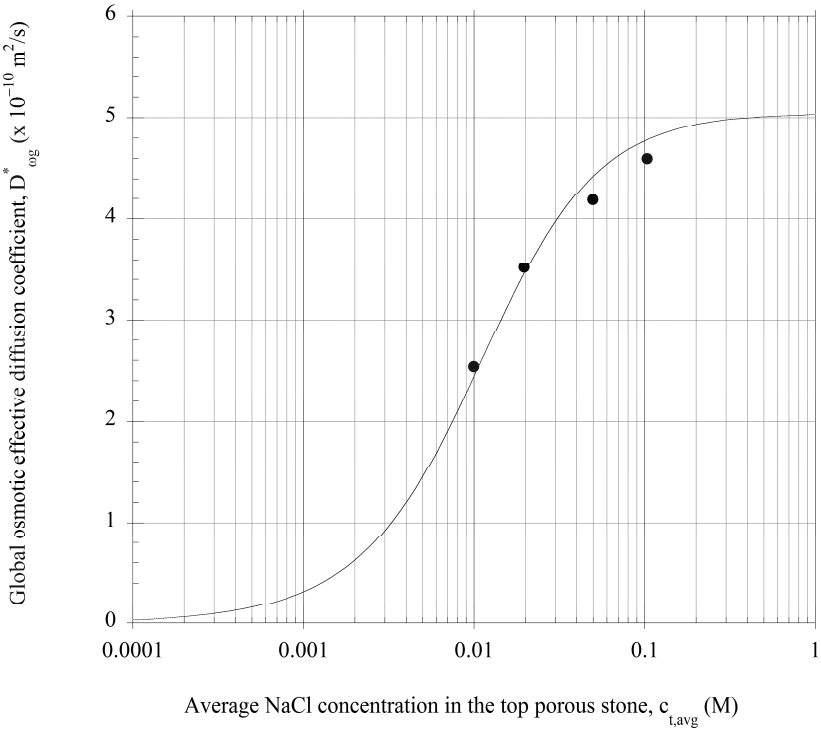

Figure 3.13 - Global osmotic effective diffusion coefficient, $D^*_{\omega g}$, as a function of the average NaCl concentration at the top boundary of the bentonite specimen, with the best fitting theoretical curve, obtained for $\bar{c}_{sk,0} = 90$ mM and $\tau_m = 0.31$ in Eqs. (3.76) and (3.77) (continuous line).

The obtained values of $\bar{c}_{sk,0}$ and τ_m are compared in Tab. 3.2 with those derived by Dominijanni and Manassero (2012b) from the interpretation of the experimental results of Malusis and Shackleford (2002a, 2002b), relative to a geosynthetic clay liner, with a bentonite porosity, n, of 0.79 for different concentrations of potassium chloride (KCl). The differences in the parameters obtained from the two studies can

be attributed to both the different mineralogical compositions of the tested bentonites and the different salts contained in the pore solutions.

The theoretical linear relationship between $D^{*}_{\omega g}$ and $(1-\omega_g)$ in Fig. 12 is a consequence of assuming that the pore-scale variations in the hydraulic pressure, ion concentrations, and water velocity within the soil are negligible: as a result, the agreement of the experimental data with the linear relationship is an indication of the acceptability of this assumption.

Table 3.2 - Comparison between the physical parameters derived from the interpretation of the experimental results in this work and those obtained by Dominijanni and Manassero (2012b) from the interpretation of the tests carried out by Malusis and Shackelford (2002a, 2002b).

Experimental data	This study	Malusis and Shackelford (2002a; 2002b)
Material	Natural sodium bentonite	Geosynthetic clay liner containing natural sodium bentonite
Method for removing soluble salts	Squeezing	Flushing
Tests	Chemico-osmotic test and swelling pressure test	Chemico-osmotic test
Salt in pore solution	NaCl	KCl
Porosity, n (-)	0.81	0.79-0.80
Solid skeleton charge concentration, $\bar{c}_{sk,0}$ (mM)	90	46
Tortuosity factor, τ_m (-)	0.31	0.14

The goodness of the linear fitting shown in Fig. 3.12 (R^2 = 0.9810) and the possibility of fitting both the global reflection coefficient and the swelling pressure data with a single value of $\bar{c}_{sk,0}$ are indications of the ability of the proposed theoretical approach to simulate the bentonite behaviour.

3.8 CONCLUSIONS

A theoretical approach that takes into account the interaction between the electric charge of the bentonite solid skeleton and the ions contained in the pore solution has been proposed. The phenomenological parameters introduced in this theoretical approach were measured for a bentonite specimen with porosity, n, of 0.81, over a range in sodium chloride concentration in the pore solution varying from 5 mM to 100 mM. Both the global reflection coefficient, ω_g, and the swelling pressure, u_{sw}, were found to decrease with an increase in the salt concentration. This result is in agreement with the trends given by the proposed theoretical model, assuming that the microscopic deviations of the pore solution state variables from their average values are negligible. If this assumption is accepted, the experimental data can be used to derive the electric charge of the solid skeleton (per unit solid volume), $\overline{c}_{sk,0}$, and the tortuosity factor, τ_m. The mechanical behaviour and the transport properties of bentonite can be estimated from these physical properties to evaluate its performance as a hydraulic and contaminant barrier in field applications. However, in order to verify the applicability of the proposed model under different boundary conditions and for different salts contained in the pore solution, further experimental evaluations must be conducted. Moreover, the results obtained for a single salt contained in the bentonite pore solution need to be extended to the more general problem of a solution containing an unspecified number of salts, in order to evaluate the performance of bentonites that are used as contaminant barriers for real leachates.

REFERENCES

Auclair, B., Nikonenko, V., Larchet, C., Métayer, M. & Dammak, L. (2002). Correlation between transport parameters of ion-exchange membranes. Journal of Membrane Science **195**, 89-102.

Coussy, O. (2004). Poromechanics. Chichester: Wiley.

Di Emidio, G. (2010). Hydraulic and chemico-osmotic performance of polymer treated clays. Ph. D. Thesis., Ghent: Ghent University.

Dominijanni, A. & Manassero, M. (2010). Chemico-osmosis and solute transport through geosynthetic clay liners. In: A. Bouazza and J.J. Bowders (Eds.), Geosynthetic clay liners for waste containment, 105-125. Leiden: CRC Press.

Dominijanni, A. & Manassero, M. (2012a). Modelling the swelling and osmotic properties of clay soils. Part I: The phenomenological approach. International Journal of Engineering Science **51**, 32-50.

Dominijanni, A. & Manassero, M. (2012b). Modelling the swelling and osmotic properties of clay soils. Part II: The physical approach. International Journal of Engineering Science **51**, 51-73.

Donnan, F.G. (1911). Theorie der Membrangleichgewichte und Membranpotentiale bei Vorhandensein von nicht dialysierenden Elektrolyten. Ein Beitrag zur physikalisch-chemischen Physiologie [Theory of membrane equilibria and membrane potentials in the presence of non-dialysing electrolytes. A contribution to physical-chemical physiology], Zeitschrift für Elektrochemie und angewandte physikalische Chemie **17**, 572-581. English translation republished in Journal of Membrane Science **100** (1995), 45-55.

Dormieux, L., Barboux, P., Coussy, O. & Dangla, P. (1995). A macroscopic model of the swelling phenomenon of a saturated clay. European Journal of Mechanics A/Solids **14**, No. 6, 981-1004.

Dormieux, L., Lemarchand, E. & Coussy, O. (2003). Macroscopic and micromechanical approaches to the modelling of the osmotic swelling in clays. Transport in Porous Media **50**, 75-91.

Ehlers, W. (2002). Foundations of multiphasic and porous materials. In: W. Ehlers and J. Bluhm (Eds.), Porous Media: Theory, Experiments and Numerical Applications, 3–86. Berlin: Springer-Verlag.

Kang, J.-B. & Shackelford, C.D. (2009). Clay membrane testing using a flexible-wall cell under closed-system boundary conditions. Applied Clay Science **44**, 43-58.

Katchalsky, A. & Curran, P.F. (1965). Nonequilibrium thermodynamics in biophysics. Cambridge: Harvard University.

Kemper, W.D. & Rollins, J.B. (1966). Osmotic efficiency coefficients across compacted clays. Soil Science Society of America, Proceedings **30**, 529–534.

Malusis, M.A. & Shackelford, C.D. (2002a). Chemico-osmotic efficiency of a geosynthetic clay liner. Journal of Geotechnical and Geoenvironmental Engineering **128**, No. 2, 97–106.

Malusis, M.A. & Shackelford, C.D. (2002b). Coupling effects during steady-state solute diffusion through a semipermeable clay membrane. Environmental Science and Technology **36**, No. 6, 1312–1319.

Malusis, M.A., Shackelford, C.D. & Maneval, J.E. (2012). Critical review of coupled flux formulations for clay membranes based on nonequilibrium thermodynamics. Journal of Contaminant Hydrology **138-139**, 40-59.

Malusis, M.A., Shackelford, C.D. & Olsen, H.W. (2001). A laboratory apparatus to measure chemico-osmotic efficiency coefficients for clay soils. Geotechnical Testing Journal **24**, 229-242.

Malusis, M.A., Shackelford, C.D. & Olsen, H.W. (2003). Flow and transport through clay membrane barriers. Engineering Geology **70**, 235–248.

Manassero, M. & Dominijanni, A. (2003). Modelling the osmosis effect on solute migration through porous media. Géotechnique **53**, No. 5, 481–492.

Shackelford, C.D. & Daniel, D.E. (1991). Diffusion in saturated soil: I. Background. Journal of Geotechnical Engineering, **117**, No. 3, 467–484.

Shackelford, C.D., Malusis, M.A. & Olsen, H.W. (2003). Clay membrane behavior for geoenvironmental containment. Soil and Rock America Conference 2003 (Proceedings of the joint 12th Panamerican Conference on Soil Mechanics and Geotechnical Engineering and the 39th U. S. Rock Mechanics Symposium), Culligan, Einstein, and Whittle, Eds., Verlag Glückauf GMBH, Essen, Germany, Vol. 1, 767–774.

Shackelford, C.D. & Lee, J.-M. (2003). The destructive role of diffusion on clay membrane behavior. Clays and Clay Minerals **51**, No. 2, 186–196.

Yaroshchuk, A.E. (1995). Osmosis and reverse osmosis in fine-charged diaphragms and membranes. Advances in Colloid and Interface Science **60**, 1-93.

Yeo, S.-S., Shackelford, C.D. & Evans, J.C. (2005). Membrane behaviour of model soil-bentonite backfill mixtures. Journal of Geotechnical and Geoenvironmental Engineering **131**, No. 4, 418-429.

3.9 FURTHER RESULTS OF CHEMICO-OSMOTIC TESTS AND CONFRONT WITH DATA FROM LITERATURE

Two further chemico-osmotic tests have been performed during the development of the Ph.D. research activity.

- The first one, performed on a calcium bentonite specimen, was aimed at analysing the osmotic behaviour of bentonite in long term landfill condition, i.e. when the cation exchange phenomenon has been developed completely and the bentonite exchange centres are entirely saturated with Calcium ions;
- The second one, performed on a sodium bentonite specimen characterised by a low porosity value (i.e. n = 0.67), was aimed at analysing the effects induced by the stress-strain properties on osmotic behaviour. Unfortunately, during the test, a loss of materials from the specimen to the outer occurred through the edge of the top porous stone, as showed in the picture in Fig. 3.14. The development of this phenomenon, on the one hand, highlighted the inadequacy of the osmotic cell in our possession to perform tests characterised by high values of swelling pressure and the necessity to design a new osmotic apparatus, that match with this need, on the other hand, have produced results that corresponds to a specimen porosity approximately equal to n ≈ 0.8, that can be compared with those obtained in the test showed in the Paper (paragraph 3.6.1).

3.9.1 Chemico-osmotic properties of calcium bentonite

The calcium bentonite was prepared in the laboratory starting from the sodium bentonite through a process of accelerated cation exchange of Sodium with Calcium, described in the paragraph 1.2.1.

The chemico-osmotic test was performed using the oven dried squeezed material, rehydrated with DW and then statically compacted, in a drained compaction mould, at a porosity, n, equal to 0.67.

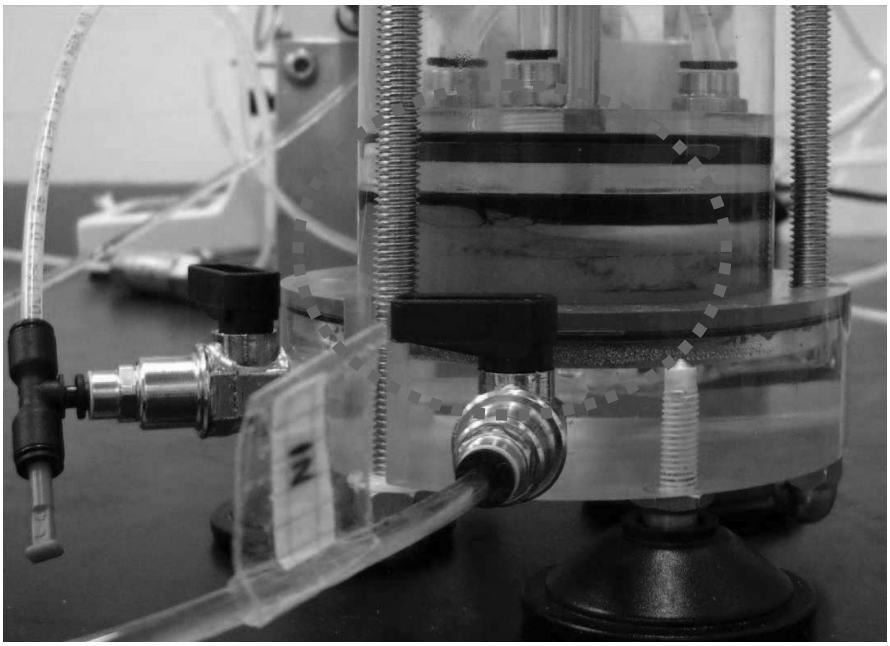

(a)

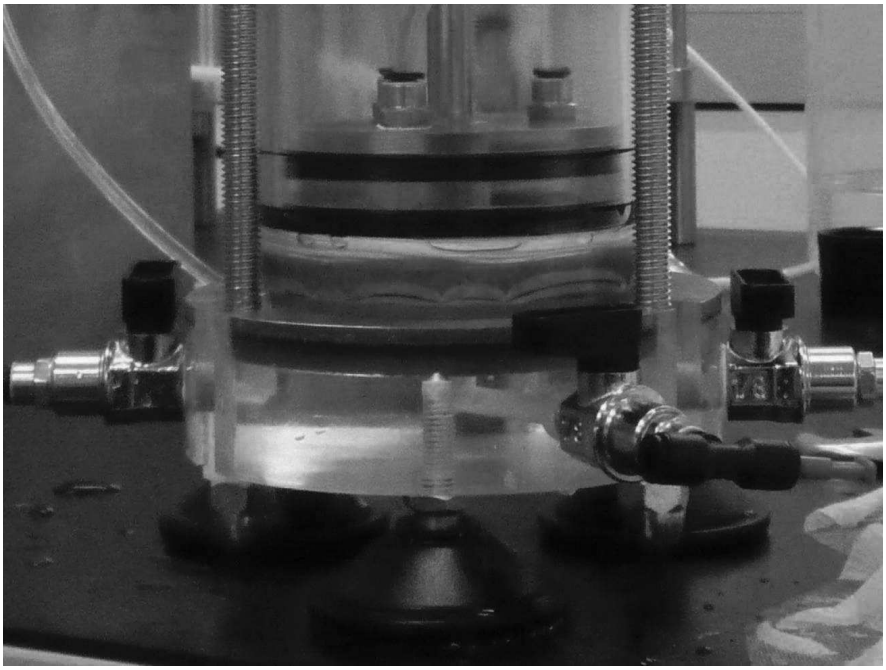

(b)

Figure 3.14 – Anomalous loss of materials from the specimen through the edge of the top porous stone (a) compared with a standard configuration of the test (b).

After assembling the cell, DW was circulated through the top piston and the bottom pedestal for two weeks in order to establish a steady baseline differential pressure, before a concentration gradient was applied to the specimen. A source concentration of $CaCl_2$ then was injected into the top porous stone, while DW was continuously circulated in the bottom porous stone.

A multiple-stage chemico-osmotic test was performed by sequential circulation of chemical solutions containing 5.37 and 10.40 mM $CaCl_2$ concentrations at a constant flow rate of 0.05 mL/min.

The EC values of the salt mass fluxes withdrawn from the top and the bottom porous stones, measured during the testing stages, are shown in Fig. 3.15 (a+b).

The measured values depend on the $CaCl_2$ concentrations imposed at the boundaries of the specimen: the EC values progressively increase during the test as the $CaCl_2$ concentration of the injected solution in the top porous stone rises. The trends of the electrical conductivity of the flux withdrawn from the top porous stone, $EC_{t,exit}$, and the electrical conductivity of the flux withdrawn from the bottom porous stone, $EC_{b,exit}$, both show that a steady state has been reached for each stage.

Moreover, the difference between the EC values measured in the flux withdrawn from the top porous stone ($EC_{t,exit}$) and the EC values of the solutions injected into the same stone ($EC_{t,ref}$) is due to the loss in $CaCl_2$ mass induced by the diffusion through the bentonite from the top to the bottom boundary.

The global reflection coefficient values, ω_g, obtained during the multiple-stage chemico-osmotic test, are shown in Fig. 3.16 as a function of time. The ω_g values are determined using Eq. (3.74), on the basis of the differential pressure, Δu, measured during the test with a time step of 10 min, and the osmotic pressure, $\Delta\Pi$, calculated from the average of the top and bottom $CaCl_2$ concentrations.

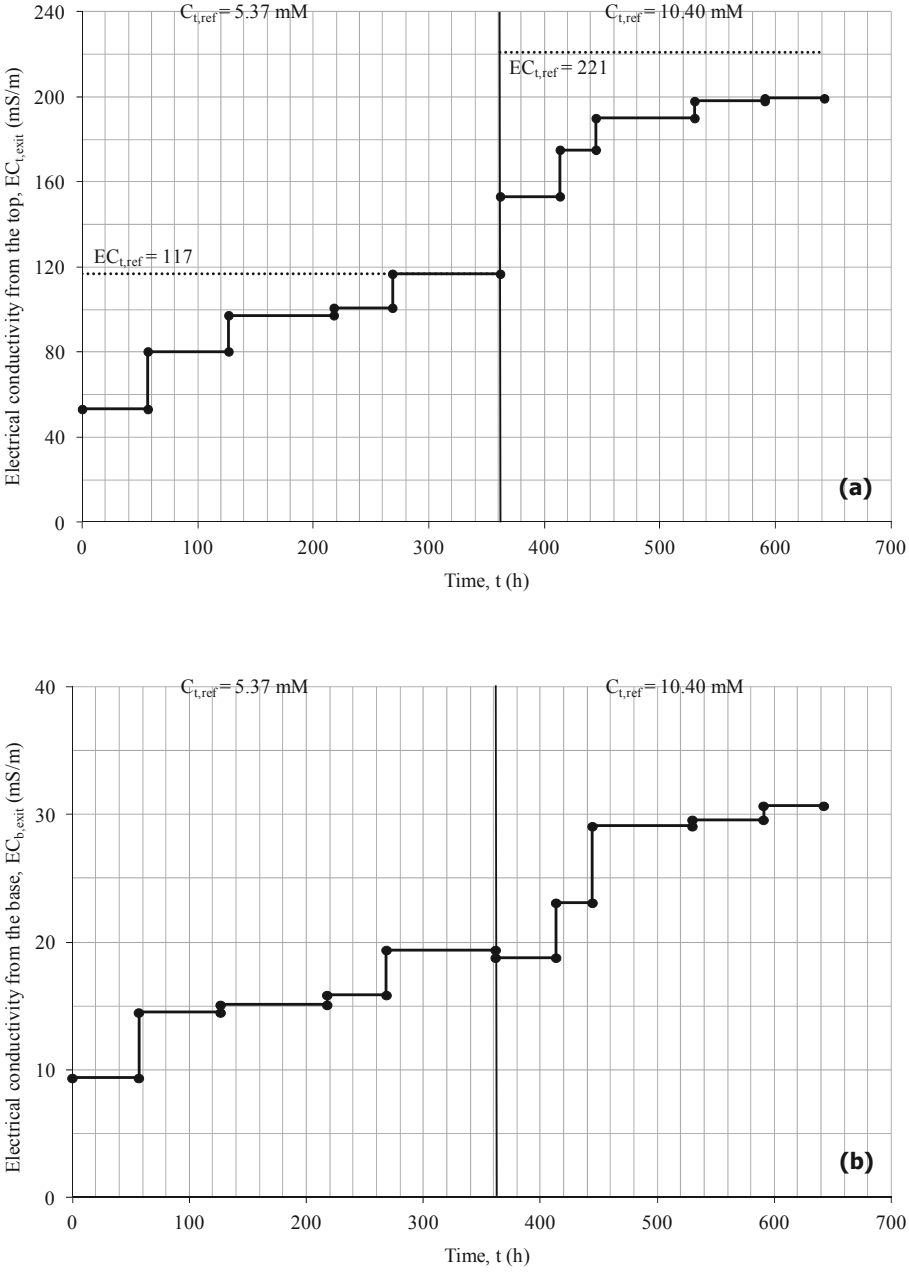

Figure 3.15 - Electrical conductivity of the salt flux flux withdrawn from the top porous stone (a) and the bottom porous stone (b) as a function of time during the multiple-stage chemico-osmotic test on calcium bentonite specimen.

As far as the EC measurements are concerned, the trend of the global reflection coefficient shows that a steady state has been reached for each stage. The steady state ω_g values tend to decrease as the salt concentration in the top porous stone increases. The recorded values are very low and range from 0.5%, for a 5.37 mM $CaCl_2$ source concentration, to 0.2%, for a 10.40 mM $CaCl_2$ source concentration. The global reflection coefficient can be assumed completely null for higher molarities. The results highlight that calcium bentonite has very low osmotic behaviour at the tested molarities values.

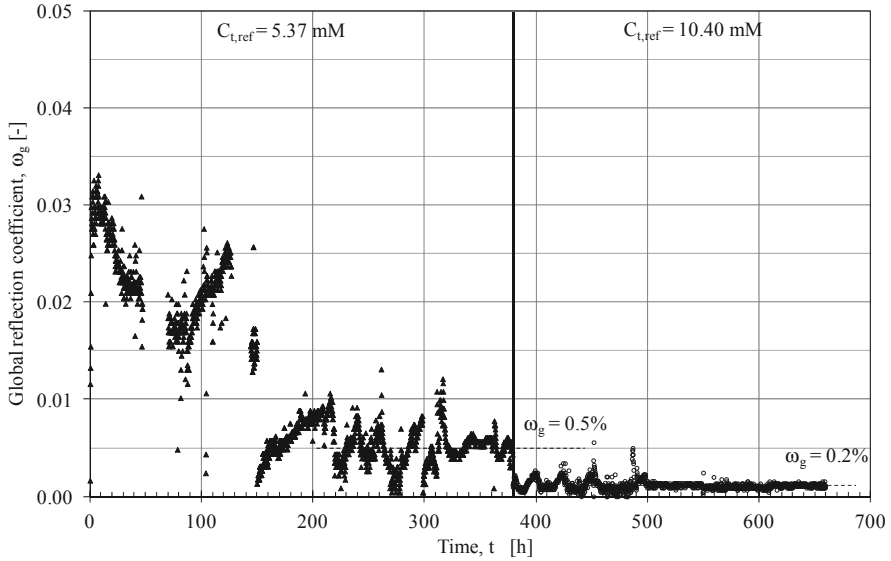

Figure 3.16 - Global reflection coefficient as a function of time during the multiple-stage chemico-osmotic test on the calcium bentonite specimen.

3.9.2 Second chemico-osmotic test on sodium bentonite

The test had been scheduled with the aim to analyse the effects induced by the stress-strain properties on osmotic behaviour. The specimen was characterised by an initial porosity of n = 0.67. Unfortunately, during the test, a loss of materials from the specimen to the outer happened and, as a consequence, the obtained results corresponded to a porosity approximately equal to n ≈ 0.8 (measured on the

specimen at the end of the test), that can be compared with those obtained in the test showed in the Paper (see Fig. 3.6).

Therefore, the results reported in this paragraph have the only function of validation of the test results reported in the Paper. In particular, since the loss of materials developed during the second stage of the test, the result of the first stage (i.e. $C_{t,ref}$ = 5.31 mM) can be influenced by the initial low porosity value of the specimen and, indeed, in this case the global reflection coefficient results significantly higher than that obtained in the test reported in the Paper (see Fig. 3.6).

A multiple-stage chemico-osmotic test was performed, using the same procedure adopted for the test reported in the Paper, by sequential circulation of chemical solutions containing 5.31, 10.06, 19.58, 51.22 and 106.96 mM NaCl concentrations at a constant flow rate of 0.05 mL/min.

The global reflection coefficient values, ω_g, obtained during this multiple-stage chemico-osmotic test, are shown in Fig. 3.17 as a function of time for comparison purposes.

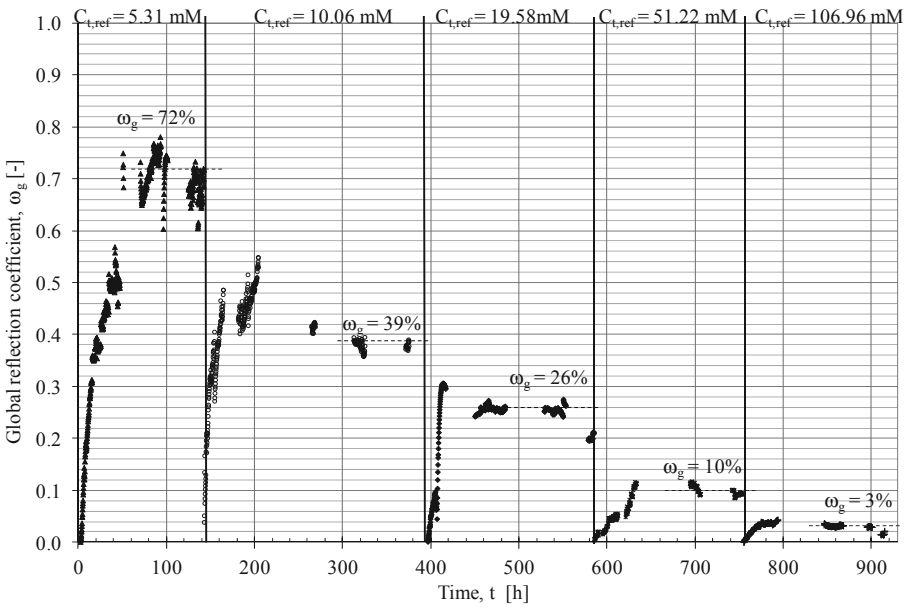

Figure 3.17 - Global reflection coefficient as a function of time during the multiple-stage chemico-osmotic test on the second sodium bentonite specimen.

The values of the global reflection coefficient were slightly lower in this test than those recorded in the test reported in Fig. 3.6 with the exception of the first stage value that resulted higher. As the bentonite specimen was subjected to an anomalous swelling in this first stage, the differential pressure measurement, Δu, could be affected by error.

3.9.3 Confront with data from literature

In Figure 3.18 the chemico-osmotic test results reported in the Paper (red crossed symbols) are compared with the global reflection coefficient values reported for sodium and calcium bentonite specimens by Kemper and Rollins (1966), open symbols, and for a sodium bentonite GCL by Malusis and Shackelford (2002), closed symbols.

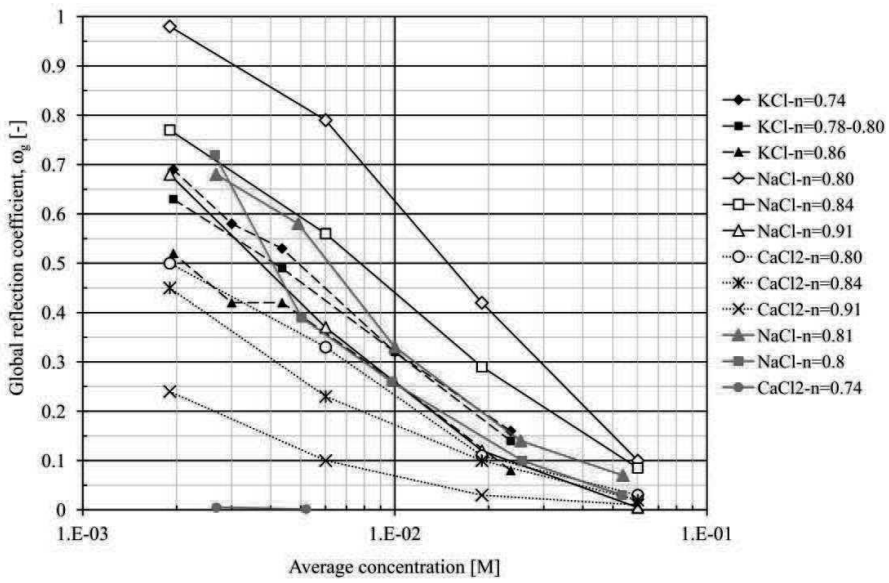

Figure 3.18 – Global reflection coefficients as a function of the average salt concentration across the specimen and the specimen porosity (n) for (open symbols) bentonite specimens (Kemper and Rollins, 1966), (closed symbols) a GCL (Malusis and Shackelford, 2002) and (red symbols) the results obtained in the Ph.D. research activity.

Fig. 3.18 shows a good agreement of the data obtained in the test performed on sodium bentonite during the research activity and those founded in Literature. In particular, the obtained data result in perfect agreement with those reported by Kemper and Rollins (1966) for the same porosity value while, for low molarity values, the obtained data result significantly higher than those reported by Malusis and Shackelford (2002) for a sodium GCL. The explanation of this last issue stays in the different specimen composition. The GCL is indeed a less homogeneous material than the consolidated sodium bentonite used in this study and, as a consequence, it presents lower chemico-osmotic performances even at the same stress-strain conditions. For higher molarities the specimen composition has lower influence.

Concerning calcium bentonite results, the data obtained during the research activity appear to be significantly lower than those reported by Kemper and Rollins (1966). In this study, in particular, calcium bentonite was founded to have a very low osmotic behaviour, which can be defined approximately null. Contrariwise, the results reported by Kemper and Rollins (1966) showed a reflection coefficient of 50% for the lowest molarity value at a porosity value similar to that used in the test performed in this study. Anyway, it is important to underline that the testing procedure and apparatus used by Kemper and Rolling (1966) was different to that proposed by Malusis et al. (2001) (see paragraph 3.5.2.1), used for both the tests reported by Malusis and Shackelford (2002) and the tests performed during this research activity.

3.10 A NEW APPARATUS TO MEASURE TOGETHER THE SWELLING AND OSMOTIC BEHAVIOUR OF BENTONITES

During the Ph.D. research activity, starting from the knowledge achieved about both the osmotic and the swelling pressure tests, a new apparatus was designed aimed at measuring together the global reflection coefficient, ω_g, the global effective diffusion coefficient, $D^*_{\omega g}$, and the swelling pressure, u_{sw}, of bentonites.

As reported schematically in Figure 3.19, the new apparatus includes the new oedometer (see the more detailed sketch in Fig. 3.20), the flow pump system and the

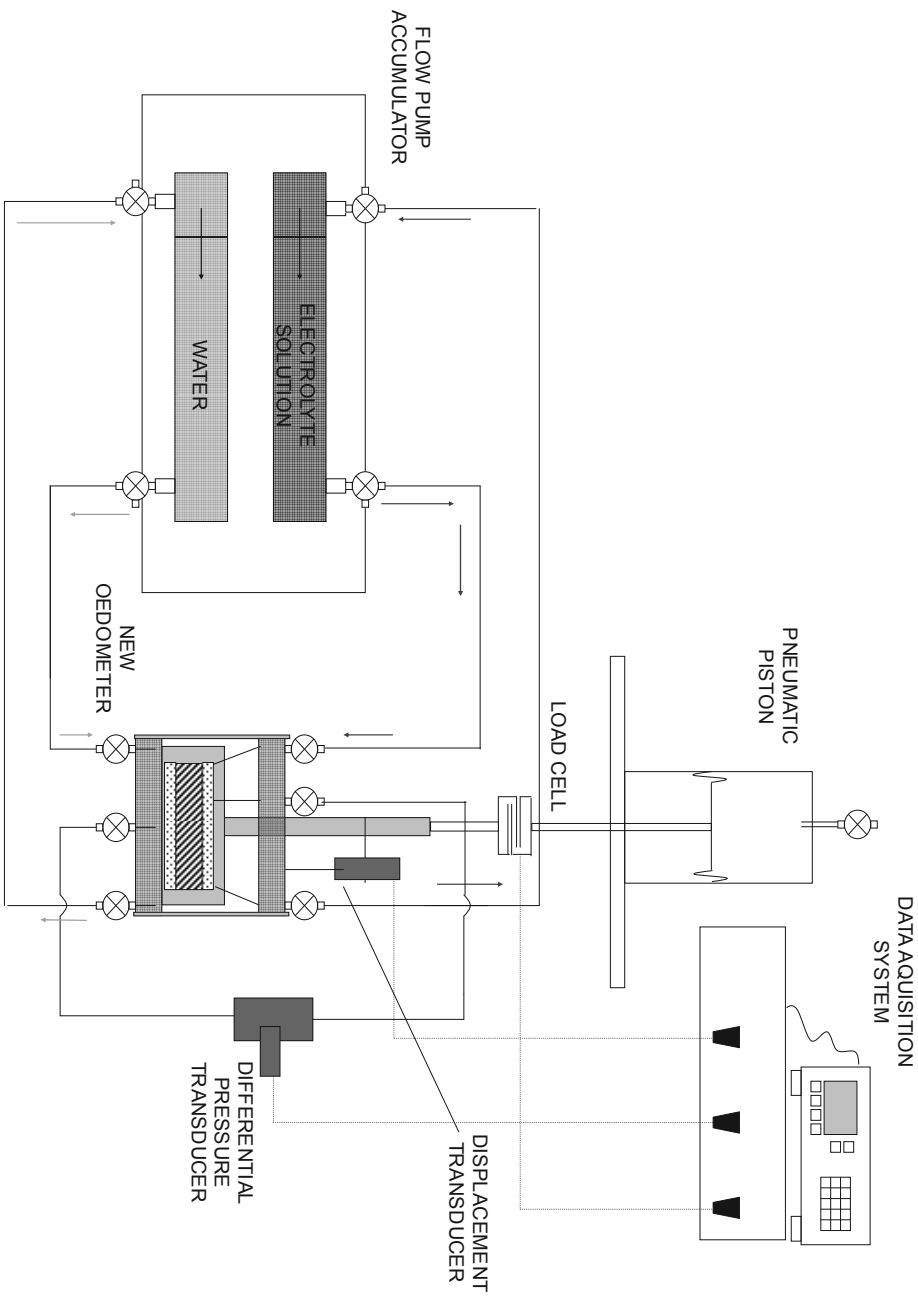

Figure 3.19 – Scheme of the new apparatus aimed at measuring together the osmotic and swelling behaviour of bentonites.

pressure transducer, which are aimed at measuring the osmotic properties of the specimen, while the displacement transducer, the load cell and the pneumatic piston are aimed at measuring the swelling pressure.

The design sketch in Figure 3.20 represents in detail the new oedometric cell.

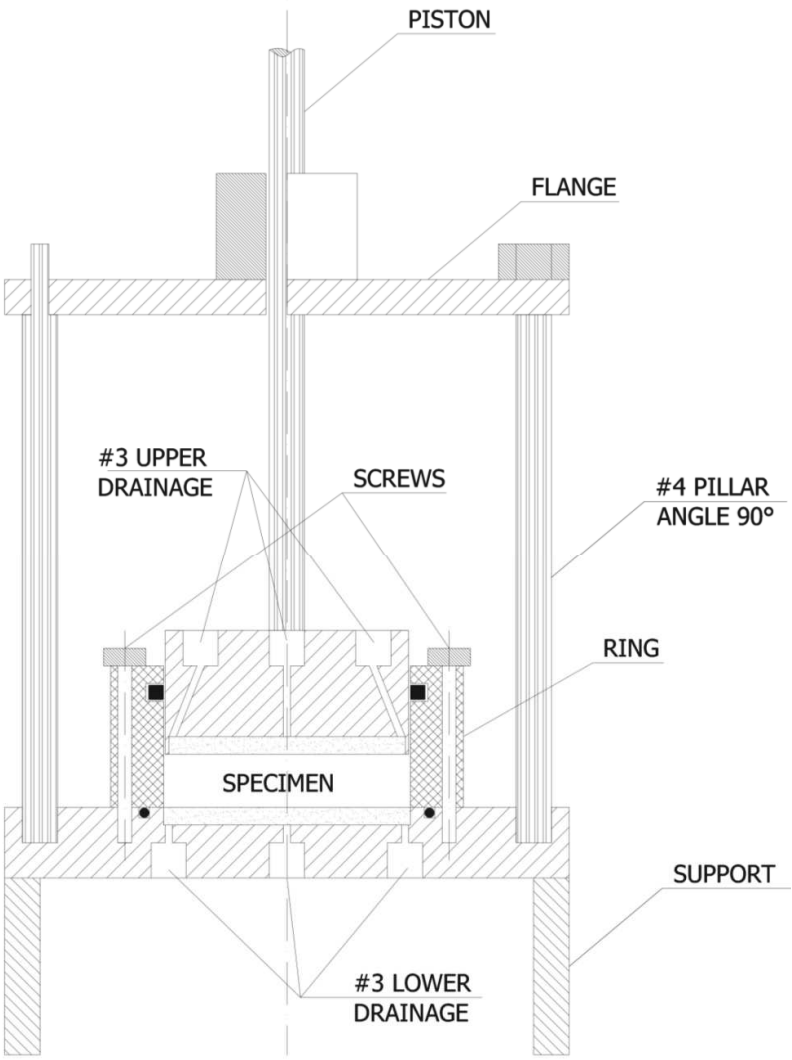

Figure 3.20 – Design sketch of the new oedometric cell.

The rigid wall permeameter, used in the chemico-osmotic test (see paragraph 3.5.2.1), has been replaced with an oedometer which match with the need of containment of specimens characterized by very high swelling pressure without allowing loss of material. The oedometric cell will permit to study the osmotic properties of specimen characterized by very low porosity value and to analyse the effects induced by stress-strain properties on osmotic behaviour.

The new oedometric cell is endowed of tree drainage lines in both the top and the bottom porous stones, which allow for the circulation of the solutions in the porous stones (i.e. through the two peripheral lines) and the simultaneous measurement of the differential pressure between the porous stones (i.e. through the central line).

In order to measure the swelling pressure, the load cell needs to detect a very small piston movement. With the aim to allow that this movement develops without constrain, the new oedometric cell is equipped with a *q-ring* (the square ring in Fig. 3.20).

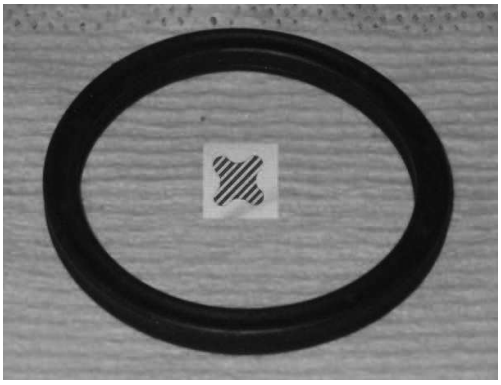

Figure 3.21 – Picture of a q-ring.

The q-ring (see Fig. 3.21) has the same features of a more typical o-ring (e.g. hydraulic tightness), but, furthermore, presents a lower contact surface with the upper steel plate of the oedometer, which is rigidly connected to the piston and the load cell.

As a consequence, the q-ring allows negligible friction forces for very small vertical strain of the specimen and permits the correct measurement of the swelling pressure in the load cell.

Chapter 4

CONTAINMENT PERFORMANCES OF POLYMER MODIFIED BENTONITE BARRIERS TOWARDS HYDROCARBONS

Background information on hydrocarbon behaviour in soils is reported in the first part of this chapter. In particular, the effects of capillary forces on the distribution of immiscible fluids in porous media and the theoretical aspects regarding the formation of tactoids induced by the low dielectric constant that characterized most of hydrocarbon species, are studied.

Moreover, this chapter reports the contents of the Paper:
S., Puma, A., Dominijanni, M., Manassero, D., Toncelli, (2011).
Title: **Hydraulic Performance of GCLs with Diesel Oil and Polymer Treatment Proposal.**
In Proceedings of the 4th International Conference Geosynthetics Middle East 2011. Abu Dhabi, United Arab Emirates, 24-25 October 2011.

Since hydrocarbons and water are immiscible fluids, hydrocarbons are generally defined Non Aqueous Phase Liquids, or NAPL. Mixed immiscible compounds do not produce a single phase but show two phases totally distinct and stable in time.
NAPL are divided into two groups based on their density:
- Light NAPLs (L-NAPLs) are characterized by a lower density than water and, as a consequence, they tend to float on water table;
- Dense NAPLs (D-NAPLs) are characterized by a higher density than water and, as a consequence, they tend to sink in water.
The bentonite behaviour with diesel oil was study in the experimental activity, developed during the Ph.D.. Diesel oil is a product of the primary distillation of petroleum and is classified as L-NAPL since it presents a density equal to 850 g/dm^3.
The purpose of the first part of this chapter is to provide a physical introduction on the main features regarding the capillarity phenomenon in porous media and the hydrocarbon behaviour in charged material.

4.1 CAPILLARITY IN POROUS MEDIA

4.1.1 Characteristic curve

In a porous medium, containing in the pore space two (or more) immiscible fluids, the interface between two fluid phases acts as a membrane under tension, since the molecules closed to the interface own an excess of energy with respect to the molecules in the bulk phases. This surplus of energy, called *interfacial energy* or *surface tension*, is due to the attractive forces existing between the molecules of the same phase. A molecule placed in the bulk of the liquid, is subjected to attraction forces from all the surrounding molecules (on all directions) and, as a consequence, it is not subjected to a net force of attraction. Otherwise, if the molecule is placed close to the interface, it is attracted by the molecules of the same phase, since a fluid cannot exercise an attractive force on another fluid if they are immiscible. Consequently, there is a net attractive force acting on the molecules at the interface that tend to draw them to the bulk.

The phase, that presents a smaller contact angle along the contact of the interface with the solid matrix, takes the name of *wetting phase*. For the common soil, the hydrocarbons have an intermediate wettability between water and air.

In porous media, capillary phenomena try to minimize the surplus of energy through minimizing the interfacial area (Charbeneau, 2007). As a consequence, the interface between two immiscible fluids is curved and there is a capillary pressure between the phases on either side (Charbeneau, 2007) which can be identified as the pressure difference between the nonwetting phase and the wetting phase.

The *capillary pressure*, p_c, is defined by the Young (1805) – Laplace (1806) equation as follows:

$$p_c = \frac{2\sigma \cos(\theta_c)}{\bar{r}} \qquad [4.1]$$

as a function of: σ = the surface tesion; θ_c = the smaller contact angle and $\bar{r}$ = the mean radius of curvature of the interface.

The relationship between p_c and the wetting fluid saturation is called *capillary pressure curve* (or simply *characteristic curve*, since it is a very important characteristic of the porous medium and it is usually used to characterize the soils). As reported in equation 4.1, when p_c increases in a porous medium, the interface between the two phases is pushed into the smaller pore space and the wetting phase saturation is reduced (in behalf of the nonwetting phase). Otherwise, when p_c decreases, the interface moves into the larger pores and the wetting phase saturation increases.

In the test performed to evaluate the sodium bentonite characteristic curve, the material was firstly fully saturated with the wetting phase (water) and later the nonwetting fluid (air) was introduced at increasing capillary pressure. The wetting phase saturation decreases until the *wetting-phase residual saturation* is reached, which represents the wetting phase fluid that is held tightly at grain contacts and as fluid skins, so that the wetting phase is no longer continuous for flow (Charbeneau, 2007), as represented in Figure 4.1.

Figure 4.1 – Schematic representation of the residual condition of the wetting phase in a porous medium.

4.1.2 Characteristic curve models

The most popular model aimed at fitting the characteristic curve measurements was developed by van Genuchten (1980) in the following mathematical form:

$$S_e = \left(1 + \left(\alpha h_c\right)^N\right)^{-M} \qquad [4.2]$$

where: S_e is the effective saturation of the wetting phase, which range between 0 and 1, and is calculated as in equation 4.3; h_c is the capillary pressure head; α, N and M are model parameters. M and N, in particular, are dependent parameters based on Mualem (1976) relationship, reported in equation 4.4.

$$S_e = \frac{S_w - S_{wr}}{1 - S_{wr}} \qquad [4.3]$$

$$\text{Mualem: } M = 1 - \frac{1}{N} \quad ; \quad N > 1 \qquad [4.4]$$

The parameter α (L^{-1}) modulates the pore dimension, higher value of α corresponds to larger pore size. Whereas the parameter N (-) specifies whether the pore space dimension is more or less heterogeneous: higher value of N corresponds to wider range in pose size.

Characteristic curves are generally derived empirically for the air-water system but the model parameters (α and N) determined for the air-water system can be scaled to another fluid combination. In particular, if it is assumed that the distribution of pore sizes does not change for different fluid systems, that is, there is neither significant shrinkage nor swelling of the porous medium for different fluid systems, the parameter N will not change for different fluid combinations (Charbeneau, 2007). Otherwise, the parameter α presents a direct dependence on the capillary pressure and, as a consequence, needs to be scaled.

The scaling equation aimed at obtaining the α parameter for the NAPL-water system, starting from the α for the air-water system, is reported in equation 4.5.

$$\alpha_{[N-w]} = \frac{\sigma_{[a-w]}}{\sigma_{[N-w]}} \alpha_{[a-w]} \qquad [4.5]$$

4.2 CHARACTERISTIC CURVE OF SODIUM BENTONITE

During the Ph.D. research activity, the capillary phenomenon in sodium bentonite has been studied. The characteristic curve of powder sodium bentonite was determined using the vapour equilibrium technique, since the suction measurements required for bentonite are higher than those commonly measured with more traditional methods, such as the oedometer with suction control, the tensiometer and the axis translation method.

4.2.1 Specimen preparation

Six small specimens were prepared starting from dry powder bentonite by means of hydration with DW and drained consolidation in a compaction mold (diameter 101.8 mm). The extruded consolidated specimens (1 and 2) was cropped with smaller

mold, characterized by a diameter of D = 38.1 mm. The average height of the final specimens (1A, 1B, 1C were obtained from specimen 1; 2A, 2B, 2C were obtained from specimen 2) was equal to H_{ave} = 13.7 mm. The saturation was measured on the extruded specimen and the average registered value was S_{ave} = 102 %. The specimen preparation steps are described in Fig. 4.2.

4.2.2 The vapour equilibrium technique

The vapour equilibrium technique is based on the relative moisture control in a closed system, which consists of an airtight container including three elements: a solution, the solution vapour phase and the pore fluid phase of the porous medium.
Two equilibrium states develop between these three elements in the system:

- The first one between the solution and the vapour phase, which is controlled by evaporation;
- The second one between the vapour phase and the pore fluid phase of the porous medium.

By this way, the vapour phase becomes a significant means between the solution and the soil specimen, which is able to spread the osmotic pressure of the container solution to the pore fluid phase even without contact between specimen and solution.
The relative moisture of the system is regulated through the osmotic potential variation of the solution in the container, which is obtained using different chemical solutions.
Several authors used the vapour equilibrium technique for suction control in many applications on clays: e. g. oedometric tests (Belanteur at al., 1997; Villar, 1999; Cuisinier and Masrouri, 2002) and triaxial tests (Blatz and Graham, 2000).
Fine grained soils, i.e. clays, sodium bentonite, need higher suction measurements than those used for coarser materials, which can be studied with more traditional methods, such as the oedometer with suction control, the tensiometer and the axis translation method. The vapour equilibrium technique allows high suction measurements.

(A) DRAINED CONSOLIDATION OF SPECIMEN #1

(B) SPECIMEN #1 CROP WITH 38.1 mm MOLD OBTAINING SPECIMENS 1A, 1B AND 1C

(C) SPECIMEN CROP UNDER STATIC PRESS

(D) FINAL SPECIMEN #1A WEIGHING

Figure 4.2 – Specimen preparation procedure for characteristic curve determination.

The test performed on sodium bentonite consisted in a static method, in which the vapour transport developed in a closed container merely through diffusion. In this method the steady state achievement takes a long time.

A schematic view of the testing equilibrium cell is reported in Fig. 4.3.

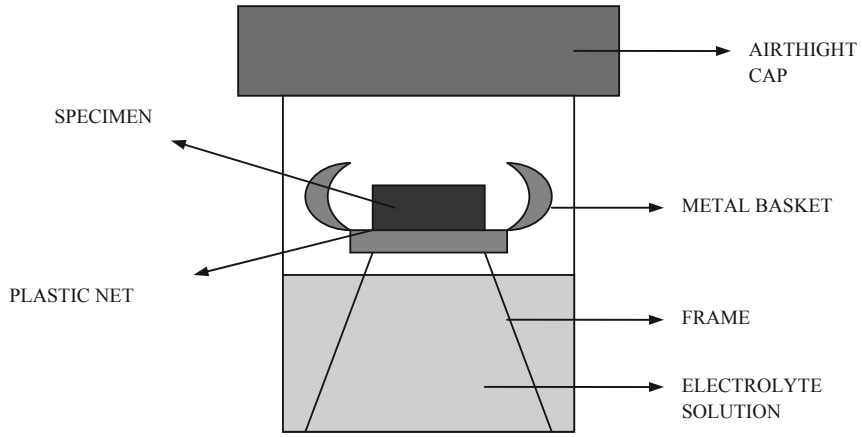

Figure 4.3 – Schematic representation of the vapour equilibrium cell used for the test.

Inside the vapour equilibrium cell, at the achievement of the state conditions, the total suction of the pore solution, ψ, inside the specimen is assumed equal to the osmotic pressure, Π, of the electrolyte solution at the bottom end of the container.
The osmotic pressure, Π, of an ideal electrolyte solution is described by the Van't Hoff equation:

$$\Pi_{id} = \nu \cdot C \cdot R \cdot T \qquad [4.6]$$

where ν is the number of ions derived from the salt complete dissociation, C is the molar concetration of the solution, R is the universal gas constant (R = 8.314 $JK^{-1}mol^{-1}$) and T is the absolute temperature (K).
While, for a non-ideal electrolyte solution:

$$\Pi = \varphi \cdot \Pi_{id} \qquad [4.7]$$

where φ is a correction coefficient for the mathematical deviation from the ideal case, ranging between 0 and 1.
The total suction of the pore solution, ψ, inside the specimen is defined as in equation 4.8.

$$\Psi = \frac{R \cdot T \cdot \rho_w}{MM_w} \cdot \ln\left(\frac{p}{p_0}\right) \qquad [4.8]$$

where ρ_w is the water density, MM_w is the water molar mass, p is the vapour pressure and p_0 is the solvent pressure in standard conditions (which is merely function of the temperature)

Seeing as, at the achievement of the state conditions, ψ can be assumed equal to Π, the correction coefficient, φ can be derived as follows:

$$\varphi \cdot \nu \cdot C \cdot R \cdot T = \frac{R \cdot T \cdot \rho_w}{MM_w} \cdot \ln\left(\frac{p}{p_0}\right)$$
$$\varphi = \frac{\rho_w}{\nu \cdot C \cdot MM_w} \ln\left(\frac{p}{p_0}\right) \qquad [4.9]$$

4.2.3 Testing procedure and results

The test was performed in six vapour equilibrium cells, containing six specimens and six different electrolyte solutions. In each cell, at the achievement of the equilibrium, the suction of the specimen pore solution was considered equal to the osmotic pressure reported in table 4.1.

The electrolyte concentrations in Table 4.1 were selected with the aim to prepare an adequate range of suction, wide enough to draw an appreciable capillary pressure curve.

The electrolyte solution filled the bottom of each cell, each specimen was weighted and placed on the plastic net in the container so that there was no contact between the specimen and the solution. Finally the cells were ermetically sealed.

The initial weights (tare, gross and net) of the six specimens were recorded. The initial saturations of the specimens ranged between 99% and 104%.

Table 4.1 – Osmotic pressure of the electrolyte solutions used during the experimental activity considered equal to the suction of the specimen pore solutions.

SALTS	CONCENTRATION	OSMOTIC PRESSURE/ SUCTION	EQUILIBRIUM CELL AND SPECIMEN ID
NaCl	0.1 mol	463 kPa	1A
NaCl	0.2 mol	916 kPa	1B
NaCl	1 mol	4,641 kPa	1C
NaCl	2 mol	9,757 kPa	2A
$Ca(NO_3)_2\,4H_2O$	156 g/ 100 g water	92,000 kPa	2B
$KOH\ \ 2H_2O$	128 g/ 100 g water	330,000 kPa	2C

The gross weight of the specimens was initially measured about every week but, during the test, a decrease of monitoring frequency has been required. The specimen monitoring is reported in Fig. 4.4.

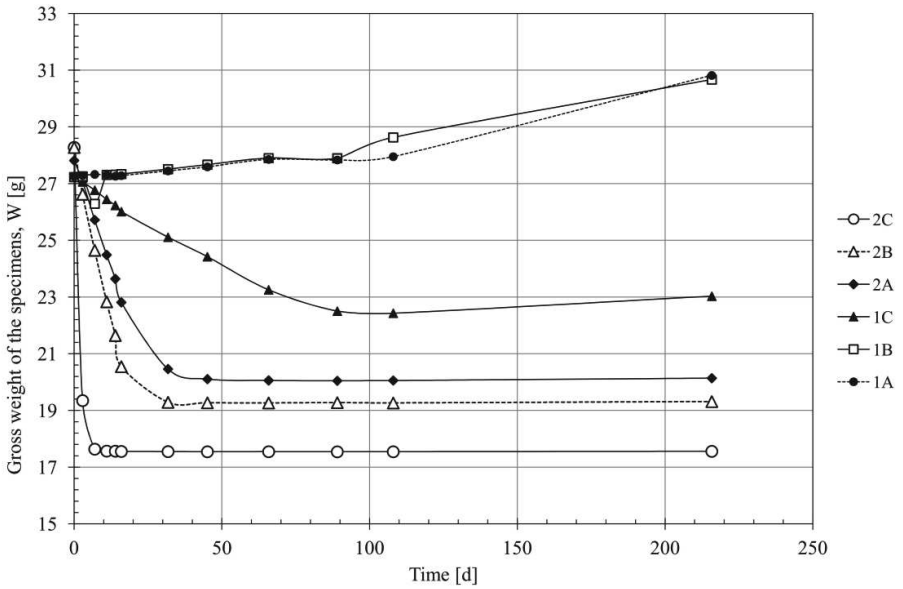

Figure 4.4 – Monitoring of specimen gross weight during the test.

The monitoring of the specimen weights highlighted that the specimens subjected to higher suction reached earlier the equilibrium condition. The specimen subjected to

suction equal to ψ = 330 MPa reached the equilibrium condition in less than 10 days. The specimens 1A and 1B, subjected to suction lower than 1 MPa, swelled during the test and increased their weight through water absorption. Otherwise, all the other specimens decreased their volume (i.e. consolidated) during the test due to the water loss and pore space reduction.

The results of the test are reported in Table 4.2.

Table 4.2 – Vapour equilibrium test results.

	INITIAL			
ID	**Tare, T [g]**	**Gross weight, W_G [g]**	**Net weight, W_N [g]**	**Volume, V_I [cm^3]**
2C	5.12	28.28	23.16	16.47
2B	5.11	28.27	23.17	16.47
2A	5.21	27.81	22.61	16.47
1C	5.14	27.25	22.10	14.80
1B	5.16	27.23	22.07	14.80
1A	5.05	27.25	22.20	14.80

	FINAL				
	Volume, V_F [cm^3]	**Solid weight, W_S [g]**	**Water weight, W_w [g]**	**Water content, w [%]**	**Saturation, S [%]**
2C	6.10	11.35	1.04	6.04	37.67
2B	7.26	11.41	2.76	21.47	83.07
2A	8.38	10.95	3.96	31.59	81.56
1C	11.05	11.36	6.44	58.72	98.65
1B	18.68	11.13	14.20	128.57	98.80
1A	17.63	11.29	14.03	128.51	100.00

The results of the test, reported in Table 4.2, are:

- the initial tare, gross weight and net weight measured for each specimen before starting the test;
- the initial volume of each specimen measured before starting the test (the specimen diameter is constant and equal to 38.1 mm, while the specimen height was not equal because the specimens #1 consolidated until the height H_1 = 12.98 mm and the specimen #2 consolidated until the height H_2 = 14.45 mm);
- the final volume of each specimen measure after ending the test;

- the final solid weight and water weight of each specimen measured after ending the test;
- the final water content of each specimen, calculated using equation 4.10.

$$w = \frac{W_w}{W_S} \cdot 100 \qquad [4.10]$$

- the final water saturation of each specimen, calculated using equation 4.11.

$$S = \frac{w \cdot G_S \cdot \left(\frac{W_S}{V_F} \right)}{G_S \cdot \gamma_w - \left(\frac{W_S}{V_F} \right)} \cdot 100 \qquad [4.11]$$

The results in Table 4.2 are plotted in Fig. 4.5 in term of specimen water content, w, as a function of the total suction, ψ, and in Fig. 4.6 (continuous line) in term of specimen water saturation, S, as a function of the total suction, ψ. This last trend represents the characteristic curve of the studied material.

The characteristic curve for *diesel oil – water* system was derived from the results obtained for *air – water* system using the scaling factor in equation 4.6. The characteristic curve for the *diesel oil – water* system has been reported in Figure 4.6 (dotted line).

Finally, the experimental data fitting with Van Genuchten-Mualem model (equations 4.2, 4.3 and 4.4) is reported in Figure 4.7. The model fit gave S_{wr} = 34%, α = 0.0004 m^{-1} and N = 2.1.

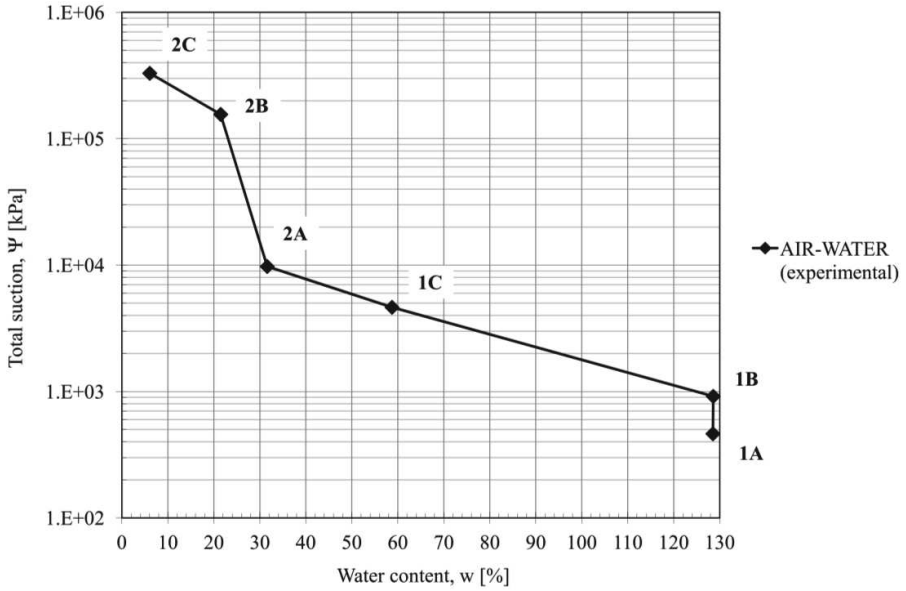

Figure 4.5 – Specimen water content as a function of the total suction at the end of the vapour equilibrium test.

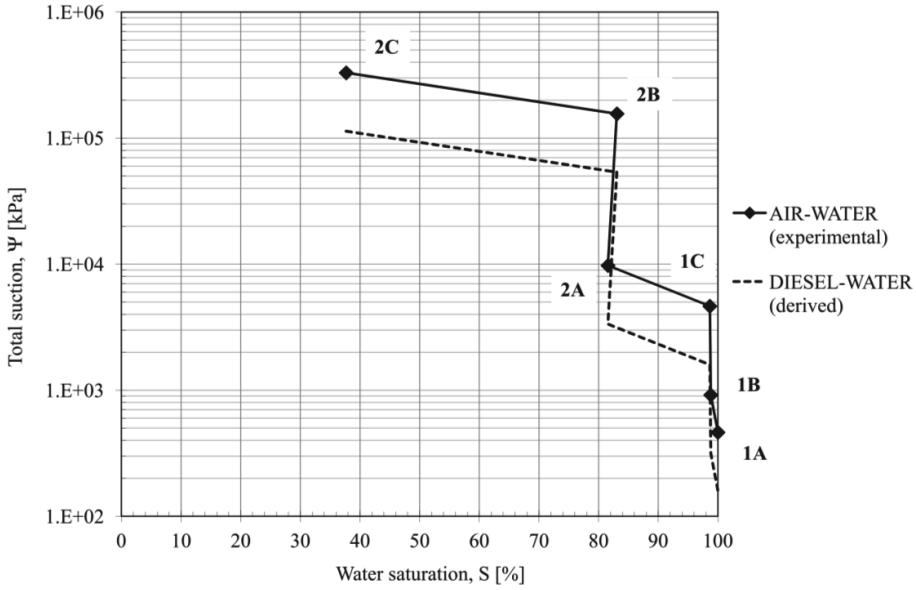

Figure 4.6 – Characteristic curve for air-water system (continuous line) obtained by the vapour equilibrium test and characteristic curve for diesel oil-water system (dotted line), derived using scaling equations (see eq. 4.6).

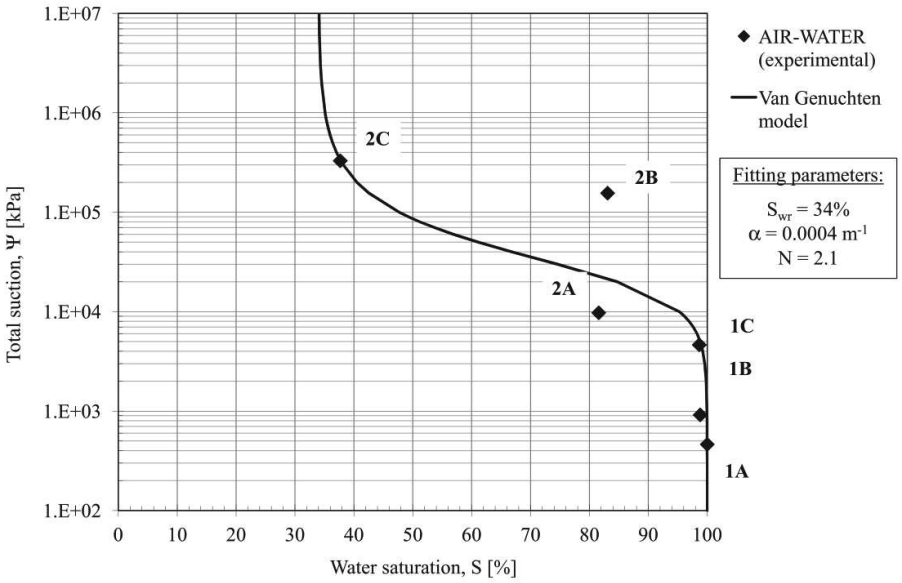

Figure 4.7 – Characteristic curve experimental data obtained by the vapour equilibrium test and Van Genuchten model fitting (eqs. 4.2, 4.3 and 4.4) obtained with fitting parameters: S_{wr} = 34%; α = 0.0004 m^{-1}; N = 2.1.

Fig. 4.6 shows the characteristic curve for diesel oil-water system, derived using the scaling equation 4.6. This equation is founded on the assumption that the distribution of pore sizes does not change for different fluid systems and, if the fluid variation produces an increase of the average pore size, it tends to overestimate the wetting phase saturation for a given total suction value.

The passage from the air-water system to the oil-water system can produce the variation of the pore size distribution as a consequence of a reduction of the dielectric constant (see paragraph 4.3) and, moreover, this phenomenon develops progressively as the oil saturation increases and the water saturation decreases in the porous medium (as experimentally demonstrated in paragraph 4.7.2). Based on the previous reflections, the characteristic curve for diesel oil-water system, reported in Fig. 4.6, acquires a qualitative valence.

4.3 HYDROCARBON BEHAVIOUR IN CHARGED POROUS MEDIA

The negative electric potential at the surfaces of bentonite particles is balanced by the charge of the cations in the pore solution, in order that the bulk clay results electrically neutral.

The cations fill the area around the surface of bentonite lamella, or tactoid, where they are retained by the balance of electrical force and thermal diffusion. The former attracts the cations toward the particle surface, creating a concentration gradient (i.e. the cations concentration is higher near the surface and lower in far from the surface) while the latter attempts to remove this gradient and to establish an homogeneous concentration.

Moreover, anion concentration gradient exists in this area with opposite sign. The area where the concentration of cations is a function of the electric potential of the negatively charged clay surface is called diffuse double layer.

The Gouy-Chapman theory describes an approximate exponential decay of the electric potential until a certain distance from the charged surface. This distance is known as Debey length, λ, and corresponds to the centroid of the diffuse double layer (Mitchell, 1993):

$$\lambda = \sqrt{\frac{\varepsilon\varepsilon_0 RT}{F^2 \sum_{i=n} c_i z_i^{\,2}}} \qquad [4.12]$$

where ε is the dielectric constant of the pore water (also referred to as relative permittivity), ε_0 is the permittivity in a vacuum, R is the universal gas constant, F is Faraday's constant, T is absolute temperature, z_i is the valence of the i-th ion, c_i is the i-th cation concentration. By convention λ usually is used as the "thickness" of the diffuse double layer, although in reality a distinct boundary does not exist between the diffuse layer and the bulk fluid (Shackelford et al., 2000).

Equation 4.12 leads to an unreal concentration of cations in correspondence of the surface because point charge cations have been assumed. As a consequence, equation 4.12 has been modified with the Stern correction, which describes a layer

of finite sized cations adsorbed to the charged surface. In this way, the potential falls linearly from Ψ_0 to Ψ_s (Stern Potential) at the surface and after it decays exponentially, as shown in figure 4.8.

As indicated by equation 4.12, the electrolyte concentration, cation valence, and dielectric constant affect λ which, in turn, effects the hydraulic conductivity and swelling of bentonite. When λ decreases a corresponding increase in hydraulic conductivity develops, induced by the aggregation of the lamellae and the consequent increase of the macro-porosity. Moreover, dramatic reduction in λ caused by liquids with low ε have resulted in shrinkage and cracking of clay with corresponding large increases in hydraulic conductivity (Bowders and Daniel, 1987; Mitchell and Madsen, 1987; Broderick and Daniel, 1990; Shackelford, 1994).

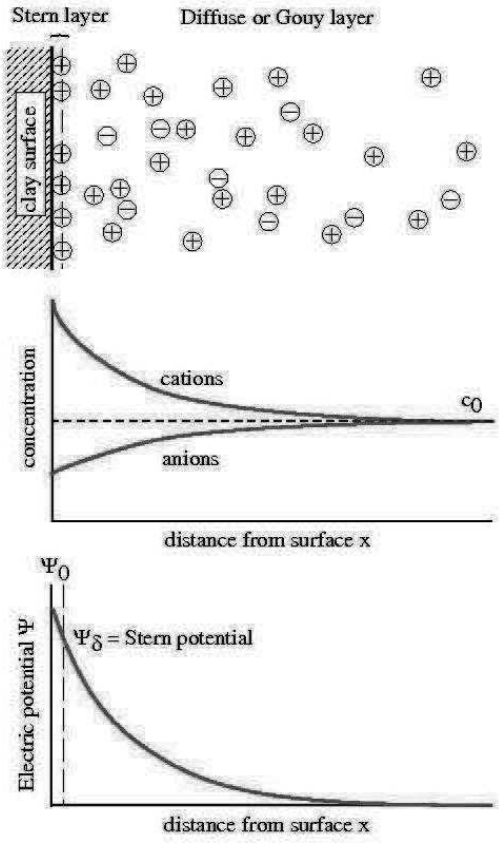

Figure 4.8 - Qualitative representation of Gouy-Chapman-Stern model (After Van Impe, 2002).

In particular, the permeation of clays with solution containing aqueous miscible organic solvents (at a concentration higher than 50%) produces relevant increases of hydraulic conductivity (Bowders and Daniel, 1987; Mitchell and Madsen, 1987; Fernandez and Quigley, 1988; Shackelford, 1994; Shackelford et al., 2000).

Moreover, clays permeated with non-polar (i.e. immiscible) organic liquids result very permeable (Fernandez and Quigley, 1985; Broderick and Daniel, 1990; Shackelford, 1994). In both cases, the hydraulic conductivity increase was attributed to the shrinkage and cracking of clay due to the compression of the adsorbed layer by the low ε of pure organic compounds (typically $\varepsilon < 40$) relative to water ($\varepsilon = 80$) (Shackelford et al., 2000).

In the experimental activity developed during the Ph.D. the hydraulic and swelling performances of sodium bentonite towards diesel oil ($\varepsilon = 2$ at 20°C) were evaluated. The study is reported in the following paper.

HYDRAULIC PERFORMANCE OF GCLS WITH DIESEL OIL AND POLYMER TREATMENT PROPOSAL

By

Sara Puma*, Andrea Dominijanni**, Mario Manassero*** and Daniel Toncelli°

* POLITECNICO DI TORINO, Dipartimento di Ingegneria per l'Ambiente, il Territorio e le Geotecnologie. C.so Duca Degli Abruzzi 24, 10129, Torino, Italy. sara.puma@polito.it

** POLITECNICO DI TORINO, Dipartimento di Ingegneria per l'Ambiente, il Territorio e le Geotecnologie. C.so Duca Degli Abruzzi 24, 10129, Torino, Italy. andrea.dominijanni@polito.it

*** POLITECNICO DI TORINO, Dipartimento di Ingegneria per l'Ambiente, il Territorio e le Geotecnologie. C.so Duca Degli Abruzzi 24, 10129, Torino, Italy. mario.manassero@polito.it

° LAVIOSA CHIMICA MINERARIA S.p.A., via Leonardo Da Vinci 21, 57123, Livorno, Italy. dtoncelli@laviosa.it